Frequency domain diffraction analysis to determine wave forces on a moored ship in a complex wave field

Hanwei Wang

Master of Science Thesis

TU Delft Delft University of Technology

Faculty of Mechanical, Maritime and Materials Engineering (3mE)

Delft University of Technology
Master Offshore and Dredging Engineering
Specialization of Floating Offshore Structures

MSc.Thesis Report:

Frequency domain diffraction analysis to determine wave forces on a moored ship in a complex wave field

Hanwei Wang

(Feb. 2018 – Sep. 2018)

This page is blank page.

FINAL REPORT

Title: Frequency domain diffraction analysis to determine wave forces on a moored ship in a complex wave field

Author: Hanwei Wang

Date: September 2018

Graduation committee:

Prof. Dr. Ir. Riaan van't Veer	Delft University of Technology
Dr. -Ing. Sebastian Schreier	Delft University of Technology
Dr. Ir. Sape Miedema	Delft University of Technology
Dr. Ir. Alex van Deyzen	Royal HaskoningDHV
Ir. Frederick Jaouen	Maritime Research Institute Netherlands

Acknowledgements

This thesis is part of the Master Programme in Offshore Engineering at Delft University of Technology. It marks the ending of two years hard working, doing interesting research, gaining knowledge and personal experiences in The Netherlands. This is an unique opportunity that will be always remembered.

I would like to thank Prof. Riaan van't Veer and Sebastian Schreier for the guidance and motivation during the project; **Royal HaskoningDHV** for giving the opportunity and all supports; Yijun Wang, Alex van Deyzen for the knowledge, experience sharing and their daily assistance; Sebastian Schreier and Frederick Jaouen for their regular guidances, which helps me to proceed this thesis project in a scientific and rigorous approach.

I would also like to acknowledge Joao P. H Dobrochinski for sharing the experience of SWASH model setting; Olaf Scholl and Fillip Schurrman for supporting and instructing SWASH parallel computation; Mark Klein and Marcela Busnelli for sharing the experience of wave modelling; Bas Reijmerink, Martjin de Jong, Arne van der Hout and **Deltares** for kindly providing and explaining the model test data used in validation phase.

Finally I would like to thank all my relatives, friends, colleagues and especially my parents for support, which helps me to overcome all the challenges during this intense but harvestable two years.

Hanwei Wang

September 2018

Summary

Moored vessels are subject to wave forces and moments at different frequencies, which induce motions of the body and can be transferred to the mooring lines and fenders. Under extreme forces and vessel motions, dangerous line breaking accidents can occur or the ship movements can be simply too large to continue the loading/unloading process, causing downtime of the port. An accurate modelling of the waves in the harbour and the response of moored ships is of prime importance to determine the safety and workability of the berths.

In Royal HaskoningDHV, a time domain conventional work flow (MIKE 21 BW - Harberth) is used for years. In this project the combination of the wave model SWASH and the frequency domain 3D diffraction model DIFFRAC to compute wave forces acting on moored ships is investigated, this proposed approach using the SWASH wave model comes as a possible alternative to the current practice of Royal HaskoningDHV, who experienced a sequence of numerical issues while simulating extreme incident waves with an operational Boussinesq-type model.

The objectives of the study leads to the following research question: To which extent can the SWASH wave model and the DIFFRAC model be combined in order to accurately compute wave forces acting on moored ships?

To answer this research question, the coupling tool to combine SWASH and DIFFRAC is developed with 'Full FFT' method and 'Partial Overlapping FFT' method. The coupling tool developed to combine the SWASH and DIFFRAC models proved to be consistent for the simplified tested conditions. The first-order forces computed using SWASH and DIFFRAC are generally well predicted, while larger deviations can occur for the second-order forces. This is mainly because the simplification of waterline geometry made by DIFFRAC in the computation of second-order forces.

The proposed approach using the SWASH and DIFFRAC models, combined with the developed coupling tool, is validated against model test data of waves and forces acting on a restrained ship (including regular, irregular long-crested and irregular short-crested waves in open water case and basin case), for validation cases of regular wave and long-crested wave propagate in open water, both SWASH model and ship response fit very well with measurements, when including wave spreading, the coupling procedure with 'Full FFT method' shows higher performance than with 'Partial overlapping FFT' method. For cases with more complicated basin geometry (involve the harbour structure), in SWASH simulation, significant wave height of wave within harbour shows significantly lower than the wave outside the harbour due to the influence of harbour geometry, this phenomenon does not match the model test in Deltares, therefore the performence of coupling procedure can not be investigated for these cases with complicated harbour geometry.

Based on the result from validation, this new developed frequency domain approach has been proven competitive with respect to the current time domain approach in both accuracy and time consuming , and can be applied to future projects.

Contents

Chapter 1

Introduction

1.1 Research problem

Vessels in harbours are subject to wave forces and moments at different frequencies, which induces motion of the body and can be transferred to the mooring lines and fenders. Under extreme forcing, dangerous line breaking accidents can occur or the ship movements can be simply too large to continue the loading/unloading process, causing down time of the port. An accurate modeling of the waves in the harbour and the response of moored ships is of prime importance to determine the safety and workability of the harbour. In Royal HaskoningDHV the DMA (Dynamic Mooring Analysis) work chain is applied to calculate the force on mooring lines, fenders and then downtime (workability) of the harbour. The beginning of this system is to define wave forces and moments acting on the floating body.

To indicate wave forces acting on moored vessel, a hybrid Boussinesq-panel method for predicting the motion of a moored ship has been investigated by Bingham(2000), with solving the wave force acting on restrained vessel in time domain by using modified Boussinesq-type wave model and simulation tool WAMSIM©, the first-order wave forces are determined using Haskind relations in a frequency-domain panel method. The ship motions are again calculated in the time-domain to include the nonlinear restoring forces of the mooring system. van der Molen (2006) used a Boussinesq wave model to calculate the propagation of the incident waves. The short-wave are phase-resolved and act as the driving force for the generation and propagation of the associated bound waves. The short wave, bound and free long wave elevations are calculated in the time domain using shallow water equations. Long wave assumptions can be used to provide simple formulations for the wave force on the ship. This is valid approach only when the infra-gravity wave is the dominating wave case. Based on the work of Bingham, in year 2008, by applying WAMIT©, a method for simulating the motions and mooring forces of a moored ship subject to wave forcing has been further developed and validated for both the open water case and inside harbour areas by Christensen2008. Contrary to Bingham2000 (2000), van der Molen and Wenneker (2008) have validated a time-domain panel method, which is applied to determine the scattering of the incident waves. By fully calculating the fluid flow around the ship it is possible to directly obtain the first-order wave forces as well as slowly varying drift forces with direct pressure integration fully in time domain without

Fourier transformations.

However, numerical issues always occur to operational Boussinesq wave models especially for extreme wave case, as reported in Monteban (2016). SWASH, which is a more advanced nonlinear wave model developed in Delft University of Technology, comparing to Boussinesq type wave models, which is also currently used in Royal HaskoningDHV, SWASH can produce more reliable wave simulation especially for extreme wave case even with several vertical layers. In principle the SWASH model is capable to resolve in a robust way the relevant processes involved in wave penetration studies, being very likely competitive with the extended Boussinesq wave models in terms of robustness and the computational efforts. This has been investigated and validated in Master thesis Dobrochinski (2014), by coupling SWASH and time domain diffraction analysis software Harberth in Royal HaskoningDHV. This 3D time domain work flow is significantly time consuming, therefore to enhance efficiency, a frequency dependent 3D solver can produce relatively accurate results with saving significant computational efforts. DIFFRAC, which is a frequency domain diffraction analysis software, has been fully developed and maintained by MARIN and has been validated for both shallow and deep water against many physical model test results with normal method (without 'User Defined Wave' option) MARIN (2017), which has been proved with great performance for frequency domain diffraction analysis. Therefore is selected as this frequency domain diffraction analysis software.

For DIFFRAC application in complex wave field, a coupling tool should be developed to couple SWASH and DIFFRAC based on built-in function 'User Defined Waves' in order to interpolate the wave data at predefined collocation points along the hull of floating body and each water line point to calculate forces and moments acting on the moored vessel, which is exposed to a complex wave field. In this master thesis, this work flow (SWASH - Developed coupling tool - DIFFRAC) based in frequency-domain calculations will be investigated and validated against with experimental measurements.

1.2 Research question and objectives

Comparing with conventional method (marked with red dots) in Royal HaskoningDHV, the new work flow (marked with green dots) based on frequency domain calculations is shown in Fig.1.1, the performance should be investigated beforehand of real application, resulting in research question:

To which extent can the SWASH wave model and the DIFFRAC model be combined in order to accurately compute wave forces acting on moored ships?

To answer this research question, the objectives listed below have to be accomplished:

- Analyze the overall approach identifying the contribution of the different steps and associated assumptions/simplifications to the accuracy of the calculation;
- Investigate the influence of SWASH model settings on the predictions of forces acting on moored ships;
- Investigate the influence of developed coupling tool on the resulted force and moment

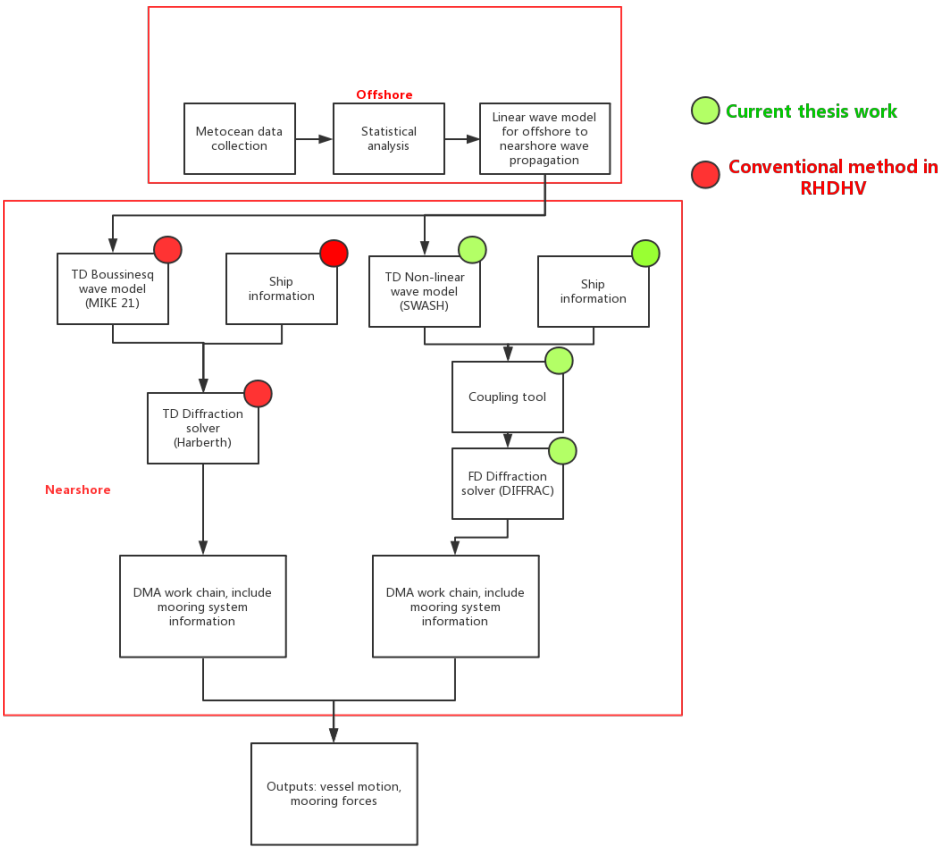

Figure 1.1: Conventional time domain method (MIKE21 BW + Harberth) and new frequency domain method (SWASH + coupling tool + DIFFRAC) within DMA whole work flow.

acting on the moored ship;

- Verify coupling tool and new work flow;
- Validate this new work flow by comparing with results from model test carried out at Deltares, Bijleveld (2004).

1.3 Research approach

The whole research approach is divided into steps as follows:

1. Review of theory and numerical tools
   - Literature review;
   - Manuals and tutorials of SWASH and DIFFRAC;
2. Developing the coupling tool to combine SWASH and DIFFRAC
3. Verification
   - Wave model set up, start with 2D regular and irregular wave model;
   - Verify this new workflow in 2D case.
4. Update the previous tool to 3D coupling tool
5. Validation
   - Wave model set up, 3D regular, irregular long-crested and irregular short-crested wave model in open water and in harbour geometry;
   - Update 2D coupling tool to 3D coupling tool;
   - Validate the this new work flow against experimental measurements.

The overall steps can be seen in Fig.1.2

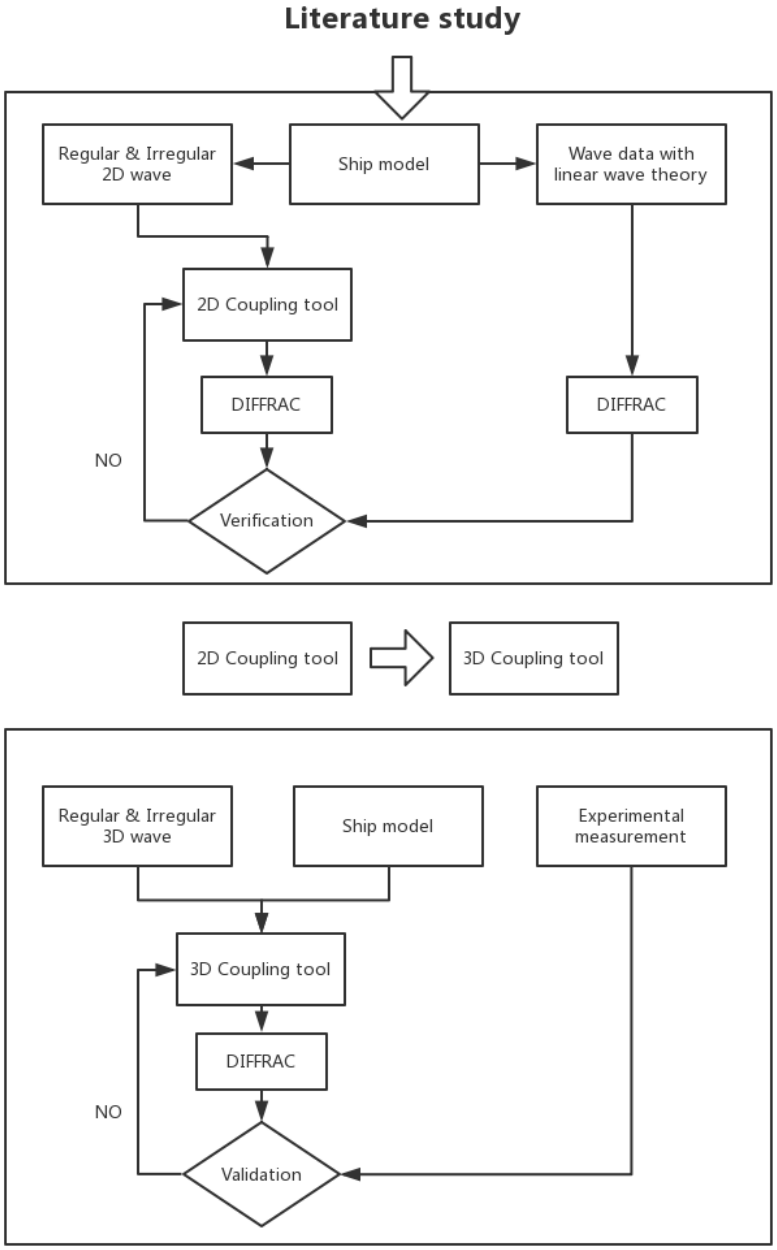

Figure 1.2: Overview of research approach

Chapter 2

Review of theory and tools

In this chapter general aspects regarding waves in coastal areas and the response of ships on waves are covered, following with attention on the theory of numerical tools (SWASH and DIFFRAC) applied in this project, end with Fourier Transform in engineering application and the methods to eliminate the influence of spectral leakage in the development of coupling tool.

2.1 Wave modelling

Sorting the various waves by their frequencies gives an overview of the wave types that can be encountered in oceanic and coastal waters (Fig.2.1). Wave periods vary from seconds up to 24 hours. kd value (wave number $\cdot$ water depth) is widely applied to indicate wave case, the waves with $kd < 3$ are the most common wave cases in coastal area, these waves are also the interest in this project.

Irregular sea and swell waves with small differences in wave frequencies are known to propagate in groups of higher and groups of lower waves due to the modulation of wave height. Non-linear interactions of the incident modulated short waves generate longer waves with the frequency of the wave groups. These long waves are referred as bound infra-gravity waves, which are phase locked (bound) and in anti-phase with the wave groups. Their amplitude mainly depends on local conditions and characteristics of the short wave spectrum. This infra-gravity wave is much more dangerous relative to other ordinary waves in coastal engineering application.

With harbours, estuaries and headlands, the ordinary waves gradually lose energy as they propagate in and around all the corners, whereas the infra-gravity waves just plough on right through to the most far-reaching pocket beaches and boat ramps. But infra-gravity waves have mostly been studied on gently-sloping beaches, where it is easy to compare their behaviour with that of the ordinary waves. Here, the ordinary waves dissipate their energy through breaking, while the infra-gravity waves just keep on going right to the shoreline.

One important feature of infra-gravity waves is that they actually increase in size as they

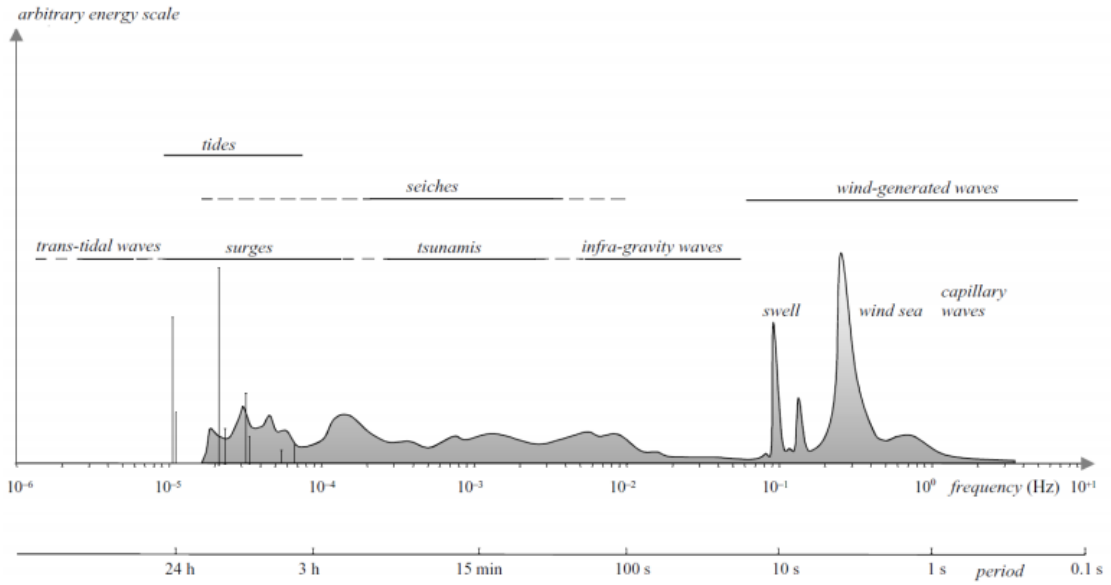

Figure 2.1: Wave categories by frequencies and period, Munk (2010).

approach the shore. Because of their exceptionally long wavelength, they never get steep enough to break. In fact, because infra-gravity waves never break, they keep on growing like to the shoreline and reach their maximum size at the shoreline itself. This process is greatly enhanced during large stormy conditions (see Figure.2.2).

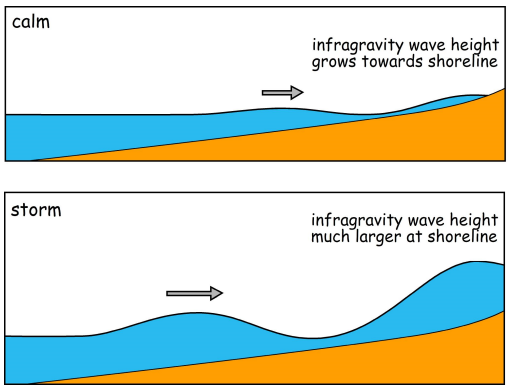

Figure 2.2: Infragravity waves are so long that they never break, therefore they squash up and get bigger as they slow down in shallow water, reaching their maximum height at the shoreline itself, Butt (2010).

In contrast, the ordinary waves, which have a much shorter wavelength, generally become steep enough to break before they reach the shoreline. Once they break and become lines of rolling whitewater, they start to dissipate their energy. On gently-sloping beaches, they tend to break a long way out, and can lose practically all their energy before they get to the shore. This is why the lines of whitewater arriving at the shoreline are usually quite weak and dribbly, even if the waves further out back are really big. In this case, the ordinary waves are said to be saturated. In theory, completely saturated waves diminish to nothing at the shoreline.

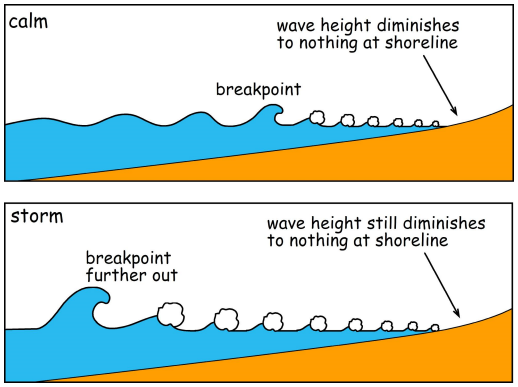

Figure 2.3: In truly saturated conditions on gently-sloping beaches it does not matter how big the offshore wave height gets, the ordinary waves still diminish to virtually nothing at the shoreline, Butt (2010).

Due to the viability of this long infra-gravity wave, even with relatively small amplitude, infra-gravity waves can influence considerably the behaviour of moored ships if their frequencies overlap the range of natural frequency of the mooring system. Thus, a proper assessment of the generation and near shore transformation of infra-gravity waves in the surroundings of harbours is of utmost importance to the design of the mooring facilities and determine practical aspects of port operations, Butt (2010).

2.2 SWASH: A time domain multi-layer wave propagation model

Over the past decades, strong efforts have been made at Delft University of Technology to advance the state of wave modeling for coastal engineering application. Within other achievements, these efforts resulted in the newly developed non-hydrostatic model SWASH. SWASH is intended to be used for simulating the transformation of surface gravity waves and shallow water flows in coastal regions up to the shore in an efficient and robust way, Zijlema, Stelling, and Smit (2011).

The model can accurately predict the evolution of waves propagating in intermediate and shallow water. The variations in total and incoming infra-gravity wave heights are also represented by SWASH, as well as reproducing the phenomena associated with the evolution of these waves in the nearshore (i.e. shoaling of bound infra-gravity waves, shoaling reflections, phase lag between the wave envelope and the incoming infra-gravity waves, nonlinear interactions and the occurrence of infra-gravity wave breaking), Rijnsdorp, Smit, and Zijlema (2014).

Zijlema et al. (2011) present a series of verifications of the SWASH model for generic wave and flow features which are expected to be encountered in most nearshore related applications, including well-controlled laboratory conditions and cases for which analytical solutions are provided. kd value (wave number $\cdot$ water depth) always used to indicate the case of wave propagation, generally, when $kd < 3$, the wave is regard as propagating in shallow water. SWASH model with two equidistant layers, accurate propagation of progressive waves is retained for $kd = 7.7$, with 3 non-equidistant vertical layers exhibits accurate wave dispersion up to $kd = 16$ when linear progressive waves are involved, this

includes typical values for most nearshore applications The SWASH Team (2017).

A detailed description of the physical and mathmetical and SWASH model are in Appendix A.

2.3 Interaction of waves and ships

The dynamics of rigid bodies due to fluid motions is governed by the combined actions of different external forces and moments (e.g. wave forces, wind forces, current forces, fender and mooring lines forces) and the inertia of the bodies themselves. Notice that the focus of this project is on the determination of wave forces acting on ships moored at areas subject to complex wave processes.

The motions of a ship, just as for any other rigid body, can be split into three mutually perpendicular translations of the center of gravity, G, and three rotations around G. Figure 2.4 presents the definitions of the basic ship motions and the body-bound coordinate system $G(x_b, y_b, z_b)$ with the origin is the center of gravity of the body. The positive x direction is towards the bow, the positive y direction is towards the portside, and z is positive upward. The signs of the rotations are right handed.

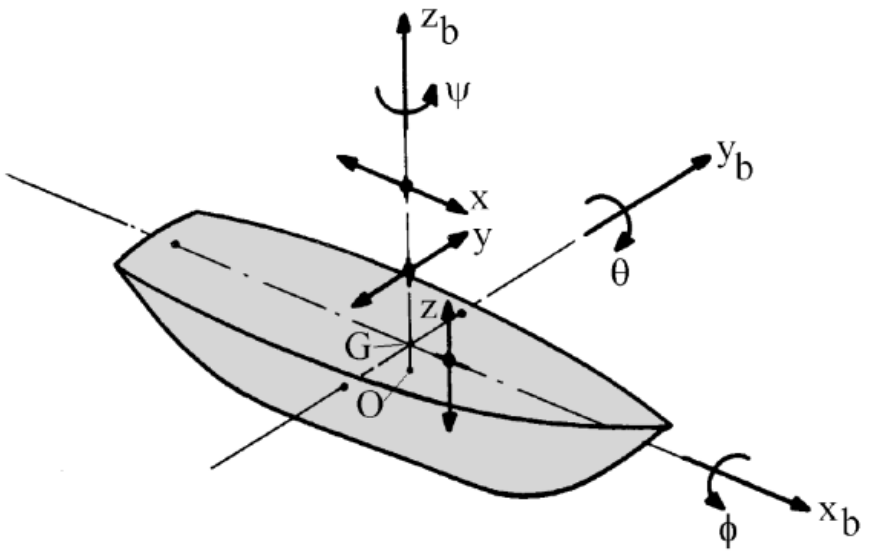

Figure 2.4: Body–bound coordinate system $G(x_b, y_b, z_b)$, Journée and Massie (2002).

To define the motions of a body in the earth fixed (EF) coordinate system, both its position and its orientation needs to be known. This can be described in a 6 component vector, which is illustrated in Figure 2.4. The first three components determine the movements of the centre of gravity of the body:

- Component 1 (surge) is positive from stern to bow (x);

- Component 2 (sway) is positive from starboard to portside (y);
- Component 3 (heave) is positive from keel towards deck (z).

Three rotation angles are used to specify the movements around the centre of gravity of the body. The order in which the rotations are applied is:

- Component 4 (roll) is a rotation around the surge axis (ϕ). Starboard down is positive;
- Component 5 (pitch) is a rotation around the sway axis (θ). Bow down is positive;
- Component 6 (yaw) is a rotation around the heave axis (Ψ). Bow to portside is positive.

The rigid body's equation of motions follow from Newton's second law. The vector equations for the translations of and the rotations about the center of gravity are respectively given by:

$$F = \frac{d}{dt}(mU) \qquad and \qquad M = \frac{d}{dt}(H) \tag{2.3.1}$$

in which:
F = resulting external force acting in the center of gravity (N)
m = mass of the rigid body (kg)
U = instantaneous velocity of the center of gravity (m/s)
M = resulting external moment acting about the center of gravity (Nm)
H = instantaneous angular momentum about the center of gravity (Nms)
t = time (s)

If the system is linear, the forces acting on a body subject to waves can be computed based on the superposition of: 1) the forces resulting from movement of the rigid body in still water (hydromechanic forces and moments); and 2) the forces on the restrained body in waves (wave exciting forces and moments). This is an important assumption usually applied in the calculation of the loads on floating bodies. Accordingly, the motions of the body in six degrees of freedom can be expressed in matrix form as:

$$\begin{gathered} \frac{d}{dt}(\rho\nabla \cdot \dot{X}) \;=\; \rho\nabla \cdot \ddot{X} \;=\; \mathbf{M} \cdot \ddot{X} \\ \mathbf{M} \cdot \ddot{X} \;=\; F_h + F_w \end{gathered} \tag{2.3.2}$$

in which:
X = vector of body motions

ρ = density of water (kg/m^3)
∇ = volume of displacement of the body (m^3)
M = inertia matrix (kg)
F_h = hydromechanic forces and moments (N and Nm)
F_w = exciting wave forces and moments (N and Nm)

The motions of the floating body induces hydrodynamic reactions that generate a time-dependent pressure field around the body. The integration of the pressures in the required direction provides the hydrodynamic forces or moments (F_h). These loads can be expressed in terms of frequency-dependent potential mass and damping coefficients, computed with relatively simple frequency-domain computer programs based on potential theory.

Loads in-phase with the body acceleration give the potential mass (or inertia) coefficients. This coefficient has the dimension of mass, being the so-called the hydrodynamic mass or added mass. The hydrodynamic reaction in this case resembles a standing wave system and does not dissipate energy from the motions. Loads in-phase with the body velocity provide the wave (or potential) damping coefficients. This hydrodynamic reaction corresponds to progressive waves propagating radially from the body, withdrawing energy and damping the motions. In a linear system the so-called wave damping is proportional to the velocity of the moving body.

A motion mode can cause a force in that same direction (e.g. heave motion causing a force in the direction of the z-axis), but also in different directions. This introduces what is called coupling between motions or between the hydromechanic forces and moments. The coupling of ships motions can be split into symmetric components about the vertical-longitudinal plane of symmetry (surge, heave and pitch) and anti-symmetric components (sway, roll and yaw). Symmetric and anti-symmetric motions do not have any effect on each other. Although, they can be coupled when external elements are influencing the motions (e.g. effects of anchor lines).

Boundary-integral 3D diffraction models (e.g. DIFFRAC and Harberth) can handle the radiation problem by computing potential flow resulting from body motions on different modes. The hydromechanic forces (F_h) are computed by integrating the pressures of the radiation problem along the 3D hull of the vessel. Similarly, the wave exciting forces (F_w) result from the integration of the total wave pressures along the hull.

An additional hydromechanic load is the restoring *spring* term, in-phase with the displacement of the body. This term is not directly related to the hydrodynamic reactions due to motions, but is an effect of the body out of its equilibrium position. The *stiffness* coefficient is obtained from A_w (area of the waterline) and S_w (first order moment of the waterline), both related to the geometry of the floating body. It is also possible to obtain the stiffness coefficients from static experiments. For free floating bodies the restoring term applies only for heave, roll and pitch motions.

By replacing the hydromechanic forces (F_h in Equation 2.3.2) by the above mentioned coefficients, the equation of motion in six degrees of freedom in the frequency-domain is obtained:

$$(\mathbf{M} + \mathbf{a})\ddot{X} \ + \ \mathbf{b}\dot{X} \ + \ \mathbf{C}X \ = \ F_w \tag{2.3.3}$$

in which:
$\mathbf{a}$ = matrix of frequency-dependent potential mass coefficient (kg);
$\mathbf{b}$ = matrix of frequency-dependent potential damping coefficient (kg/s);
$\mathbf{C}$ = matrix of hydrostatic restoring coefficient (kg/s^2).

In time-domain, the motions on a given time are influenced by the motions before this interval. The reaction force due to the accelerating body is also expressed in terms of an added mass coefficient, while the 'memory' is included in simulations with the so-called retardation functions. These coefficients can be calculated using time-domain computer programs based on potential theory or using the frequency-dependent added mass and damping coefficients.

Viscous effects such as skin friction and vortices around the corners of the hull can introduce additional damping to the body motions. Viscous damping coefficient cannot be calculated with a potential flow model, therefore when relevant a viscous damping coefficient is prescribed explicitly. Specially for sway, heave, pitch and yaw motions of ships, viscous effects are sufficiently small relative to the potential damping and can be neglected. However, for surge and particularly roll the potential damping is generally small, so the contribution of viscous effects can be relevant to the overall damping of these motion modes.

With the mass matrix of the ship defined, as well as the hydromechanic (F_h) and wave exciting forces (F_w), the equation of motions of the ship can be integrated on time. Other forces such as the effect of a mooring system, fenders, winds and currents can be included in those computations as external source terms. The results of the integration are time records of ship motions and forces in mooring lines and fenders. These outcomes can be compared to the allowable motions and forces for an economic loading and safe mooring. Finally, the expected downtime of the port with respect to wave action on moored ships can be determined.

2.4 DIFFRAC: Frequency domain diffraction analysis software

2.4.1 DIFFRAC Introduction

DIFFRAC is a wave diffraction program based on a three-dimensional source distribution technique for the solution of the linearised velocity potential problem. For this approach the fluid is assumed to be inviscid, homogeneous, irrotational and incompressible. DIFFRAC computes fluid pressures and wave loads on the basis of the velocity potential around the vessel, given as a scalar function in space and time.

For the computations, the mean wetted part of the hull of the vessel is approximated by a number of panels. Each element represents a distribution of source singularities, each of which contributes to the velocity potential describing the fluid flow.

The rigid lid method is used to suppress the effect of irregular frequencies, this method is

well introduced in Appendix 1 in MARIN (2017). A damping lid may be used to damp resonant water motions, for example in the gap between side-by-side moored vessels. It is capable of calculating the wave loads and motion response of free floating or moored structures in regular waves, including their hydrodynamic interaction. The program is applicable to both shallow and deep water and has been validated against many physical model test results (normal method without 'User Defined Wave' option) MARIN (2017).

2.4.2 'User Defined Wave' Option

However, the wave field is not always simple (regular), so in some cases, for example the case when wave entry into a harbour, the effect of passing ships, or the wave generation on bathymetries in coastal regions have to be considered. In such a case a built-in function 'User defined wave' option allows user to calculate the wave loads due to incoming waves and diffracted waves in any incoming wave field, user may specify their own undisturbed water pressure and water velocities at the panel collocation points. For that purpose, a file must be provided that contains the undisturbed water velocities and water pressures in the collocation points and undisturbed wave elevation in the waterline points, for all specified wave frequencies and wave directions.

To achieve this purpose, the file that contains all the required wave quantities should be provided, for regular wave, the frequency domain wave quantities is given by DIFFRAC, for more complicated wave cases (long-crested wave, short-crested wave, etc.), the function 'User Defined Wave' help DIFFRAC to recognize the frequency domain wave quantities defined by user, this user defined frequency wave quantities are:

- Both real and imaginary parts of incident velocity in x, y and y direction (V_x, V_y, V_z) and dynamic incident water pressure (P) in all the collocation points;
- The incident water elevation (ζ_{inc}) in the waterline points. Each line in the file should contain real and imaginary parts of ζ_{inc}.

INPUTS (For calculation in complex wave field)

- Structure's geometry
- Position of center of gravity
- Raddii of inertia about the axes
- Water depth
- Wave information in complex wave field through 'User Defined wave' option

OUTPUTS

- Added mass and damping coefficients;
- Wave forces and moments;

- Wave induced motions;
- Pressure distribution over the body surface;
- Mean 2nd order wave drift forces.

2.5 Discrete Fourier Transform to predict the wave spectra in irregular seas.

Fourier transform is applied to convert the time series into spectra, a continuous time series in real case can only be recorded and processed as finite discrete data points in computer, in mathematics, the discrete Fourier transform (DFT) converts a finite sequence of equally-spaced samples of a function into a same-length sequence of equally-spaced samples of the discrete-time Fourier transform (DTFT), which is a complex-valued function of frequency. The traditional method of representing irregular seas is by discrete Fourier components with constant frequency span. This method is commonly referred to as the FFT (Fast Fourier Transform) of the wave spectrum, Rahman, Riordan, Susilo, and Mousavizadegan (2011).

2.5.1 Spectral leakage and window function

In reality, signals are of time-limited nature and nothing can be known about the signal beyond the measured interval. For example, if the measurement of a never ending continuous train of sinusoidal wave is of interest, at some point of time we need to terminate our measurement to do further analysis. Fourier Transforms implicitly assumes that the signal essentially repeats itself after the measured time, Mathuranathan (2011).

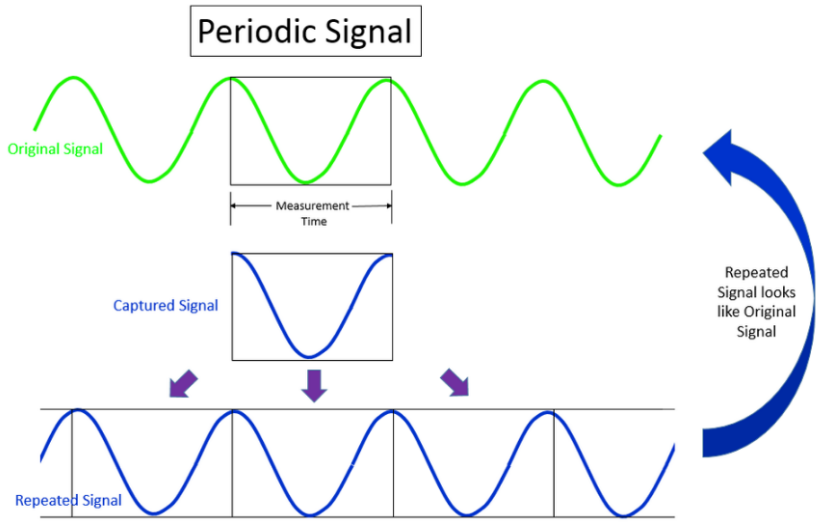

Figure 2.5: Periodic signal.

Fig.2.5 and 2.6 illustrate the scenario in which a continuous train of sinusoidal signal is observed over a finite interval of time ("measured signal"). As discussed, the FFT as-

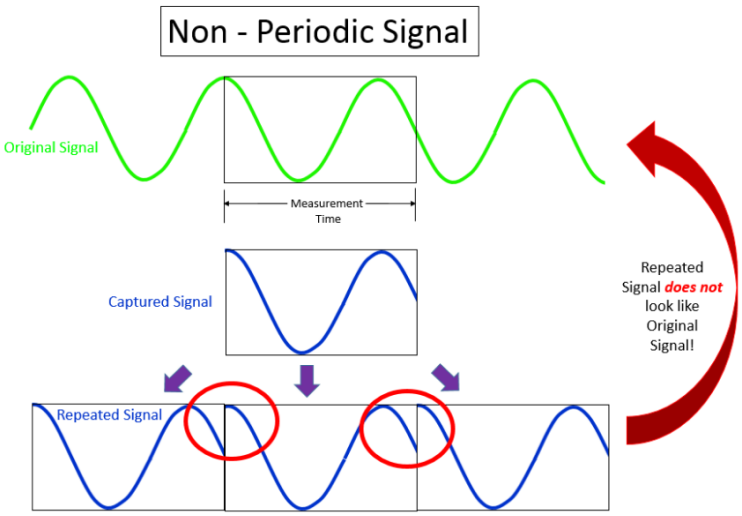

Figure 2.6: Non-periodic signal.

sumes the signal to be continuous (conceptually, it does this by juxtaposing the measured signal repetitively). Observe the glitches in the assumed signal. These glitches are the manifestations of the measurement time relative to the frequency of the actual signal. If measurement time is an integral multiple of the rate of the actual signal (i.e. the inverse of the frequency of the signal), then no glitch will be observed in the assumed signal. These sharp discontinuities will spread out in the frequency domain, which leads to much wider spectra than FFT of a fully periodic signal, as given in Fig.2.7. This is called spectral leakage. However the information for both amplitude and phase still remain in resulted spectrum, and can be inverse transformed to original time series by using inverse Fourier transform with entire spectrum.

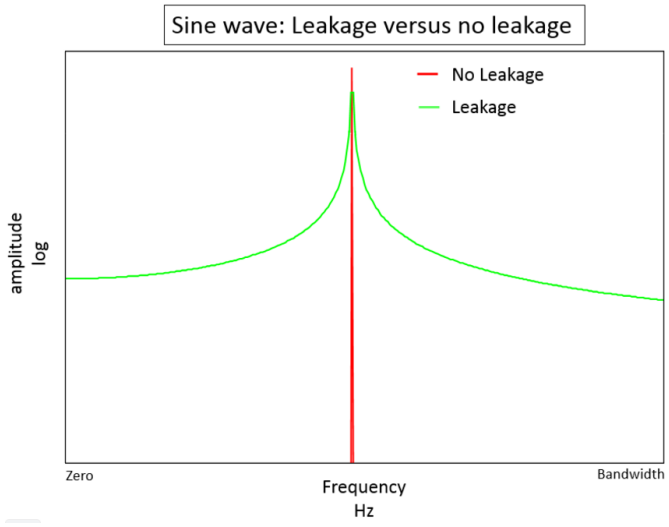

Figure 2.7: Periodic and non-periodic signal in frequency domain.

The only method to solve this problem is whole cycle sampling demodulation, which means the period of sampling should be the integer of the period of signal, then the frequency of

signal can exactly coincide the one of the spectral line and correctly produced in spectra without any further procession. However, for a real irregular wave, with infinite wave components, this perfect sampling duration can not be defined and fit all the frequency components, therefore, using so-called window function to correct the resulted amplitude spectra.

The formula of Hanning window follows

$$w(n) = 0.5(1 - cos(2\pi\frac{n}{N})), 0 \leq n \leq N \tag{2.5.1}$$

which with 0 values at both beginning and end point, as given in the second row of Fig.2.8

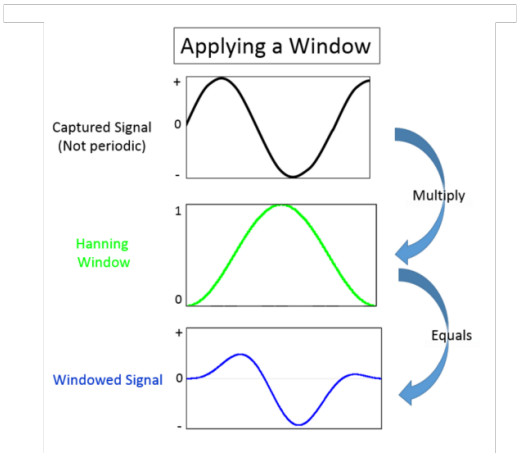

Figure 2.8: Window.

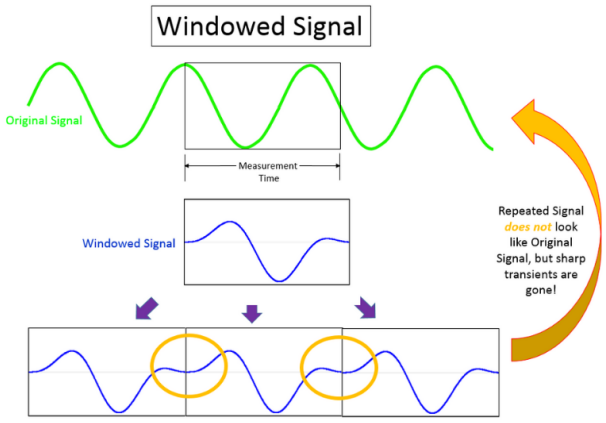

Figure 2.9: How window method correct the non-periodic signal.

The length of window function is the same as the length of input time series, with 0 at both the beginning and end, therefore, after multiplying the window function with original time signal, both the beginning and end of original signal are 0, therefore, still periodic as shown in Fig.2.9. Through this method, some spreading energy due to spectral leakage will be put back into the peak in spectra, therefore the amplitude spectra from FFT can be corrected as given in Fig.2.10.

2.5.2 Partial overlapping window method

When directly applying FFT for the whole time series of sample water elevation (either from record of real irregular seas or from SWASH simulation), significant deviations and oscillation appears when the quantities of samples is insufficient, in real case, the method to produce smooth wave spectra from time series is averaging over sufficient number of samples to describe statistical parameters, one find that the results converge to the original spectrum after averaged 1000 sample spectrum, Bakkedal (2014). For cases with sample FFT and 1000 averaged FFT are shown in Fig.2.11 and 2.12. The resulting smooth wave spectrum is averaged over samples, the phase information is lost.

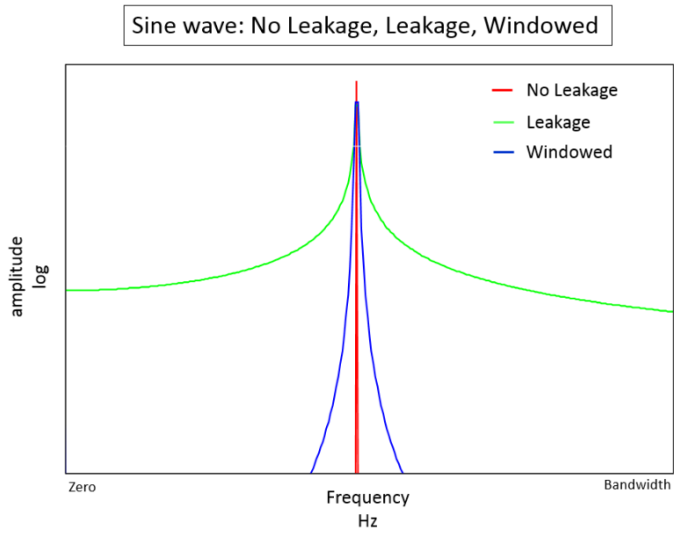

Figure 2.10: Periodic, non-periodic signal and non-periodic signal with window in frequency domain.

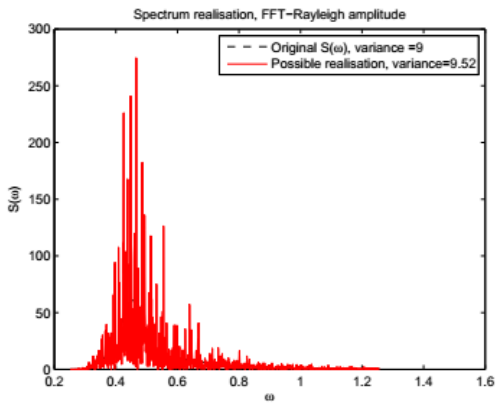

Figure 2.11: Spectrum from FFT with one sample

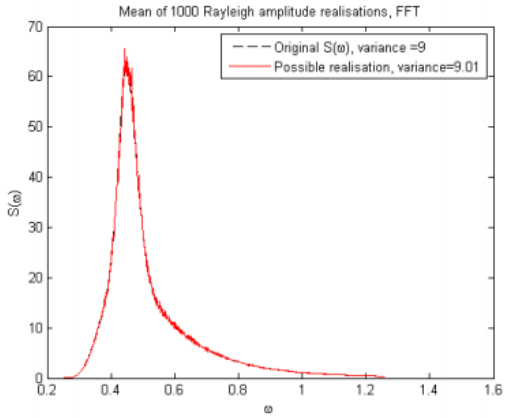

Figure 2.12: Spectrum averaged over 1000 samples

However, for engineering application, the quantities of sample (number of SWASH simulation) is not sufficient to produce converged wave spectra, to solve this problem, an partial overlapping FFT algorithm is applied. For a given time series with N data points, first truncate this time series with length n (n should equal $2^{integer}$ for FFT calculation), which length should still be sufficiently representative for the whole time series, then introduce an increment Δn, at step i, the time truncated time series is from $N_{(i-1)\Delta n}$ to $N_{i\Delta n-1}$, the

number of the iteration $Num = \frac{N-n}{\Delta n}$, then the average can be easily got from

$$S(\omega) = \sum_{i=1}^{Num} FFT(N_i)/Num \tag{2.5.2}$$

With N_i is the number i truncated time series in the whole time series.

By adapting the length of increment Δn, sufficient number of samples can be achieved, however, small increment per step produces more samples but the less difference between neighbour truncated time series at each iteration, therefore the resulting averaged spectrum is less precise than the real averaged spectrum from 1000 samples. The resulting power spectral density spectrum and theoretical power spectral density spectrum (amplitude density spectrum) are shown in Fig.2.13

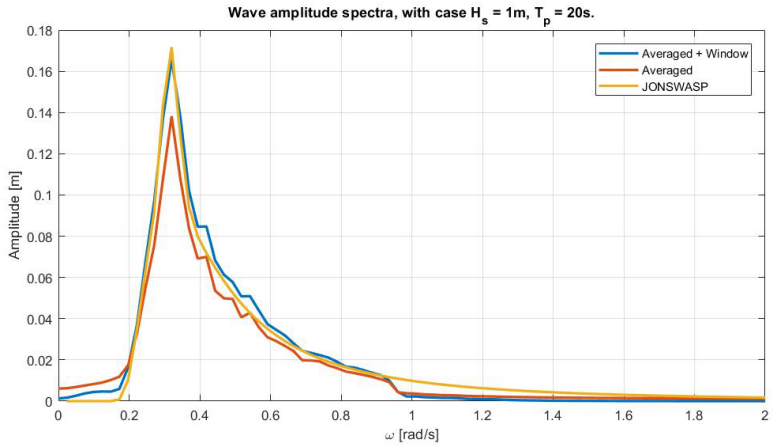

Figure 2.13: Wave amplitude density spectra from (1) Standard JONSWAP calculation (2) Averaged spectrum over 1056 samples with overlapping time window (3) Averaged spectrum with overlapping Hanning window over 1056 samples.

The data indicated in orange and blue color are the resulting averaged wave amplitude density spectrum over 1056 samples with and without overlapping Hanning window, the water elevation time series comes from SWASH simulation at same record point. Wave spectrum is in terms of the ocean wave surface energy spectrum, to verify the resulting amplitude density spectrum against SWASH data, firstly, the energy spectrum has to be transformed to amplitude spectrum after applying Eq.2.5.3,

$$\zeta_(\omega) = \sqrt{2S(\omega)\Delta\omega} \tag{2.5.3}$$

with:
$\zeta(\omega)$ is the wave amplitude density spectra;
$S(\omega)$ is the JONSWAP wave spectra;
$\Delta\omega$ is the frequency step (width of spectral bin).

From Eq.2.5.3, the width of each spectral bin ($\Delta\omega$) is directly related to resulted wave amplitude density spectra, therefore keep identical $\Delta\omega$ for mentioned methods to verify the resulted wave amplitude density spectrum against each other.

2.5.3 Phase spectrum correction

Due to the spectral leakage mentioned in the last section, on each panel, the resulted phase spectrum is unreliable as well, even with overlapping Hanning time window method, in 'User Defined Wave' option, both real and imaginary parts of the wave quantities should be given, therefore both the amplitude spectrum and phase spectrum of wave quantities need to be correctly calculated.

In DIFFRAC calculation, the phase of ship motion and wave force acting on the ship are all with respect to the phase of incident wave acting at CoG of the ship, these relative phases of forces, moments and motions with respect to incident wave are the contribution of relative phases of the wave quantities at all the panel. Therefore if this relative phase shift at all the panels along the ship hull can be defined, the total relative phase should be defined as well.

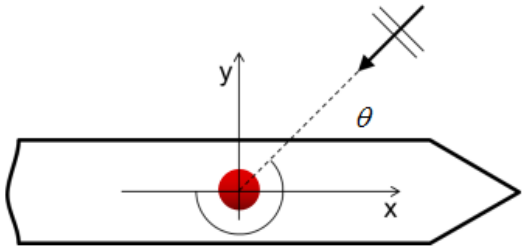

Figure 2.14: Ship and incident wave

Assume a regular wave act at CoG of the ship with wave formula

$$A_0 = asin(\omega t - kx_0 cos(\theta) - ky_0 sin(\theta)) \tag{2.5.4}$$

with x_0 and y_0 are the coordinate of CoG of the ship, and θ is the wave propagation direction.

At a random panel on the ship hull with coordinate x_i and y_i, this wave formula for the regular wave is

$$A_i = asin(\omega t - kx_i cos(\theta) - ky_i sin(\theta)) \tag{2.5.5}$$

then the phase of wave acting on the random panel i relative to the wave acting on the CoG of the ship is

$$\phi = k(x_0 - x_i)cos(\theta) + k(y_0 - y_i)sin(\theta) \tag{2.5.6}$$

For irregular seas, including wave directional spreading, the short-crested waves need to be taken into account, therefore Eq.(2.5.6) becomes to

$$\phi(\omega) = k(\omega)(x_0 - x_i)cos(\theta(\omega)) + k(\omega)(y_0 - y_i)sin(\theta(\omega)) \tag{2.5.7}$$

wave number $k(\omega)$ follows dispersion relation, with the direction of short-crested wave $\theta(\omega)$, the relative shift of irregular seas can also be calculated.

From potential theory, water particle velocity U, V and W and dynamic pressure P are all derived from wave potential with partial derivation of x, y, z and t together with Bernoulli equation.

For a regular wave propagates in random water depth,

$$A(x,y,t) = \zeta_a sin(\omega t - kxcos(\theta) - kysin(\theta)) \tag{2.5.8}$$

the incident wave potential is Eq.2.5.9, Krogstad (2000)

$$\phi_w(x,y,z,t) = \frac{\zeta_a g}{\omega}\frac{cosh(k(z+h))}{cosh(kh)}cos(\omega t - kxcos(\theta) - kysin(\theta)) \tag{2.5.9}$$

then derive other wave quantities based on this incident wave potential,

$$\zeta = \zeta_a sin(\omega t - kxcos(\theta) - kysin(\theta)) \tag{2.5.10}$$

with dispersion relation, wave number k is

$$\omega^2 = gk \cdot tanh(hk) \tag{2.5.11}$$

then we get

$$U(x,y,z,t) = \frac{\partial \phi_w}{\partial x}(x,y,z,t) = \zeta_a \omega \frac{cosh(k(z+h))}{sinh(kh)} sin(\omega t - kxcos(\theta) - kysin(\theta))cos(\theta) \tag{2.5.12}$$

$$V(x,y,z,t) = \frac{\partial \phi_w}{\partial y}(x,y,z,t) = \zeta_a \omega \frac{cosh(k(z+h))}{sinh(kh)} sin(\omega t - kxcos(\theta) - kysin(\theta))sin(\theta) \tag{2.5.13}$$

$$W(x,y,z,t) = \frac{\partial \phi_w}{\partial z}(x,y,z,t) = \zeta_a \omega \frac{sinh(k(z+h))}{sinh(kh)} cos(\omega t - kxcos(\theta) - kysin(\theta)) \tag{2.5.14}$$

In general the pressure in the water is equal to the atmospheric pressure + the hydrostatic pressure (depth induced pressure) and a dynamic part due to the wave motion, from Bernoulli equation

$$\frac{p}{\rho} + \frac{\partial \phi_w}{\partial t} + \frac{1}{2}(U^2 + V^2 + W^2) + gz = \frac{P_{atm}}{\rho} \tag{2.5.15}$$

If the wave amplitude is small, neglect the term $(U^2+V^2)/2$, therefore obtain the following simple equation:

$$p(x,y,z,t) = -\rho \frac{\partial \phi_w}{\partial t}(x,y,z,t) - \rho g z + p_{atm} \tag{2.5.16}$$

The time varying part is usually called the dynamic pressure and equals to

$$p(x,y,z,t) = -\rho\frac{\partial\phi_w}{\partial t}(x,y,z,t) = \rho\zeta_a g\frac{cosh(k(z+h))}{cosh(kh)}sin(\omega t - kxcos(\theta) - kysin(\theta)) \tag{2.5.17}$$

For each of the derived wave quantities, the approach to calculate the relative phase on a random panel is same as the approach for calculating the relative phase of wave at random panel.

Chapter 3

Development of coupling tool

In this chapter, the method to couple SWASH and DIFFRAC is detailed introduced, this coupling procedure is based on MATLAB, start with reading SWASH outputs, follows with the interpolation and extrapolation to define the time domain wave quantities on ship panels, then with two methods to transfer the time domain SWASH output into frequency domain DIFFRAC input at each collocation point and waterline point, end up with DIFFRAC model setting and processing DIFFRAC outputs.

1. Reads outputs from SWASH model
2. Produce ship model in DIFFRAC (Panels and waterline points)
3. Define time wave quantities at panels
4. Transfer the interpolated time domain wave data into frequency domain wave data ('Full FFT' method and 'Partial Overlapping FFT' method)
5. Organize the DIFFRAC input files and run DIFFRAC calculation
6. Process DIFFRAC outputs

3.1 Read SWASH outputs

In SWASH model, the time dependent wave quantities (water velocity components, dynamic pressure, dynamic layers, etc) are located at each grid point of the wave mesh in horizontal plane (3D wave model) or the grid points along axis (2D wave model).

In vertical dimension, SWASH model is formed as several dynamic vertical layers, the thickness of each layer can be defined as percentage of the total water depth (eg. 5%, 15% and 80% as 3 layer distribution) or a certain water depth in meter (eg. 1m, 3m and 16m for 20m still water depth), and the thickness of each layer will redistribute as the oscillation of water surface, which is so-called dynamic vertical layer.

To get the required wave quantities as mentioned in Chapter 2, several wave quantities need to be selected as outputs from SWASH simulation:

- Time of wave modeling: in SWASH, user can specify both the duration and time step of simulation
- Coordinate values X_p and Y_p of each grid point;
- Thickness of each dynamic vertical layer;
- Water elevation at each surface grid point;
- Water particle velocities in horizontal $U(x, y, z, t)$ and $V(x, y, z, t)$ at each grid point and middle points of each dynamic layer;
- Vertical water particle velocity $W(x, y, z, t)$ at each grid point and interface (including surface and bottom) of each dynamic layer;
- Dynamic pressure from water density and water elevation;
- Non-hydrostatic pressure locates at each grid point and interface (including surface and bottom) of each dynamic layer, however, this data is normalized by water density in SWASH, so need to be back transformed into standard unit (kPa).

As shown in Fig.3.1, all the time domain wave data are located on each grid point of the wave mesh in horizontal plane, the structure in wave field can also be included.

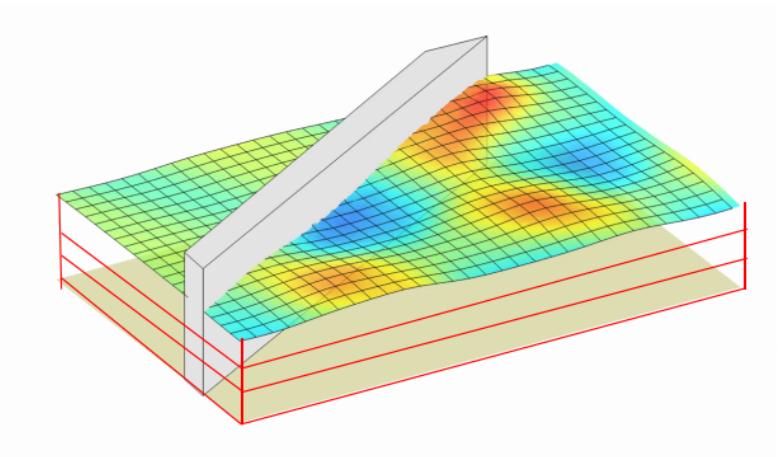

Figure 3.1: SWASH simulation at mooring site, with 3 vertical layers

3.2 Produce ship model in DIFFRAC

There is no restriction to the maximum number of independent moving bodies in DIFFRAC, in DIFFRAC version 2.62 or higher, to reduce or avoid the jump in integral equation from irregular frequency, a method using internal lid to close off the inner ship flow in the body, thereby restricting the non-uniqueness of the sources. For multi-body problem, the so-called damping lid between the floating bodies are also modeled as a part of the floating body. The location of center of gravity of and heading of the ship model should be given in DIFFRAC. Then the panel method is used to describe the geometry of the ship hull

and waterline, the 3D ship hull will be discretized to a number of square and triangle panels, if superposition of irregular frequencies is required then also the free surface part of the vessel or construction has to be approximated by panels.

3.3 Define the wave quantities at panels

In SWASH simulation, the ship information is not involved, the ship model will then be put into wave at mooring site (area of interest) by using the same coordinate system as in SWASH simulation with predefined offset in X and Y at CoG and a heading angle in DIFFRAC.

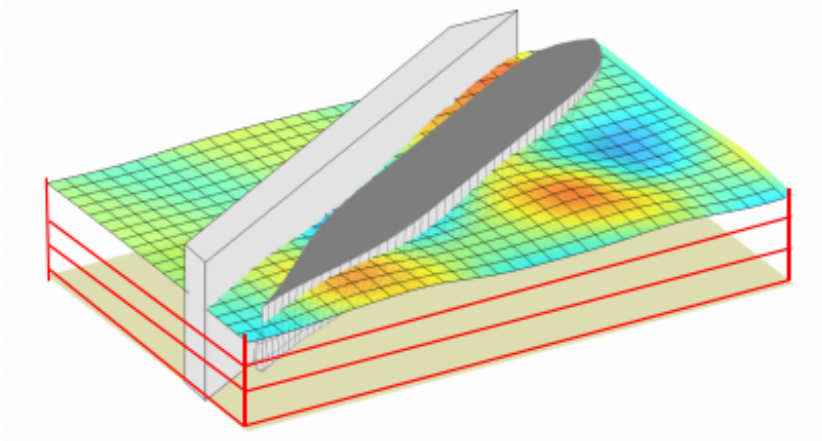

Figure 3.2: SWASH with ship at mooring site

The interpolation of SWASH model results to the collocation points (x_{hull}, y_{hull} and z_{hull}) is divided in three steps aiming to speed up the procedure.

First four wave model grid points surrounding each collocation point are identified, wave quantities at these grid points will be used to interpolate the wave data at the collocation point. The water elevation at water line points along the ship are also interpolated from the surrounding four grid points.

Large gradients of pressure and velocity components may occur along the vertical axis. The vertical interpolation of wave quantities is relatively trivial when a large number of vertical layers is considered in SWASH. However, especially when a few vertical layers are considered, information along vertical is scarce to define the quantities in the collocation point level (z_{hull}). The wave the vertical velocity are provided by SWASH at the edge of layers, so these results can be linearly interpolated along the vertical axis to determine the value at panel's level. However, not all the wave quantities locate at the layer surface and interface, Fig.3.3 shows the wave quantities layout (Box layout) in SWASH model outputs, horizontal velocity components and dynamic pressure are located in the middle of each layer, which means the surface panel with $z_{hull} = 0$ is beyond the range of interpolation.

Method to approximate the wave quantities at these surface panels is extrapolating the

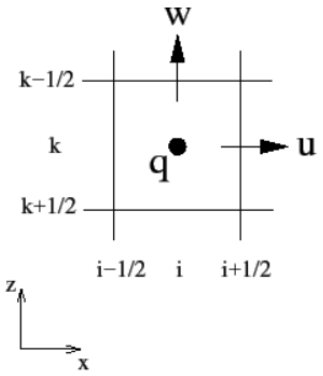

Figure 3.3: Applied arrangements of the unknowns in a staggered grid (u is horizontal velocity, w is the vertical velocity and q is the non hydrostatic pressure).

data from closest two points, therefore, two relatively thiner layers need to be put on the top of SWASH model:

$$q_{z=0} = \frac{q_{z=2} - q_{z=1}}{h_{z=2} - h_{z=1}} \times (-h_{z=1}) + q_{z=1} \tag{3.3.1}$$

where:

- q is the wave quantities (horizontal velocity components and dynamic pressure);
- h is water depth at center of the cell in vertical dimension;
- index 1 and 2 corresponding with the first and second vertical layer.

3.4 Transform interpolated time domain wave quantities into frequency domain

The interpolated and extrapolated time domain wave quantities will be transfered to frequency domain wave data by using FFT. As introduced in previous sections, the biggest challenge is the spectral leakage. Two method will be applied in coupling procedure to eliminate (reduce) the spectral leakage and achieve a correct DIFFRAC calculation.

3.4.1 'Full FFT' method and 'Partial overlapping FFT' method

Full FFT method

Although spectral leakage leads oscillation in both amplitude and phase spectrum, however all the information still remain in the spectrum after applying FFT to the whole

time series, which means by applying IFFT with the whole response spectrum, we can reproduce the correct response time series without losing information. This character helps to achieve the realization of so-called 'Full FFT method', the wave quantities spectrum derived from FFT method is double- side spectrum, both of them are the mirror of the other part (conjugate part), therefore the one locates at the positive frequency domain is organized as 'User Defined Wave' inputs to execute DIFFRAC calculation, during the DIFFRAC calculation, the whole DIFFRAC system is regard as a kind of 'filter', the filtered outputs are the response spectrum at all the exciting frequency (all frequencies in spectrum), since the input are the whole wave quantities spectrum, therefore no information lost in both excitation side and response side, the 'double-side' response spectra can be produced after gluing the original response spectra with their associated conjugate part, with applying IFFT of these double-side response spectra, the response time series can be obtained. With the mentioned partial overlapping window method in this chapter, we can also get smooth averaged response spectra. Since all the frequency components in the frequency domain need to be taken into account in DIFFRAC calculation, therefore, this method is relatively time consuming.

Partial overlapping FFT method

With respect to the 'Full FFT method', a much quicker 'Partial overlapping FFT' method can be achieved by combining partial overlapping window method (for amplitude spectrum correction) and phase correction method (for relative phases spectrum calculation). The biggest challenge of this approach is the method to define the wave propagation direction, which will be applied in phase correction.

For unidirectional wave, such as regular wave and long-crested spectral wave, since the wave direction is uniform and does not change during wave propagation, the main wave direction can be applied for all the wave components. However, for short-crested wave, the directional information should be involved in the wave spectrum, in short-crested wave group, each wave component has its own wave direction (Krogstad, 2000), the introduced 'maximum entropy' method from Lygre and Krogstad (1986) developed in Royal HaskningDHV can derive the 3D wave spectrum (including the wave directions) at specified position in SWASH model by using the information (water elevation, horizontal velocity components in x and y) at this location, for unidirectional wave, the wave direction from this method has been proved stable at any locations in SWASH domain. However, for short-crested wave, the wave direction is only known at the boundary (where user can define the input of SWASH model), therefore potential uncertainties still exist in this method and may influence the whole coupling procedure. The 3D spectrum from this method, with SWASH outputs at a random location in short-crested wave model is shown in the Fig.3.4 and 3.5.

As can be seen in the Fig.3.5, the peak direction is unique for each wave component and will be applied to represent the main wave direction θ_ω of this wave components A_ω, with wave number k_ω and coordinate all the panels and CoG of ship, all the information is required in the phase correction of short-crested spectral wave follows Eq.(2.5.9) is offered. With both the correction of amplitude and phase at interesting frequencies, the interesting response spectral zone can be calculated independently. However, the shortcoming of this method is that only partial information involved in DIFFRAC calculation, which

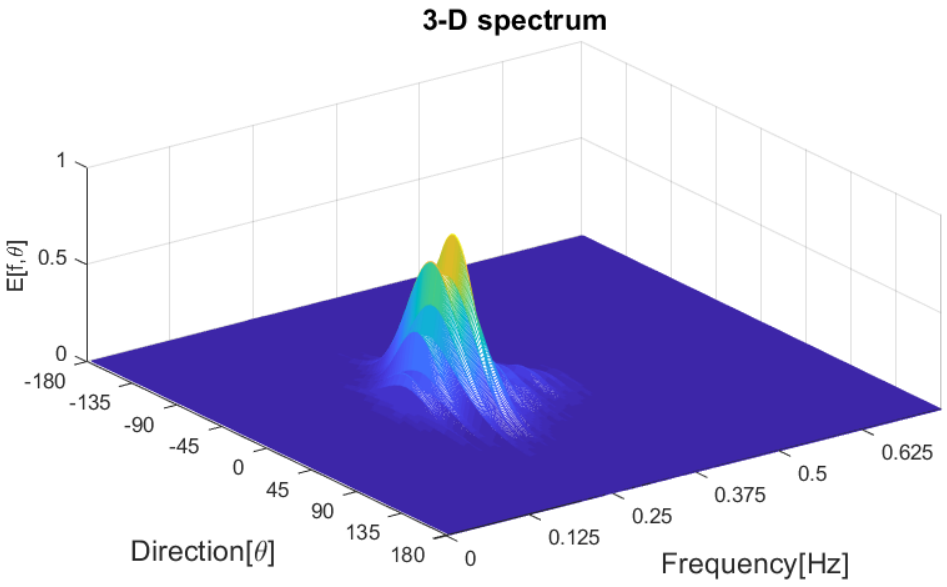

Figure 3.4: 3D wave spectrum at random location in SWASH short-crested wave model

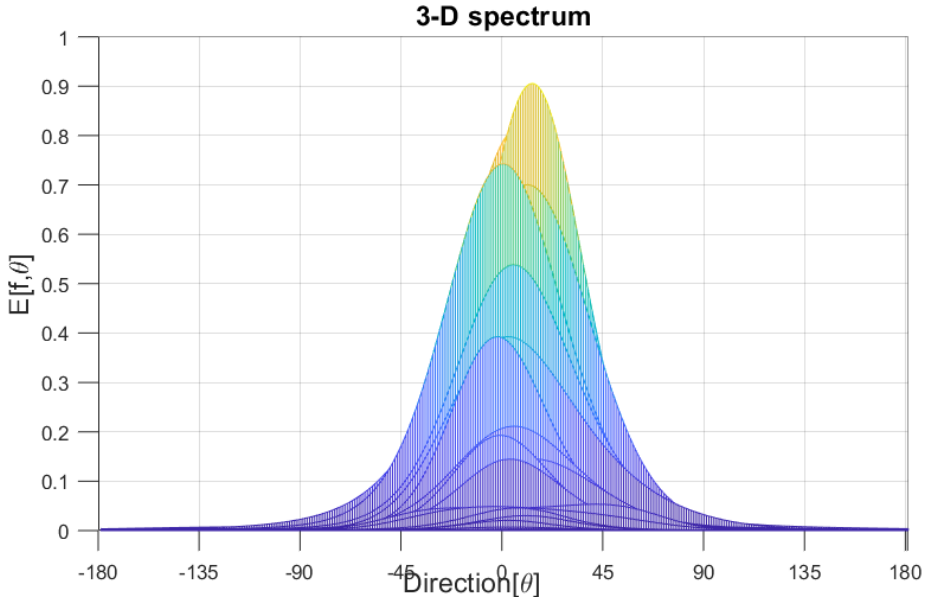

Figure 3.5: Direction distribution of wave components in short-crested SWASH wave model

means impossible to reproduce the whole response time series through IFFT with partial frequency domain information.

Since the 'max entropy' is only verified at the boundary of SWASH model (where user know the directional information), as reported from verification against the results from MIKE 21BW, potential uncertainties still within this method.

The time domain wave quantities can be transfer to frequency domain wave data with sufficiently accurate amplitude spectrum and correct relative phase spectrum by using wither 'Full FFT' and 'Partial overlapping FFT' method mentioned in previous chapters.

When apply 'Full FFT method' method, the whole frequency domain of excitation (input wave data) will be taken into calculation, the length of frequency domain (0 to $F_s/2$ Hz) is depend on the sampling frequency F_s in SWASH simulation. Then both the real and imaginary parts of complex number are obtained.

When apply 'Partial overlapping FFT' method, only the interesting parts in excitation side will be taken into account, these parts can be the frequency range around the peak of wave spectrum and the peak of ship response function. Then both the real and imaginary parts of complex number at interesting frequencies can be obtained.

3.5 Organize the DIFFRAC input file

When 'User Defined Wave' option is invoked in DIFFRAC, a file userdefincwave.dat is expected in the working directory. It contains for all frequencies and wave directions for the water velocity in x, y and z directions and the dynamic pressure in all collocation points. Each line in the file should therefore contains eight numbers, as both the real and imaginary part of these quantities are prescribed. It also contains the incident water elevation at the waterline points. Each line in the file should therefore contain two numbers. i.e. the real and imaginary parts.

- The incident water particle velocity in X,Y and Z directions (U, V, W) and dynamic water pressure (P) in all collocation points each line in the file should contain 8 numbers:
  1. Real part U
  2. Imaginary part U
  3. Real part V
  4. Imaginary part V
  5. Real part W
  6. Imaginary part W
  7. Real part P
  8. Imaginary part P
- The incident water elevation (ζ) in the waterline points. Each line in the file should contain 2 numbers:

1. Real part ζ
2. Imaginary part ζ

User should keep the number of ω, $\Delta\omega$ and the ω_{start} identical for both DIFFRAC model setting and in file userdefinecwave.dat.

Chapter 4

Model verification

A general assessment of the applicability of the new work flow (SWASH - Coupling tool - DIFFRAC) for simple regular wave cases and irregular wave cases will be covered in this chapter. The test involves regular wave with different wave periods and irregular wave follows JONSWAP wave spectrum with different peak wave period. The simulations are perform in 2D mode with flat bottom. The coupling tool from the last chapter with 'Partial overlapping FFT' method is used to convert SWASH model outputs into the input files required for DIFFRAC calculation, the computed forces and moments are explored in order to verify the consistency and assess the accuracy of the coupling, highlighting possible limits of application of the computational approach combining SWASH, coupling tool and DIFFRAC model.

4.1 Model preparation

For all the verification cases in this chapter (both regular and spectral wave), 2D plane waves (in x - z plane) will be simulated in SWASH, without considering bottom friction, the origin of 2D SWASH model is located at the left end, with domain length 2002m, the sponge layer is set with 50m length at end of the domain to absorb the coming waves, then this 2D model is copied and pasted in Y dimension for 3 times to get the 3D SWASH model with 400m domain length in Y. The required computational effort in SWASH simulation can be estimated by calculating the number of computation points in time and space. This number increases linearly with the number of vertical layers and is inversely related to the grid spacing and time steps. The computational time step is proportional to the grid spacing, since it is adjusted during the simulation to keep the Courant number sufficiently low (0.3 and 0.5 as lower and upper limits respectively, for a definition of the Courant number and CFL stability condition in SWASH, see Appendix A).

Two sets of numerical schemes from Dobrochinski (2014) were selected for the discretization of advection terms in the momentum equations. The numerical schemes associated to the different terms are presented in Table.4.1. More details about these choices are provided in Appendix A and The SWASH Team (2017).

Table 4.1: Discretization of advection terms in the momentum equations. BDF: 2^{nd} order Backward Difference Scheme; CDS: 2^{nd} order Central Differences Scheme; UPW: 1^{st} order Upwind Scheme.

Term		Default set	Adapted set
$u\frac{\delta u}{\delta v}$	(H. Adv. of H-momentum)	BDF	BDF
$w\frac{\delta u}{\delta z}$	(V. Adv. of H-momentum)	UPW	CDS
$u\frac{\delta w}{\delta x}$	(H. Adv. of V-momentum)	Ignored	BDF
$w\frac{\delta w}{\delta z}$	(V. Adv. of V-momentum)	Ignored	UPW

192 2D SWASH simulation of regular wave executed in by Dobrochinski (2014), with concluding three different kinds of errors:

- Celerity (dispersion) error relative to linear wave theory;

  For general applications of SWASH simulation of wave penetration into harbour the observed errors are low (magnitude of this dispersion error is around 1%, error lager than 1% only found when grid resolution lower than 10 grids per wave length) and generally not relevant.

- Wave amplitude error near the incoming boundary

  This error quantifies a relatively abrupt drop in wave amplitude in the vicinity of the incoming boundary ($0 < x < 1\lambda$). The amplitude errors in the vicinity of the incoming boundary are more prominent for larger kd numbers (say $kd > 3$), for which the vertical profile of wave quantities is more curved. This unwanted behaviour under high kd condition is likely caused by inaccuracies in the imposed velocities at the boundary, making necessary the use of more vertical layers to proper represent the vertical profile. The maximum relative amplitude error is in the order of 15% for $kd = 5$, $H = 1$m and two layers. This deviation is considerable and should be accounted whenever wave conditions with large associated kd numbers are relevant ($kd > 3$). However, the area of interest in SWASH model is always far away from the wave makers side, therefore, this kind of errors can be neglected at the position of interest.

- Wave amplitude error per wave length along the domain

  The third error considered in this analysis is the decay in wave amplitude, the simulations do not consider dissipation due to bottom friction effects, so ideally the wave height would remain constant along the domain, at a selected area, which is far from the force boundary, after wave fully developed, this amplitude decay clearly shows up along the domain. Since a sponge layer has been placed at the end of domain to prevent wave reflection from the outgoing boundary, therefore, any difference between SWSAH outputs and inputs (model setting) with the analyzed region is due to numerical effects.

  The magnitude of this error is influenced by all variable considered in the tests. For small linear waves the gradual decay of wave height due to numerical diffusion is negligible, the vertical and horizontal grid resolution have relatively small influence on this error. For the test with wave height of $1m$ ($H/d = 0.05$) and horizontal grid resolution of 20 points per wave length, errors can be in the order of 1.5%. Considering the same wave condition an settings but only 10 grid points per wave length, the errors are up to 2.5% per wave length.

The amplitude errors per wave length are not linearly related to the wave height, so increased relative errors are expected for wave heights larger than *1m*. These deviations are specially relevant for waves with high kd number, not only because the error is larger for those waves, but also due to the cumulative effect along the simulation domain. Because those waves are relatively shorter, more 'wave lengths' are traveled thought a given domain.

It must be noted that generally kd reduces as the wave propagates towards the shore and the water depth decreases, thus the relative error per wave length is also expected to diminish. Furthermore, $kd > 3$ is already rather large for practical applications involving wave penetration in harbours.

In this chapter the ship model remains identical for all verification cases. The ship is a $125000m^3$ LNG carrier. The dimensions of the ship are given in Table.4.2 and the mesh describing the hull in Fig.4.1. The ship CoG locates at (926m, 200m), which is far from wave maker side and sponge layer side and with zero heading angle, therefore experiences a bow wave, as shown in Fig.4.2.

Table 4.2: Dimension of the $125000m^3$ LNG carrier.

Designation	Symbol	Unit	Magnitude
Length between perpendiculars	L_{pp}	m	273
Breadth	B	m	42
Draft	d	m	11.5
Displacement	∇	m^3	98740
Center of gravity above keel	kg	m	13.7
Transverse radius of gyration	k_{xx}	m	14.7
Longitudinal radius of gyration	k_{yy}	m	65.52

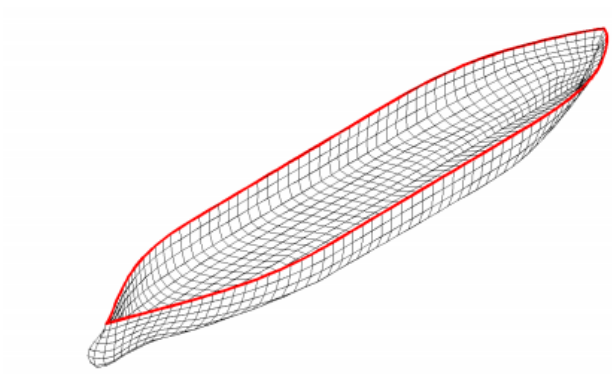

Figure 4.1: LNG Carrier with 1426 panels and 144 water line points.

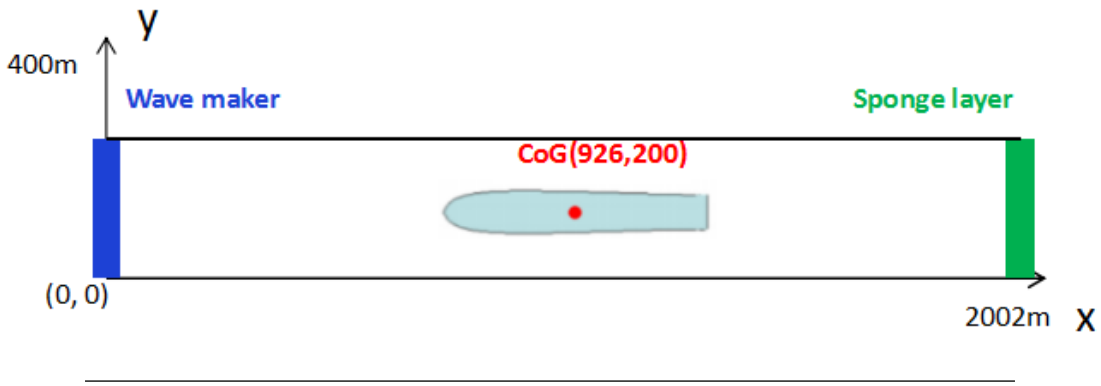

Figure 4.2: SWASH domain and ship position

4.2 Verification of 2D regular wave case

4.2.1 SWASH 2D regular wave simulation

Waves are dispersive when traveling in deep and intermediate waters, meaning that the phase speed and wave length are a function of the wave period. The kd number (with k the wave number and d the water depth) is a measure of the water depth relative to the wave length. A lower kd value indicates wave propagate in a shallower water conditions. The vertical variations of the wave quantities, such as wave pressure and orbital velocity amplitudes, is directly related to the kd number, this vertical distribution more homogeneous for lower kd's. Further more, this is an important parameter in short wave modelling. Models like SWASH and Boussinesq models are generally less accurate in the simulation of wave conditions with large kd numbers (deep water case).

It is often convenient to have an optimized model with simulations requiring feasible computation times. On the other hand, model results should be sufficiently accurate for the given application. Therefore, verification of SWASH outputs is always necessary before further procession. Generally, wave case with kd value lower than 3 is sufficient for engineering application in near shore area, therefore, in verification part wave with kd values 1.0, 2.1 are investigated, with wave period 10s and 6.28s and 20m water depth.

Because in practice the same computational grid is used to simulate longer and shorter waves, therefore, the required computation time will be dictated by how well the shorter wave of interests is represented on the grid (In The SWASH Team (2017), the recommended value is 100 grids per peak wave length, however, the performance of relatively rough grid resolution will be investigated in this chapter). The number of vertical layers will also be relevant since an increment in the number of vertical layers leads to a proportional increase in the number of computational points.

The wave parameters and basic setting in SWASH are summarized below:

- Wave period(2): 10, 6.28s;
- Wave amplitude(1): 0.1m;
- Water depth(1): 20m;

- Direction of wave propagation(1): 0° (bow wave);
- Number of vertical layers(6): 3, 4, 5, 6, 7, 8;
- Numerical schemes in momentum equation: Default set and Adapted set.

The domain length is identical for both wave cases, wave length are about 121 m and and 61 m for $T = 10s$ and $T = 6.28s$ respectively, therefore with grid resolution (Δx) 6m and 3.1m ($\lambda/20$) in SWASH simulations, to eliminate the influence from grid resolution for the wave model with the same water depth and number of layers.

Layer thickness distribution for cases with different number of layers shown in Tab.4.3, every time a top layer with constant 5% (when layer number over 4) of total water depth is added at top to extrapolate wave quantities at water surface to minimize the influence from stagger points distribution.

Table 4.3: Layer thickness distribution

Case	Percentage (%)
3 layers	5, 10, 85
4 layers	5, 5, 30, 60
5 layers	5, 5, 20, 20, 50
6 layers	5, 5, 10, 20, 20, 45
7 layers	5, 5, 10, 10, 20, 20, 30
8 layers	5, 5, 10, 10, 10, 20, 20, 20

4.2.2 Verification of wave quantities

Beside the output water elevation, other wave quantities have to be verified before interpolating them on the collocation points. The wave quantities at 2 random points (one in front of ship with x = 740m and one behind of the ship with x = 1112m from force boundary) are verified before interpolating the wave data on ship panels. the results are shown in Tables.4.4 and 4.5.

Table 4.4: Verification of SWASH outputs on both points of wave case kd = 2.1 and 3 vertical layers

Item	Depth	Theory	Point 1	Point 2	Unit
U	3m	0.037	0.037	0.037	m/s
V	3m	0	0	0	m/s
W	3m	0.036	0.036	0.036	m/s

Table 4.5: Verification of SWASH outputs on both points of wave with kd = 1 and 3 vertical layers

Item	Depth	Theory	Point 1	Point 2	Unit
U	3m	0.028	0.028	0.028	m/s
V	3m	0	0	0	m/s
W	3m	0.026	0.026	0.026	m/s

For both wave cases, the SWASH simulation fits quite well with data from theoretical calculation, therefore the wave quantities in between these two points can be considered

as well simulated by SWASH and will be used to interpolate and extrapolate the wave quantities on ship panels.

4.2.3 Verification of SWASH interpolated wave quantities

After applying 'Partial Overlapping FFT', the interpolated wave data are transfered to frequency domain. Since regular wave only has one wave frequency, therefore only one peak at wave frequency in wave spectra, the same for other wave quantities for regular wave, when wave time series is sufficient long, with 'Over lapping window' to reduce the effect of spectral leakage, the energy spreading is acceptable. On the other side, wave quantities from theoretical calculation for the same wave case is performed on each panel as bench mark to verify the SWASH interpolated data.

Algorithm 1

for $i = 1 : 1426$(Number of panels) **do**
  FFT(U) & record the peak in spectra
  FFT(V) & record the peak in spectra
  FFT(W) & record the peak in spectra
  FFT(P) & record the peak in spectra
end for
for $k = 1 : 144$(Number of Waterline points) **do**
  FFT(ζ_a) & record the peak in spectra
end for

Algorithm 2

for $i = 1 : 1426$(Number of panels) **do**
  Calculate U at $panel_i$ with potential theory
  Calculate V at $panel_i$ with potential theory
  Calculate W at $panel_i$ with potential theory
  Calculate P at $panel_i$ with potential theory
end for
for $k = 1 : 144$(Number of Waterline points) **do**
  Calculate ζ at $Waterline_i$ with potential theory
end for

Based on frequency domain potential theory, the magnitude of wave quantities are closely related to the depth, therefore the depth distribution of all the panels on the ship hull is given in Fig.4.3

Here, for a detailed illustration, the wave quantities on each panel and waterline point of case T = 10s and 5 vertical layers are verified against theoretical calculation. The verifications on all panels and waterline points are shown in Fig.4.4 and Fig.4.5.

Generally the magnitude of interpolated data fits well with theoretical calculation, the mean deviation averaged over all panels is 1.0%, 1.6%, 0% and 0.3% respectively for dynamic pressure , particle velocity U, V and W, since the wave model is a fake 3D wave

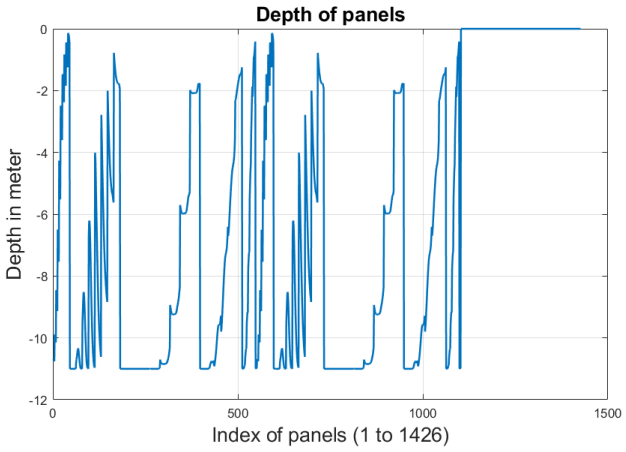

Figure 4.3: Depth distribution of all panels

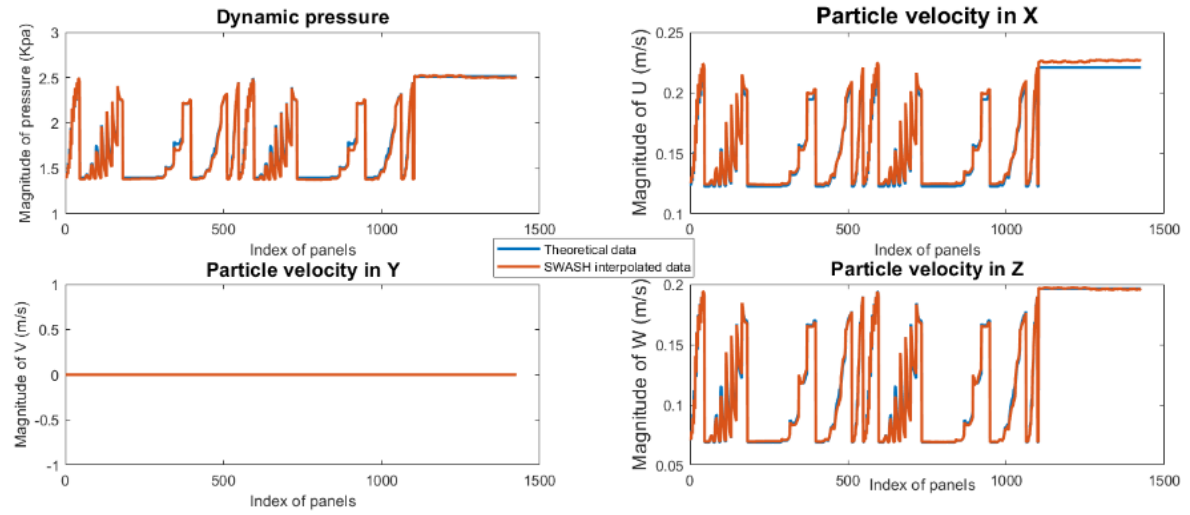

Figure 4.4: Comparison of magnitude of wave quantities on each panel.

model from 2D wave model, thus the velocity components in Y are 0 at all panels, the shape of magnitude of the rest wave quantities are indeed follows the same shape as in Fig.4.3, however some differences clearly show up.

1. The oscillation of SWASH interpolated data

   This oscillation shows up in all the wave quantities, which comes from the sampling error of SWASH model and coupling procedure. In SWASH model, the sampling rate is predefined for the whole simulation, finite discrete time series recoded to represent the real infinite time series, this discrete time series can not capture all the features of irregular wave and even regular wave, therefore the magnitude at different position has slightly difference (oscillation), on the other hand, due to so-called spectral leakage, discrete Fourier Transform can not perfectly transfer the discrete time series into spectra, these two mentioned problems are impossible to be fully solved in practice.

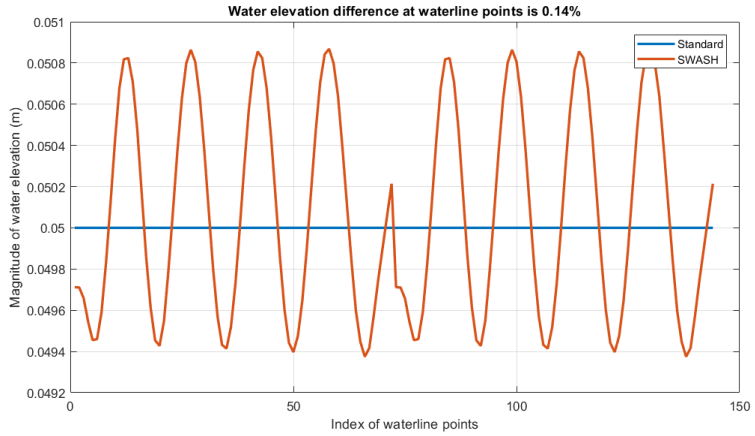

Figure 4.5: Comparison of magnitude of water elevation on each water line point.

This oscillation clearly shows up in Fig.4.5, since all the waterline points have the same z coordinate (z = 0), the frequency domain water elevation at all waterline points have the same magnitude 0.05m, the averaged interpolated data oscillating around this standard value and with 0.14% difference, which can be neglected.

2. Magnitude deviation at the tail of plot

   Beside the oscillation, all surface panels with zero depth are at the tail of the panel series, therefore this magnitude deviation at the tail of U, V and P due to the approximation from extrapolation. From overall perspective, the oscillation does not greatly contribute to the total deviation (averaged deviation), this will be proved again for irregular wave case and with more complicated wave case.

4.2.4 Verification of DIFFRAC results

The frequency domain wave quantities from previous section together with the ship model will be organized as DIFFRAC 'User Defined Wave' inputs. The resulting force and moment for both wave cases will be verified in this section. The different contributions to the total forces/moments are discussed separately (ie. First-order force and moments (Froude-Krylov forces, diffraction forces) and mean second-order drift forces and moments), and the total force and moments. After investigating wave model with vertical layer distribution as in Table.4.3, the influence of different layer thickness will also be discussed, more emphasize on the influence of top layer, which is closely related to data extrapolation on surface panels, all the SWASH simulations are with adapted set numerical scheme.

The forces and moments acting on the floating body are small when the waves are very short relative to the body size. A proper representation of those short waves along the hull of the ship would require a large number of panels, increasing considerably computation effort but not necessarily improving the accuracy of overall results, since the associated transfer functions are negligible, therefore, these short period wave components are not the interesting parts mooring study.

First order forces and moments

In this section, the first order forces and moments computed from both approaches (mentioned in last section, approach.1 (DIFFRAC + SWASH interpolated data) and approach.2 (DIFFRAC + theoretical data) with adapted discretization set. An overall evaluation of the performance of both default set and adapted set presented in Appendix C.

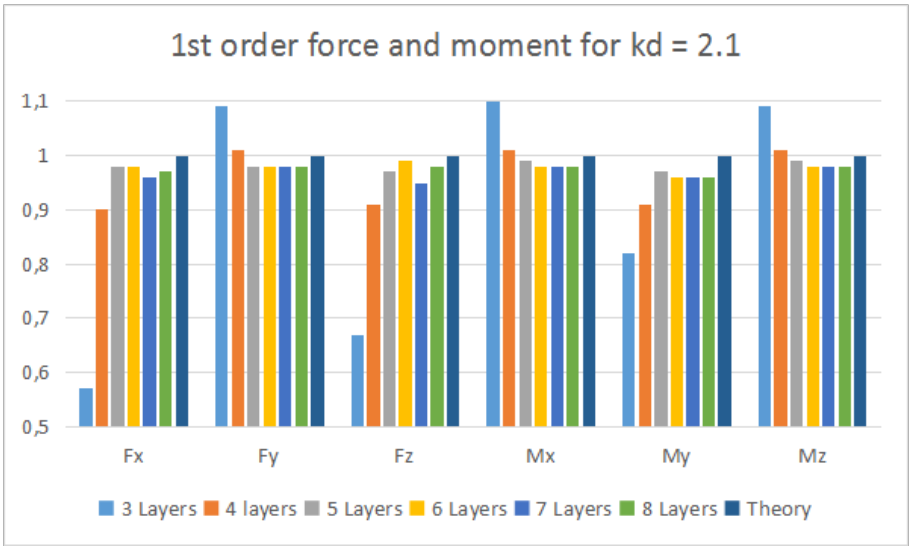

Figure 4.6: 1st order normalized force and moment for wave case kd =2.1 (Adapted set)

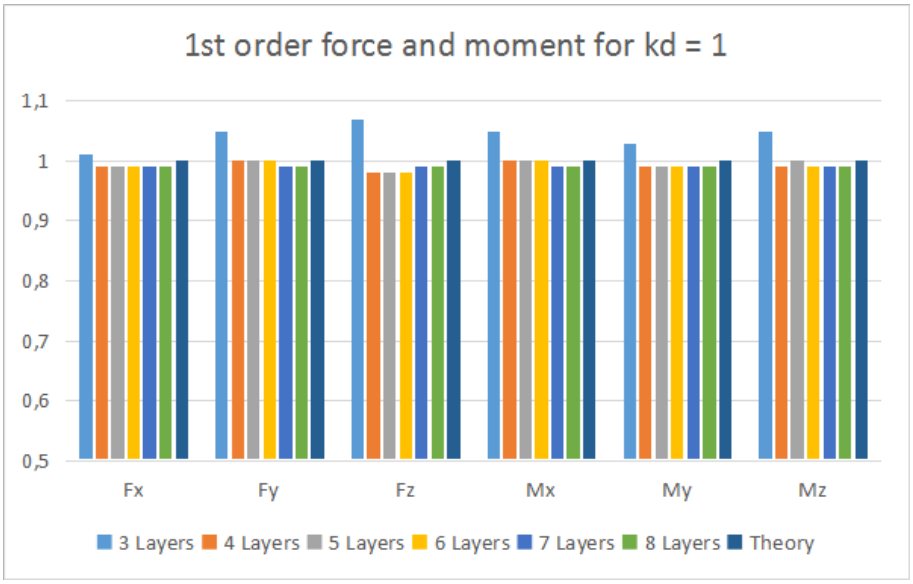

Figure 4.7: 1st order normalized force and moment for wave case kd = 1 (Adapted set)

Data for all the cases are normalized by results from theoretical calculation (approach.2) to show differences in a decent way, lager deviations among different SWASH models can be seen in wave case with higher kd value, simulated forces and moments start converge when the number of vertical layer increase, for wave case with larger kd value ($kd = 2.1$),

a significantly convergence can be seen when number of vertical layers increase from 3 to 4, then follows with a less significant convergent tendency when continuously adding more layers, for both wave case the convergent rate reduces crucially after increasing vertical number over 4, so we can say the resulted force and moments almost converge at number = 4, and fully converge at number = 7.

Second order forces and moments

For regular wave case, first-order wave forces acting on a ship are oscillatory with the same frequency as the prime regular wave, in mooring studies those forces will be relevant due to the excitation of the system (ship and mooring system) at resonant frequencies, potentially amplifying the resulting loads and motions. However the second order mean drift force is small compared to first-order forces, from perspective of the magnitude of both forces and moments, the contribution of second order components are less than 2% to the total wave forces and moments as shown in both Table.4.6 and 4.7.

Meanwhile, the 2*nd* order force and moments from approach.1 is unreliable, first of all, only the mean 2*nd* order drift force and moments can be calculated from DIFFRAC, furthermore, these 2*nd* order components are significantly influenced by the errors induced from extrapolation in coupling procedure (the data on surface panels), and produce incorrect mean 2*nd* order force and moments therefore will not be discussed in this section. However, since these second order components contribute much less to total force and moment than first order components, the influence can be neglected.

Table 4.6: Ratio of 2nd order components over 1st order components in percentage [%] (kd = 1)

	F_x	F_y	F_z	M_x	M_y	M_z
3 layers	1.4	0.3	1.9	0.5	1.1	0.5
4 layers	1.9	0	0,7	0.5	0.9	0.5
5 layers	1.5	0.4	1.9	0.5	1.2	0.5
6 layers	1.5	0.4	1.9	1.2	0.5	0.5
7 layers	1.5	0.4	1.9	1.2	0.5	0.5
8 layers	1.5	0.4	1.9	1.2	0.5	0.5

Table 4.7: Ratio of 2nd order components over 1st order components in percentage [%] (kd = 2.1)

	F_x	F_y	F_z	M_x	M_y	M_z
3 layers	2	1.5	0.7	0.6	0.9	0.2
4 layers	1.8	1.6	0.6	0.6	1.1	0.2
5 layers	1.7	1.6	0.5	0.7	1.1	0.2
6 layers	1.7	1.6	0.5	0.8	1	0.2
7 layers	1.7	1.6	0.5	0.7	1.1	0.2
8 layers	1.7	1.6	0.5	0.8	1.1	0.2

Total forces and moments

As conclusion of the verification of 2D regular wave case, the total forces and moments from both approaches need to be investigated.

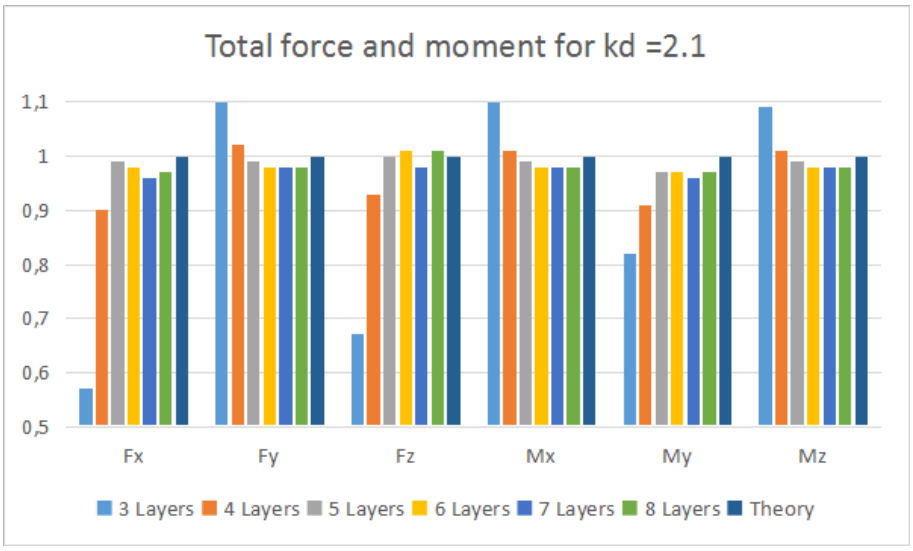

Figure 4.8: Total normalized force and moment for wave case kd = 2.1(Adapted set)

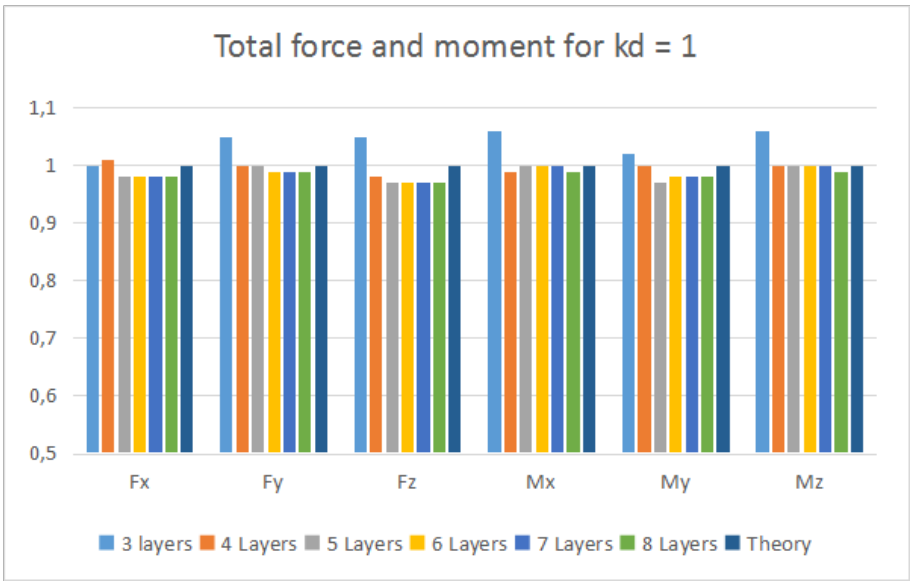

Figure 4.9: Total normalized force and moment for wave case kd = 1(Adapted set)

From overall perspective, wave case with larger kd number (wave propagate in intermediate and deep water) always need more vertical layers in SWASH simulation than in wave case with smaller kd value, therefore a more significant convergence shows up when number of layers increase in wave case with higher kd value. For both wave cases, resulting force and moment almost converge at layer number = 6, the difference among resulting forces and moments with 5, 6, 7, 8 vertical layers are within 3%. Since computational effort in SWASH simulation is linearly dependent on number of vertical layers, for engineering application, both SWASH simulation with 4 and 5 vertical layers and adapted discretization set are recommended, this conclusion need to be further investigated with irregular wave model.

4.2.5 Verification of top layers influence

The influence of vertical layers on DIFFRAC calculations has already been investigated in last section, to minimize the errors induced during coupling procedure, from Eq.(3.3.1), the thickness of top layer should be sufficiently small, in this section the influence of top layer thickness to the whole coupling procedure will be investigated. Beside the top layer, comparing the Table.4.8 and Table.4.3, for both wave cases a SWASH model reference case from Table.4.3 is appended. Therefore the influence of layer thickness for layers, which are located beneath the top layer can also be investigated.

Table 4.8: Layer thickness distribution to investigate the influence of top layer thickness

Case	Percentage (%)
4 layers	1, 5, 14, 80
	2, 5, 13, 80
	3, 5, 12, 80
	4, 5, 11, 80
	5, 5, 30, 60
5 layers	1, 5, 10, 14, 70
	2, 5, 10, 13, 70
	3, 5, 10, 12, 70
	4, 5, 10, 11, 70
	5, 5, 20, 20, 50

The layer thickness distribution is shown in Table.4.8. With the same approach.1 and approach.2 applied in last section, the resulted force and moment for each case with different top layer thickness will be verified against the result from theoretical calculation, SWASH model setting is as follows

- Wave period(1): 10s;
- Wave amplitude(1): 0.1m;
- Water depth(1): 20m;
- Direction of wave propagation(1): 0°(bow wave);
- Number of vertical layers(2): 4, 5;
- Thickness of first layer(5): 1%, 2%, 3%, 4% and 5%;

- Numerical schemes in momentum equation: Adapted set.

The result force and moment of different cases are shown in Fig.4.10 in and Fig.4.11

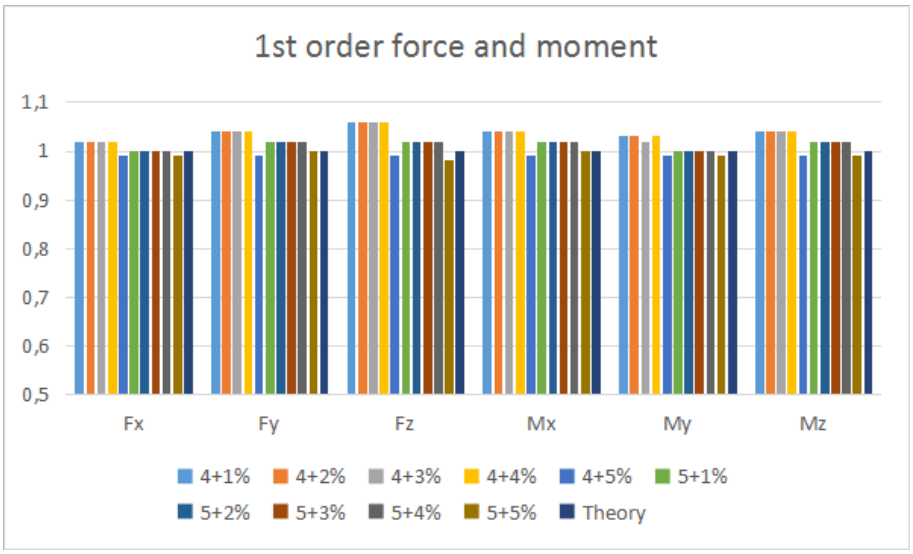

Figure 4.10: 1st order normalized force and moment of cases with different top layer thickness

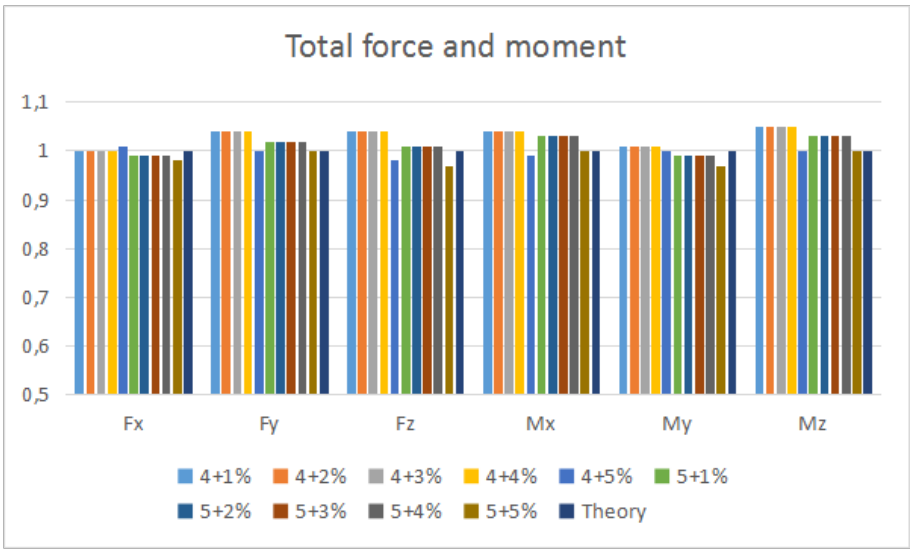

Figure 4.11: Total normalized force and moment of cases with different top layer thickness

From Fig.4.10 and Fig.4.11 the difference of top layer thickness almost has no influence on the resulted force and moment, the reason of this result has already been mentioned, since the contribution to force and moment from surface panels is quite small with respect

to the panels below water surface, therefore the difference among top layer with 1% , 2%, 3% and 4% thickness are negligible for both cases with 4 and 5 vertical layers.

Different vertical layer distribution does influence the overall result, a rough layer distribution (lets say the layer thickness difference among different layers is lager) produce an overestimated result than result from a smooth layer distribution (lets say the layer thickness difference among different layers is smaller), meanwhile lager derivation among results from rough layer distribution than smooth layer distribution is obvious.

Comparing the resulted force and moment from SWASH model with default model set, the adapted set of discretization of advection terms gives better SWASH model and therefore better performance of the whole coupling procedure. Therefore, for verification of irregular wave case, SWASH model with 4 (5%; 5%; 30%; 60%) and 5 (5%; 5%; 20%; 20%; 50%) vertical layers and adapted set of discretization of advection terms will be applied in verification of 2D spectral wave.

4.3 Verification of 2D irregular long-crested wave

4.3.1 SWASH 2D irregular long-crested wave simulation

In this section, more complicated irregular wave conditions are considered, irregular seas result from the superposition of infinite number of primary wave components with different wave height, phase and different wave frequency, therefore different wave number and wave period, by using Fourier Transform, all the wave components in irregular wave can be decoupled into wave components in wave spectra, with wave amplitude and phase at corresponding wave frequency, then each wave component can be regarded as a single regular wave.

In this section, the irregular wave simulated in SWASH follows a JONSWAP wave spectrum. 'Partial overlapping FFT' method is applied to verify the coupling results directly against the results from potential theory in frequency domain in a efficient way.

The model setting of SWASH simulation is in Tab.4.9, similarly to the test with regular wave, the computational domain is a 2D domain, and then copy all the wave data along the third dimension to produce the 3D irregular long-crested wave model, considering a flat bottom with 20m below still water level, as recommendation from last section, 4 and 5 layers through the vertical dimension, the ship model and location remains identical as in the last section, as shown in Fig.4.2.

Table 4.9: SWASH simulation setting for irregular wave case

Parameters	#1	#2
$H_s(m)$	1	1
$T_p(s)$	15	20
γ	3.3	3.3
Water depth(m)	20	20
f_{cutoff}	$3f_{peak}$	$3f_{peak}$
$F_s(Hz)$	2	2
Time length	2hrs	2hrs
Window length	512	512
length of Window overlapping	500	500
Number of windows	1056	1056

where:

- H_s: significant wave height
- T_p: Peak wave period
- γ: peak enhance parameter

A standard JONSWAP spectrum with given parameters is produced by MATLAB. To verify with the result spectrum from SWASH simulation, this standard spectrum should be processed and transferred to an amplitude density spectrum by using equation (2.5.3).

With the overlapping time window method mentioned in Chapter 2, time window length for each step FFT is 512, with 500 points overlapping with neighbour time window,

therefore, a $2hrs$ SWASH simulation with sampling frequency 2Hz (record wave double times per second) can produce 1056 number of samples, which is sufficient to let averaged spectrum convergence.

The resulted wave amplitude density spectrum from SWASH simulation with both 4 and 5 vertical layers at point 1 and point 2 are shown in Fig.4.12 and 4.13, for both wave cases the overall amplitude density spectrum from SWASH simulation fits quite well with amplitude density spectra from JONSWAP spectra around peak frequency.

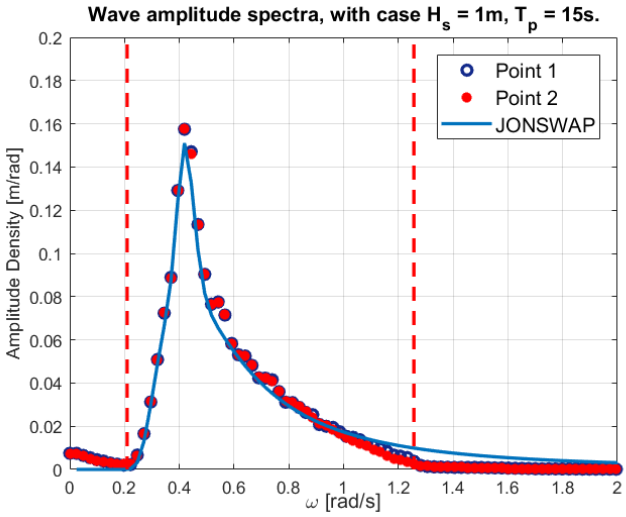

Figure 4.12: Amplitude density spectrum at both recording points for case T = 15s with 4 layers

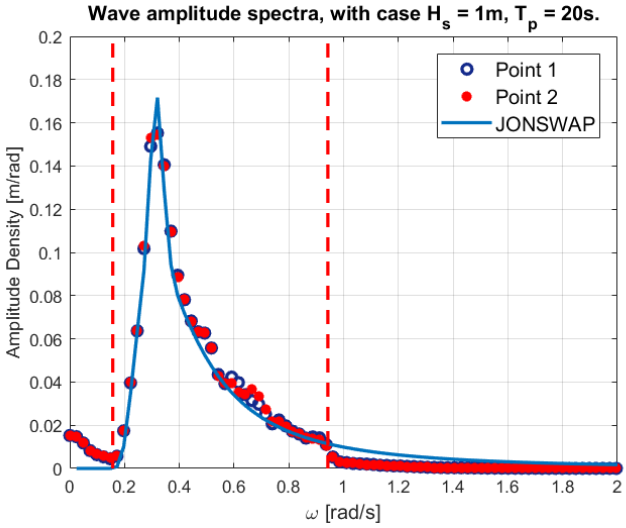

Figure 4.13: Amplitude density spectrum at both recording points for case T = 20s with 4 layers

4.3.2 Verification of DIFFRAC results

Algorithm 3

for $i = 1 : 1426$(Number of panels) **do**
  FFT(U) & record all spectral components in between cut-off frequency & set initial phase to zero
  FFT(V) & record all spectral components in between cut-off frequency & set initial phase to zero
  FFT(W) & record all spectral components in between cut-off frequency & set initial phase to zero
  FFT(P) & record all spectral components in between cut-off frequency & set initial phase to zero
end for
for $k = 1 : 144$(Number of Waterline points) **do**
  FFT(ζ) & record all spectral components in between cut-off frequency & set initial phase to zero
end for

Algorithm 4

for $i = 1 : 1426$(Number of panels) **do**
  Calculate U with potential theory with random phase for all the components in between cut-off frequencies
  Calculate V with potential theory with random phase for all the components in between cut-off frequencies
  Calculate W with potential theory with random phase for all the components in between cut-off frequencies
  Calculate P with potential theory with random phase for all the components in between cut-off frequencies
end for
for $k = 1 : 144$(Number of Waterline points) **do**
  Calculate ζ with potential theory with random phase for all the components in between cut-off frequencies
end for

Wave forces and moments

From overall perspective the resulting force and moment from approach.3 with 'Partial overlapping FFT' method fit very well with the results from theoretical calculation, the difference of $1st$ order forces and moments between 4 layers SWASH simulation and 5 layers SWASH simulation is negligible.

Big relative errors show up in F_y, M_x and M_z for both wave cases, this because the absolutely value of these components are small, therefore lead to comparably large relative error, for the rest $1st$ order components, the relative deviations among approach.3 and approach.4 are sufficiently small.

Since all the wave components in this 2D irregular wave model propagate in uni-direction, the phase correction method introduced from regular wave verification still valid for this 2D irregular model, for wave component with unique wave frequency, from dispersion relation, with unique wave number k, from Eq.(2.5.7) the phase shift on different panel per frequency can be obtained. To verify the phases ϕ_ω of 1st order response spectra, IFFT (Inverse Fast Fourier transform) is used to transfer the response amplitude spectra with response phase spectra back to response time series, however, only 41 frequency components are selected to execute DIFFRAC calculation with 'Partial overlapping window FFT' method, therefore resulted response time series from IFFT will only contain 41 time

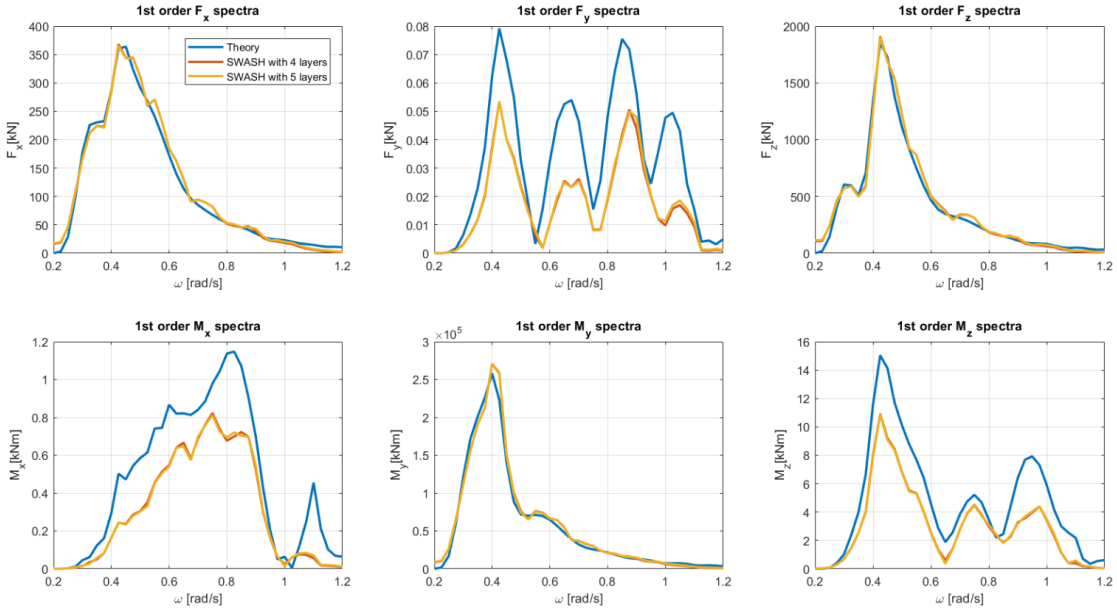

Figure 4.14: 1*st* order components of wave case with $T_p = 15$s with 'Partial overlapping FFT' method

points, which can not be used to represent the whole response time series, but sufficient for verifying the phase response.

For both wave cases, from Figs.4.16 and 4.17 the response time series fit quite well between approach 3 and approach 4, which means the relative phase response spectra has been correctly reproduced by mentioned phase correction method.

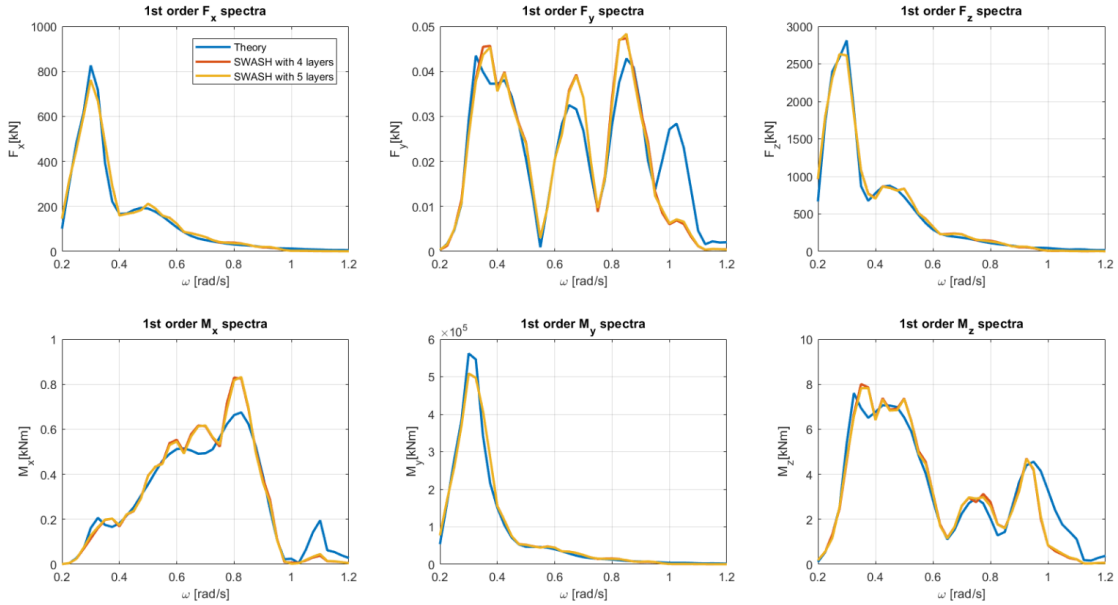

Figure 4.15: 1*st* order components of wave case with T_p =20s with 'Partial Overlapping FFT' method

For the same reason as mentioned in regular wave case, only the mean 2*nd* drift force is included in DIFFRAC calculation, although the error during coupling procedure has been reduced after applying 'Partial overlapping FFT' method, the difference of 2*nd* order force and moment between approach.3 and approach.4 are still obvious, as can be seen in Figs.4.18 and 4.19.

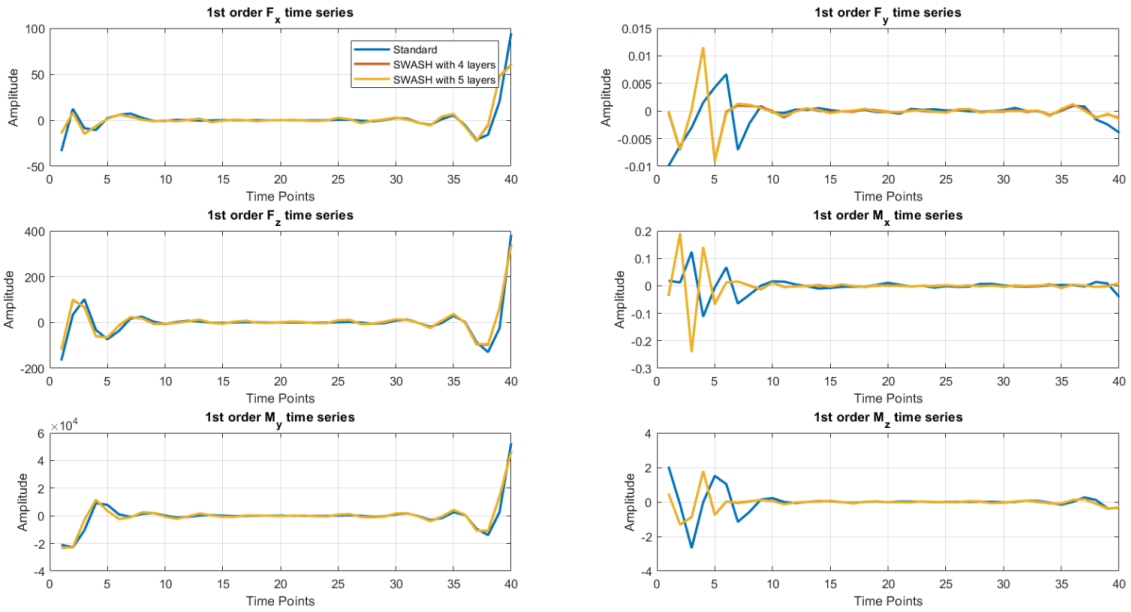

Figure 4.16: Response time series for wave case with $T_p = 15$s

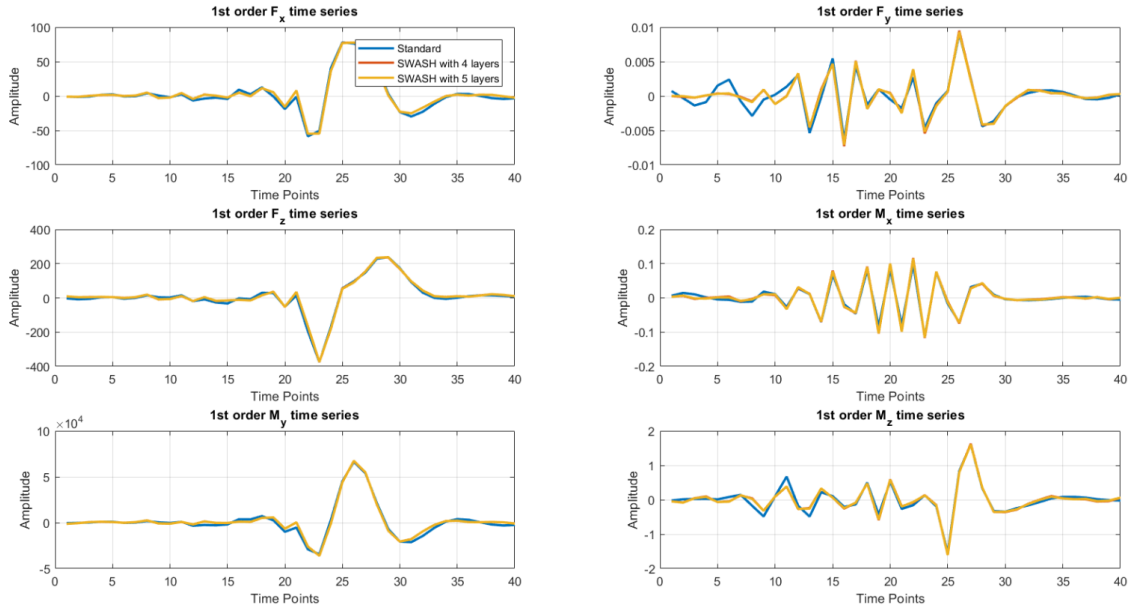

Figure 4.17: Response time series for wave case with $T_p = 20$s

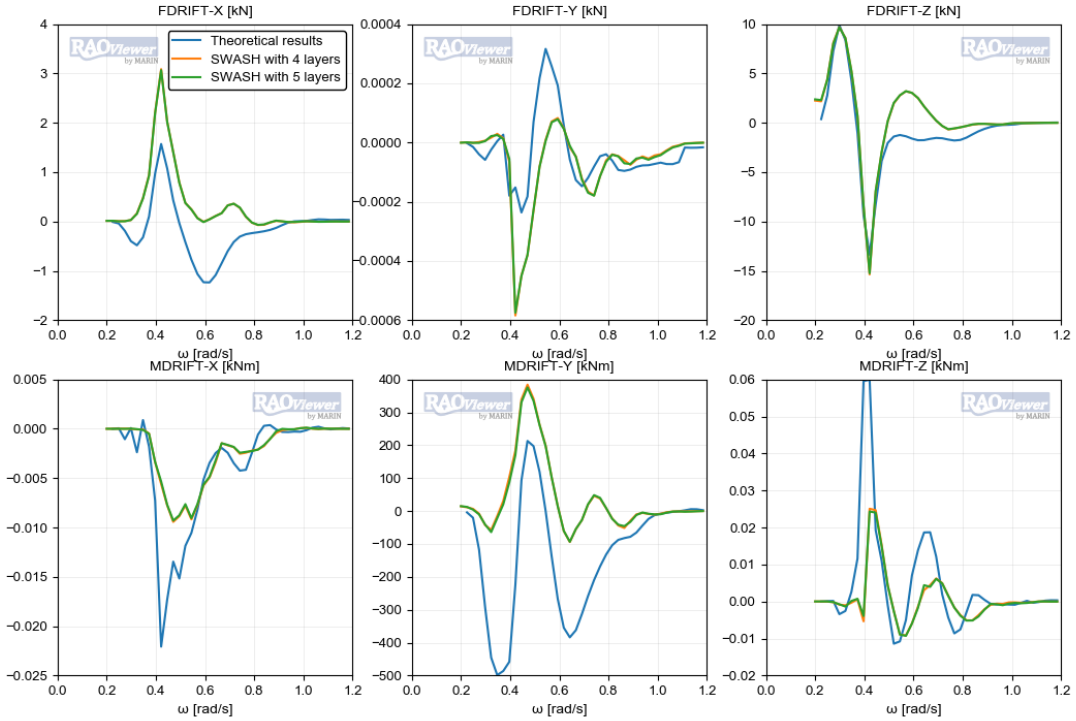

Figure 4.18: 2*nd* order force and moments of wave case with $T_p = 15$s

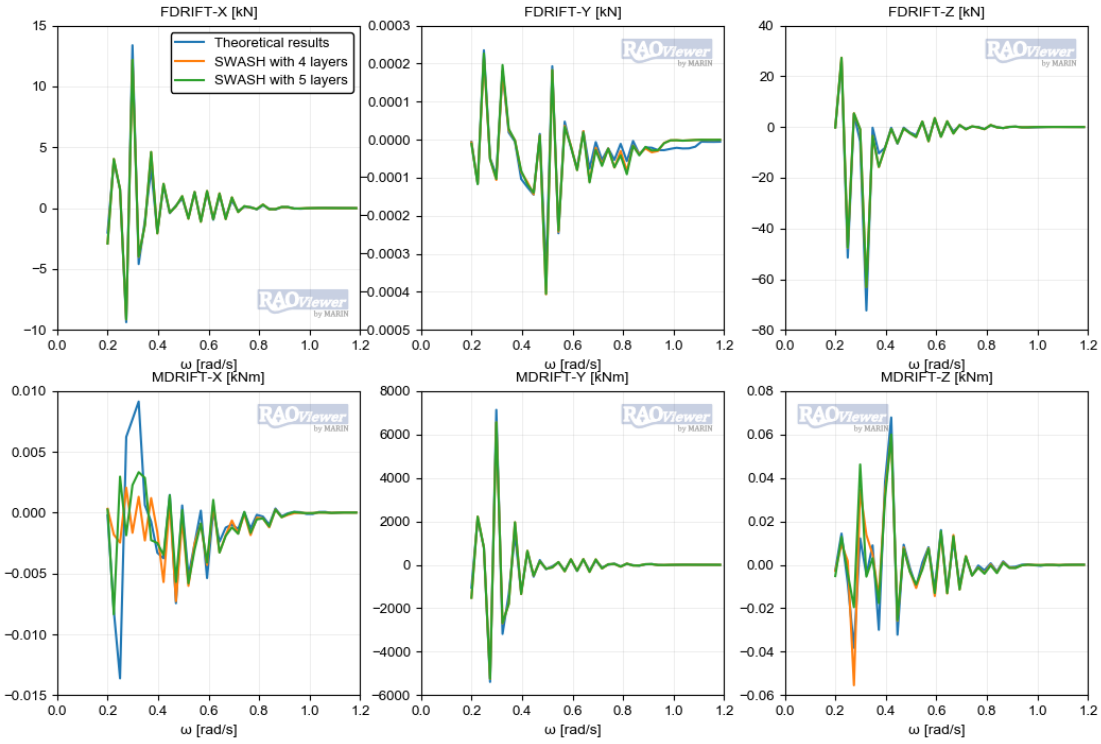

Figure 4.19: 2*nd* order force and moment of wave case with $T_p = 20$s

4.4 Conclusions

The main findings from this chapter are listed below:

- The required computation time in SWASH simulations is strictly related to the horizontal resolution of the model. In practical applications a trade-off should be made between the representation of the higher frequencies in the spectra and the computation time. 20 grid points per wave length can perform sufficiently accurate SWASH simulation.
- For waves with high kd value (say $kd \geq 3$), a drop in wave energy near the boundary can lead to considerable wave amplitude errors in SWASH. These errors can be partially reduced by increasing the number of vertical layers. Although, waves with large kd values in coastal areas have usually only little energy and therefore are not of prime relevance in wave penetration studies. For example, in 25m water depth, which is a representative water depth at the incoming boundary of detailed coastal wave models, kd values larger than 3 correspond to wave periods shorter than 5.8 seconds. These periods are generally away from the peak of the wave spectra for energetic conditions. 4 vertical layers with adapted numerical setting is SWASH simulation is sufficient to minimize the influence from coupling procedure for regular and irregular wave case, therefore the same SWASH model setting will applied in validation.
- The agreement between DIFFRAC model results for the different wave models (i.e, defined from SWASH simulations and determined based on linear wave theory) indicate that the coupling procedure is consistently implemented in the developed tool, however the $2nd$ order forces and moment for both regular wave case and irregular wave case are not representative, this because DIFFRAC can only calculate the mean $2nd$ drift force and moment, together with the errors induced from coupling procedure, makes an unreliable $2nd$ order force and moments.
- In regular wave model verification without applying 'Partial overlapping FFT' method, due to spectral leakage, wave energy spread out from the peak of wave spectra, therefore produce underestimated results for all force and moment components, after applying 'Partial overlapping FFT' the spectral leakage significantly reduced.
- The relative phase spectrum has been reproduced by applying phase correction method, even lost the initial phase information of incident wave, the phase response of wave force and moment acting on the ship can still be obtained from the relative phase contribution from all the panels.

Chapter 5

Validation of the tool

5.1 Description of the validation model

In this chapter the results obtained from the combination of SWASH, the developed coupling tool and DIFFRAC are compared with data from physical scale model. The model tests were conducted at WL|Delft Hydraulics (actual Deltares), in the directional wave basin with a modeled uniform water depth of 20m (Bijleveld, 2004). Fig.5.1 gives a impression of the basin setup during the experiments.

The measured dataset include waves at different locations in the basin and forces as well as moments acting on a restrained ship. The ship used in the test is a Panamax container vessel (L $\times$ W$\times$ D = 255m $\times$ 32.26m $\times$ 12.00m) at a model scale of 1:100 (Table.5.7). The data are provided on prototype scale using Froude scaling. The equality in Froude number between the model and full scale ensure that gravity forces and therefore surface waves are correctly scaled.

Table 5.1: Dimensions of the Panamax container vessel

Designation	Symbol	Unit	Magnitude
Length between perpendiculars	L_{pp}	m	255.00
Breadth	B	m	32.26
Draft	D	m	12.00
Displacement volume	δ	m^3	58566.00
Centre of gravity above keel	KG	m	13.50
Transverse radius of gyration	k_{xx}	m	12.40
Longitudinal radius of gyration	k_{yy}	m	69.25
Longitudinal radius of gyration	k_{zz}	m	70.35

A large steel frame is used to hold the ship on its position and to provide support for six force transducers to measure the forces on ship in six degrees of freedom. The purpose of the experiment is to model the wave forces only, therefore the ship is restrained and the mooring lines did not have to be represented in the physical model. The simulation of ship motions excited by the wave forces is rather straightforward, although the representation of the low-frequency wave forces is critical for the correct modeling of the horizontal ship

motions (van der Molen, 2006).

The test consisted of series of regular waves, irregular long-crested waves (neglect the directional spreading characters) and irregular short-crested waves.

Measurements of waves and forces are done for two basin situations:

1. The ship in open water: ship is in the center of the basin (position GRSM in Fig.5.2), and the x-axis of the ship coordinate system makes an angle of 120° with the Cartesian coordinate system given on Fig.5.2.
2. The ship in a schematic harbor basin: the position of the ship in the basin is the same as in open water tests. The internal dimensions of the harbor basin are 1200 × 400m (prototype scale), with the ship located in the middle of the longest wall (i.e. 600m to each side from the center of the ship). The ship's mid line is 20m away from the quay wall, resulting in a gap of approximately 4m between the ship and the wall. The outer part of the wall is filled with gravel in order to minimize reflection back to the wave maker.

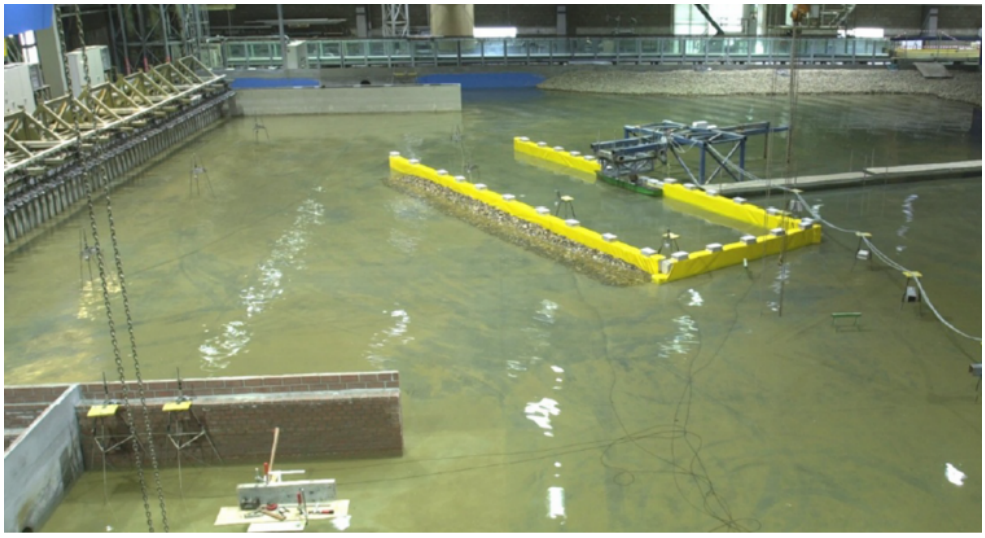

Figure 5.1: Model test set-up.

To specify the wave directions, a global coordinate system is used with the origin at left lower corner of the basin, the x-axis directed into the basin and perpendicular to the wave maker, and y-axis points upward. The harbor basin and the ship are placed under an angle of 120° with respect to the global coordinate system. Fig.5.2 shows the layout of the test, with the wave maker on the left side and gravel slopes on the opposing side to minimize wave reflection. The wave gauges GHM01, GHM02 and GHM03 are located at 300m from the wave maker and 660m apart.

The wave maker in the basin consists of independent piston type paddles, enabling wave generation in all directions including directional spreading. The second order long waves are included in the wave board control signals to produce the correct wave motions in the basin up to second order and avoid otherwise generated spurious long waves. The wave board is equipped with active reflection compensation to absorb waves reflected from the

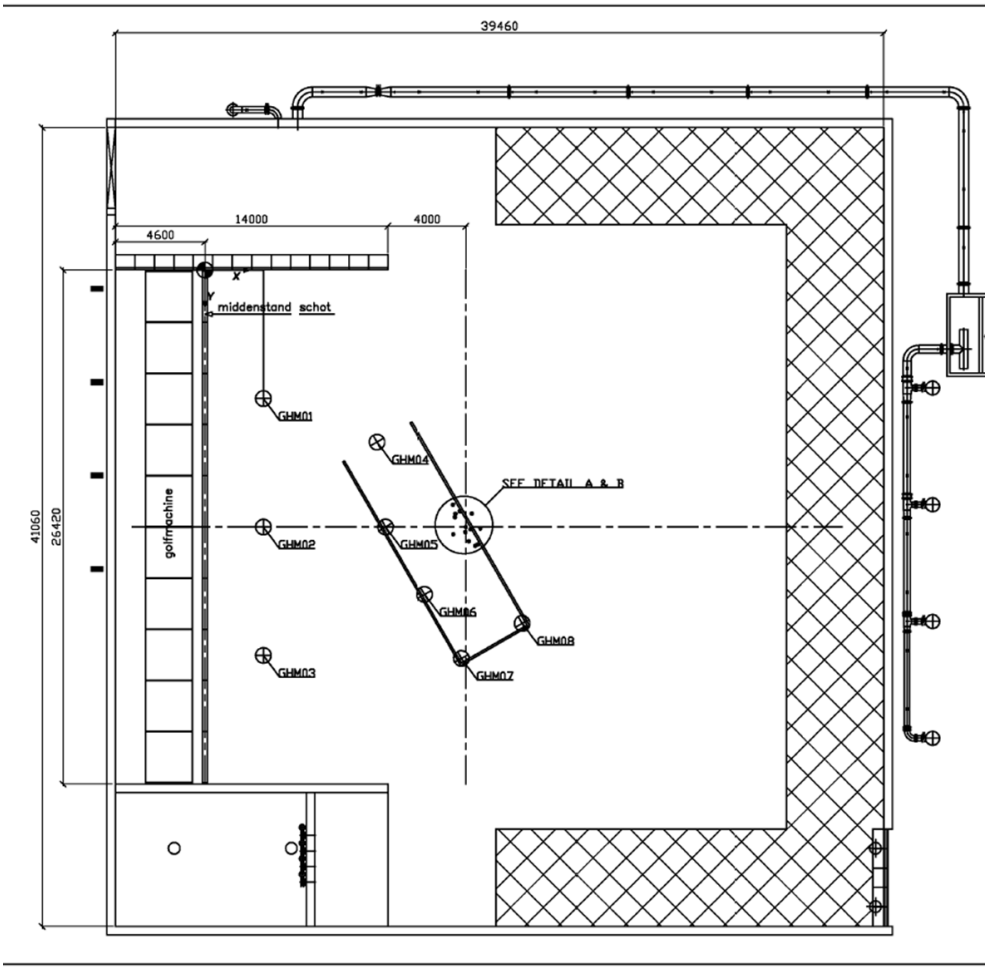

Figure 5.2: Layout of the test basin (Bijleveld ,2014).

basin, thus reducing the development of unwanted oscillations (van Dongeren, Klopman, Reniers, and Petit, 2002).

The structure (walls, harbour and gravel slope) are simulated in SWASH by using height and porosity, the porosity of all structures and gravel slopes are set to be 0 and 0.45 respectively, which means the water can not penetrate into the structure but partially into the gravel slope, the porosity of water (porosity = 1), which not present in porosity mesh of structures. Mesh of test series 2 (waves propagate in open water case) are shown in Figs.5.3 and 5.4. For test series 4 (waves propagate in basin with harbour), the mesh are shown in Figs.5.5 and 5.6, the same method is applied to simulate the existence of harbour.

The physical modeling of low-frequency waves rather difficult is because the active reflection compensation method can not eliminate all spurious effects, especially if the reflected waves are obliquely incident on the wave maker. The reflected short waves, on the other hand, are much lower than the incident waves due to breaking of short waves against the

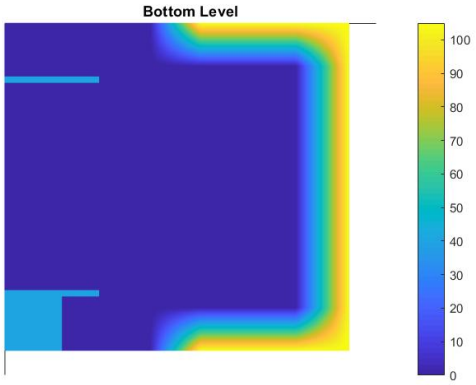

Figure 5.3: Bottom mesh in open water case.

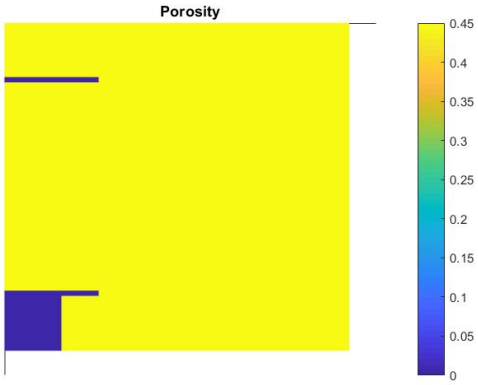

Figure 5.4: Porosity mesh in open water case.

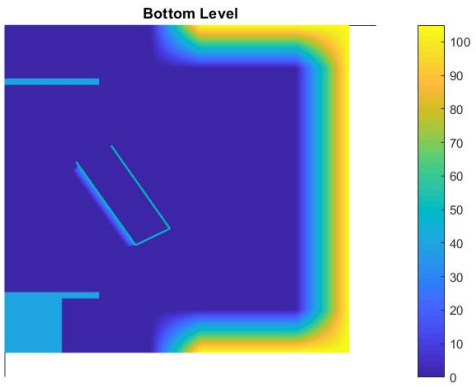

Figure 5.5: Bottom mesh in harbour case.

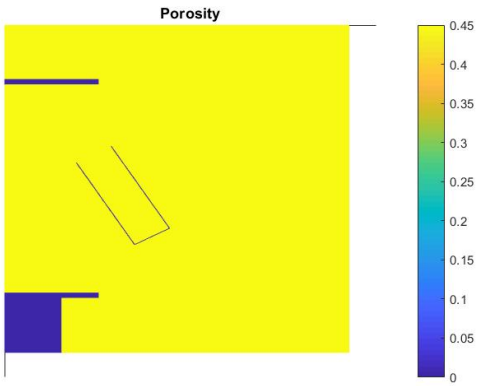

Figure 5.6: Porosity mesh in harbour case.

slopes.

Regarding the measurement of forces on the ship connected to measurement frame, problems occur especially in the correct measurement of the roll moments (M_x). This is because M_x is mainly measured as (relatively small) differences between two vertical forces.

To cover possible wave model within limit numbers of simulations, the regular wave, irregular long-crested wave and irregular short-crested wave in both open water and in harbour will be simulated, the wave conditions considered in validation are listed in Table.5.2

Table 5.2: Wave conditions considered in the validation of the approach (wave directions on the global coordinate system). In tests A_1, B_1 and C_1 the ship is in open water; in tests A_2 and C_2 the ship is in the harbour basin.

Test	Reference	H_s [m]	T_p [s]	Dir [◦]	Spreading	γ
Open water						
$A_{1.1}$	t212	2.0	10	0	0	No
$A_{1.2}$	t215	2.0	10	30 (Upward)	0	No
B_1	t2212	1.5	10	0	0	3.3
C_1	t2312	1.5	10	0	cos^2	3.3
With harbour basin						
A_2	t411	2.0	10	0	0	No
B_2	t4211	3.0	10	0	0	3.3
C_2	t4311	3.0	10	0	cos^2	3.3

5.2 Wave modeling and computation of wave forces acting on a ship

The SWASH wave model was configured to represent the testing basin. For all the test cases, the dominant wave component is with $T = 10s$ ($T = 10s$ for regular wave, $T_p = 10s$ for spectral wave), typical wave length for such a wave is around 121m, to have a feeling of the performance between DIFFRAC and Harberth, a conservative wave mesh with grid size of 4x4m is applied to simulate the wave propagation as mentioned in (Dobrochinski,), with 30 grid points per dominant wave length .

When the model is forced with a wave spectrum, higher frequency components are present in the simulation, which might be not so well represented by the numerical grid. For instance, a wave with 5s period in 20m water depth is 39m long. In this case the finer grid resolution corresponds to approximately 10 grid points per wave length, which may lead to inaccuracies especially if the height of the short waves is relatively large. It is considered, however, that only a limited amount of energy is associated with the high-frequency bands of the spectra and the corresponding forces and moments acting on a ship are relatively small, also because these waves are short relatively to the ship size. Therefore the drawbacks related to the grid spacing are expected to be marginal.

The water depth is 20m. The vertical side walls near the wave maker (left side of the domain) and the gravel slopes are included in the simulations as structures. The vertical side walls are 40m high from the bottom. The side slopes have steepness of 1:5. Reflection,

dissipation and transmission through the structures are determined by SWASH based on its porosity and d_{50} (normal stone diameter, the mesh size of structure). The porosity of the side walls is defined as zero, which mean that this structure is impermeable. The porosity considered for this side slopes is 0.45. The d_{50} of structure is 2m.

Similarly to the active reflection compensation used in the model tests, the incoming boundary condition in SWASH is weakly reflective, which means that up to a certain extent reflection can be minimize by compensating the signal for the outgoing waves. It is known, however, that both the mechanical and numerical wave maker have limitations to compensate for short waves and waves approaching in a large angle (say more than 30 degree with the wave maker normal). Because their individual characteristics may differ, it may cause differences between the wave fields in the physical tests and numerical simulation (Dobrochinski, 2014).

The first 9 minutes of the measured and simulated dataset are neglected to prevent the influence of the still initial conditions on the different analysis. This is approximately the time required for a wave with $T_p = 10s$ to cross the domain. The celerity of longer waves is larger and therefore the same distance is covered in a short time. The 9 minutes spin up time proved to be sufficient for the test A with regular waves of $T = 10s$. For test B and C ($Tp = 10s$) with spectral conditions, this main components of the spectra are assumed to be stabilized along the basin after the considered spin up time.

The bottom friction coefficient is calculated using the Manning formula with a coefficient of $0.019m^{\frac{1}{3}}s$ (typical value of smooth bottom). The 'Adapted set' of numerical schemes for the advective term is applied in these simulations. As identified on the tests with regular waves, with these numerical schemes the amount of numerical dissipation is considerably reduced relative to the 'Default set' of schemes. This is specially the case under non-linear wave conditions.

Depth induced wave breaking is not a dominating process in these tests, still the *Breaking* option in SWASH was activated in the initial tests. This option might be included to better reproduce the development of bore-like flows in the surf zone when poor vertical grid resolutions are applied, for a detailed description one is referred to Smit et al(2013).

The mesh of the Panamax ship representing the modeled vessel is given in Fig.5.7

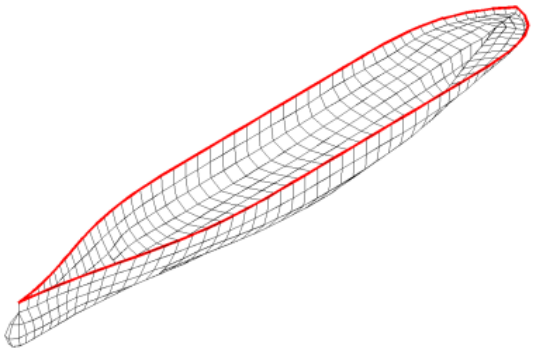

Figure 5.7: Panel description of the Panamax container vessel

5.3 Test A1.1: Regular wave with ship in open water

Regular waves with $H = 2m$ and $T = 10s$ are considered in this test. The propagation direction relative to global x-axis is 0°. The characteristics of the wave maker are uniform for test $A_{1.1}$.

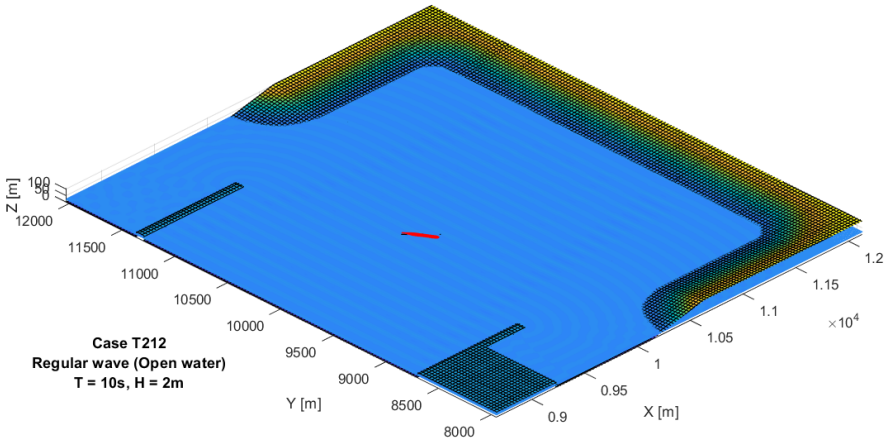

Figure 5.8: Test A1.1, regular wave propagation in open water

Table 5.3: Measured and simulated wave amplitudes in meters, the imposed regular wave amplitude for the simulation is 1m.

Wave gauge	Measured	SWASH	Difference
GHM01	0.90m	0.85m	6%
GHM02	0.68m	0.85m	25%
GHM03	0.60m	0.85m	42%

The wave condition was simulated in the SWASH model considering 4 layers. Fig.5.8 gives an overview of the model results along the entire domain, including the dissipation of the wave energy along the porous side slopes, as can be seen in 5.10.

The mean wave amplitudes measured and simulated for the wave gauges GHM01, GHM02 and GHM03 are given in Table.5.3, These are computed from the recorded time series of water surface elevation, excluding the first 9 minutes of simulation to prevent the influence of the still initial condition. For regular wave case, the wave condition can be assumed as fully developed after the initial period, therefore the simulation time in SWASH is set to 20 minutes, which is sufficient to present the regular wave component, the water elevation (the last 10 mins in simulation) at position of ship is shown in Fig.5.9. The instantaneous wave map at the end of SWASH simulation can be seen in Fig.5.10

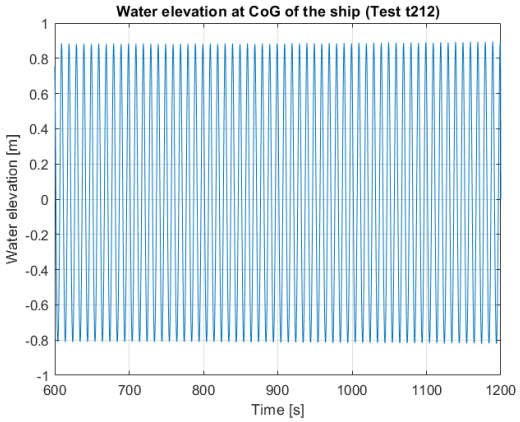

Figure 5.9: Water elevation at CoG of the ship (Test A1.1)

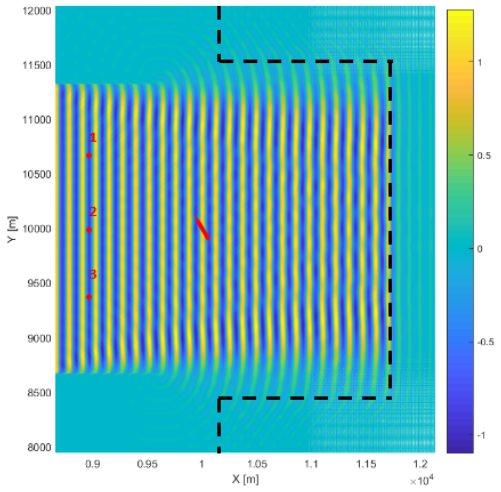

Figure 5.10: Wave map at the end of simulation (Test A1.1)

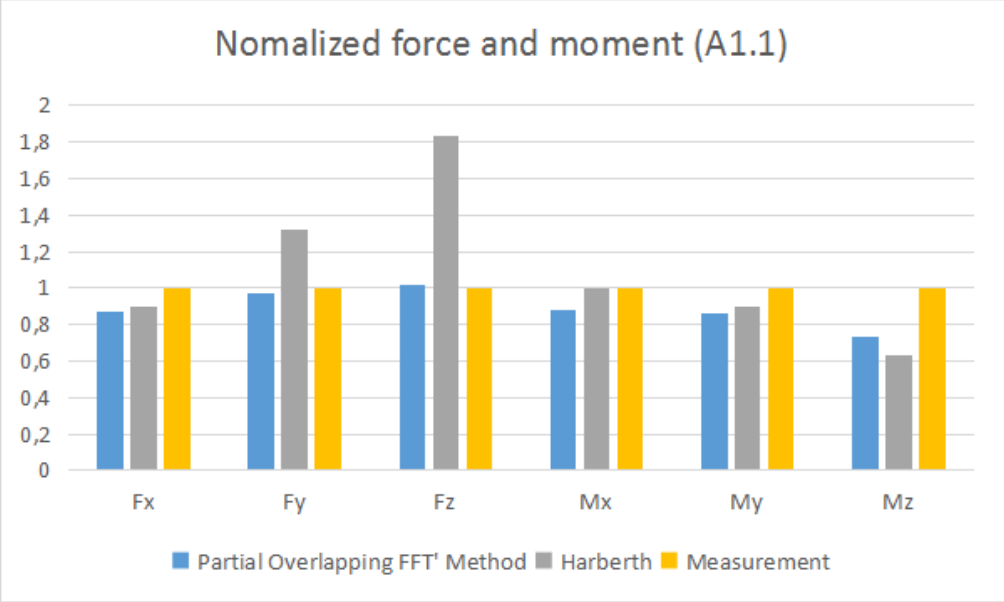

Figure 5.11: Normalized force and moment of measurement and simulation (Test A1.1).

The results given in Table.5.3 indicate a variation of wave height along the wave gauges, which is more pronounced on the measured data set. Although, the wave signals at different locations are indeed regular with 10s period. The wave height variations can be attributed to the superposition of the wave imposed by the wave maker and reflected along the limits of the basin/computational domain. Regarding the measurements they can also be due to inaccuracies in data sampling and/or on the wave maker. Wave reflection against the restrained ship, which is present only in the physical scale tests, however, since the presence of floating structure can not be simulated in SWASH model, therefore the real effect due to the existence of the ship can not be investigated.

SWASH model results around the hull of the ship were converted into DIFFRAC input files using the coupling tool described in Chapter.2 to handle 3D model results. In test case A1.1, the results of dominating forces and moments from simulation with 'Partial overlapping FFT' method is compared with measured forces and moments on Fig.5.11, to have a feeling of the performance of Harberth, the results from Harberth calculation (Dobrochinski,2014) are also included.

In general the comparisons of the measured and simulated wave forces acting on the ship are satisfactory, the performances between DIFFRAC and Harberth is comparable, the simulated yaw moment in both DIFFRAC and Harberth are lower than value from measurement.

5.4 Test A1.2: Oblique regular wave with ship in open water

Oblique regular waves with $H = 2m$ and $T = 10s$ are considered in this test. The propagation direction relative to global x-axis is 30°.

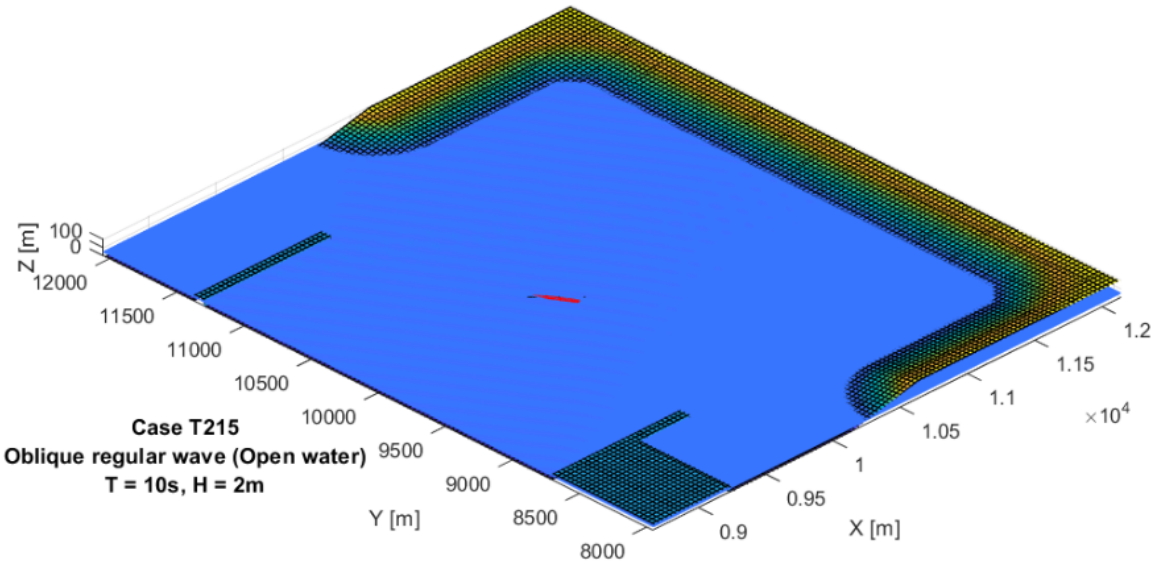

Figure 5.12: Test A1.2, oblique wave propagation in open water

The instantaneous wave map at the end of SWASH simulation is shown in Fig.5.14, Wave reflection against the vertical wall can be noticed on the upper left corner of Fig.5.14 causing the so-called diamond pattern resulted from the interaction of two wave trains with different directions of propagation. For the test A1.2 the wave direction and ship orientation have 90° difference, the ship experiences beam waves.

For this oblique regular wave propagation model, a more conservative 30 minutes SWASH simulation is performed, the water elevation at location at CoG of the ship is given in Fig.5.13 (only the last 10 minutes). The mean wave amplitudes measured and simulated for the wave gauges GHM01, GHM02 and GHM03 are given in Table.5.4. With excluding the first 9 minutes of simulation to prevent the influence of the still initial condition.

Table 5.4: Measured and simulated wave amplitudes in meters, the imposed regular wave amplitude for the simulation is 1m.

Wave gauge	Measured	SWASH	Difference
GHM01	1.17m	1.05m	10%
GHM02	1.07m	1.06m	1%
GHM03	1.36m	1.04m	24%

Better wave simulation in test A1.2, with comparing to wave simulation in Test A1.1, biggest deviation still shows up in data at wave gauge GHM03, the wave height variations can be attributed to the superposition of the incident wave and reflected wave, another possibility to explain this phenomenon is the existence of the ship in model test, since the ship heading is 120° according to the global system, both test A1.1 and A1.2, the reflected

wave will go back with direction around 270° and 240° respectively, therefore the wave field at location of GHM03 will experiences the biggest influence among all three wave gauges, the ship is not involved in SWASH calculation, leading a much more uniform wave field along wave maker in simulation, this can also prove the influence of the ship can not be ignored.

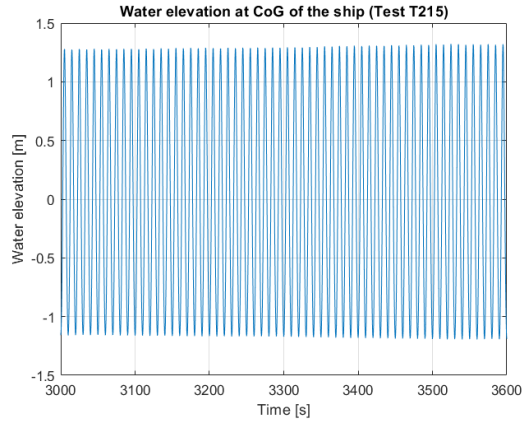

Figure 5.13: Water elevation at CoG of the ship (Test A1.2)

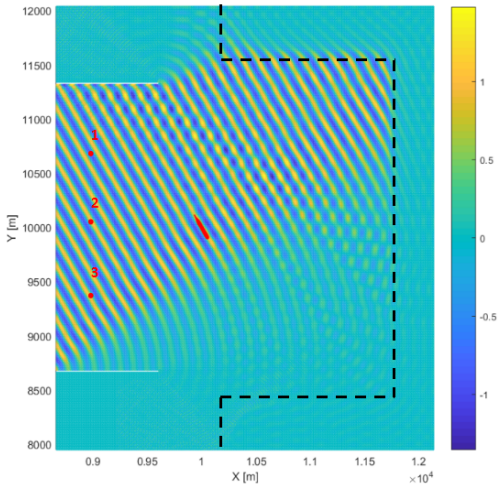

Figure 5.14: Wave map at the end of simulation (Test A1.2)

A big underestimation of F_x in shown in DIFFRAC calculation, since ship experiences a beam wave, the absolutely deviation in F_x is not significant (873.2kN lower than measured surge force), but the relative deviation, The comparison of moments around the x-axis indicate good agreement for Test A1, whereas for A2 the simulations underestimate this moment component. This mismatch may be related to the difficulties in determining the 'roll moment' (Mx) from the forces measured by the transducers, since the roll moment is measured as a (small) difference between two large components (van der Molen, 2006), similar as in tes A1.1, yaw moments in both DIFFRAC and Herbarth calculation are smaller than measurement.

As reported in Dobrochinski (2014), van der Molen (2006) used data from the same

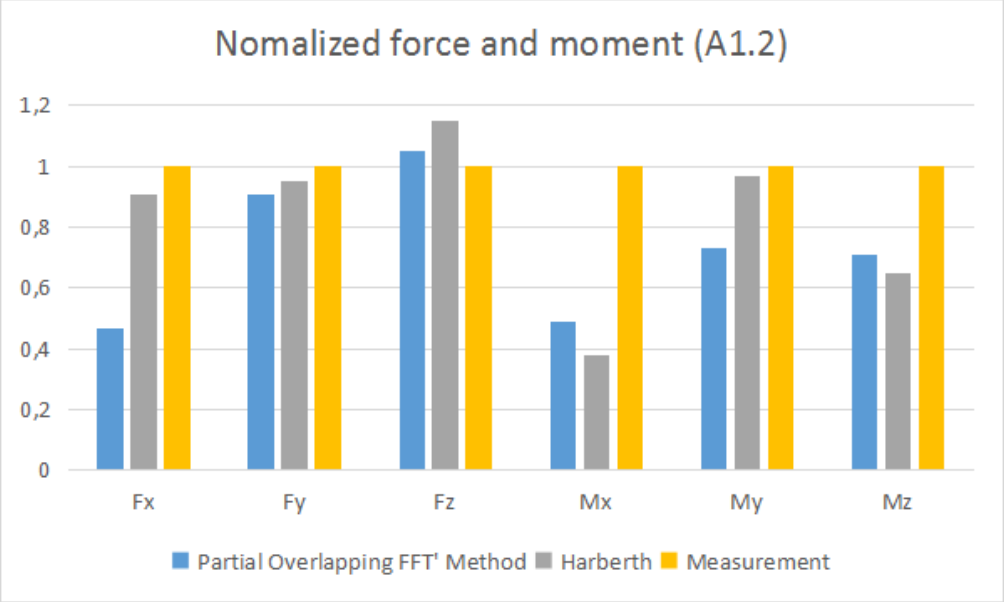

Figure 5.15: Normalized force and moment of measurement and simulation (Test A1.2).

experiment in the validation of Harberth model. In a test with passing ship waves similar differences between measured and simulated roll and yaw moments were found. The comparisons also included the results of computations using the frequency-domain panel model DELFRAC, which is widely validated and can be considered a reliable tool. The results of DELFRAC were nearly identical to the ones associate to Harberth for all force and moment modes. This suggests that the observed differences are likely associated to factors not directly related to the numerical tools applied, such as inaccuracies on measurements and on the representation of the hull of the ship in the mesh. Nevertheless, possible differences between the wave fields in the vicinity of the ship may also explain the observed differences in the associated wave loads.

5.5 Test B1: Long-crested waves with ship in open water

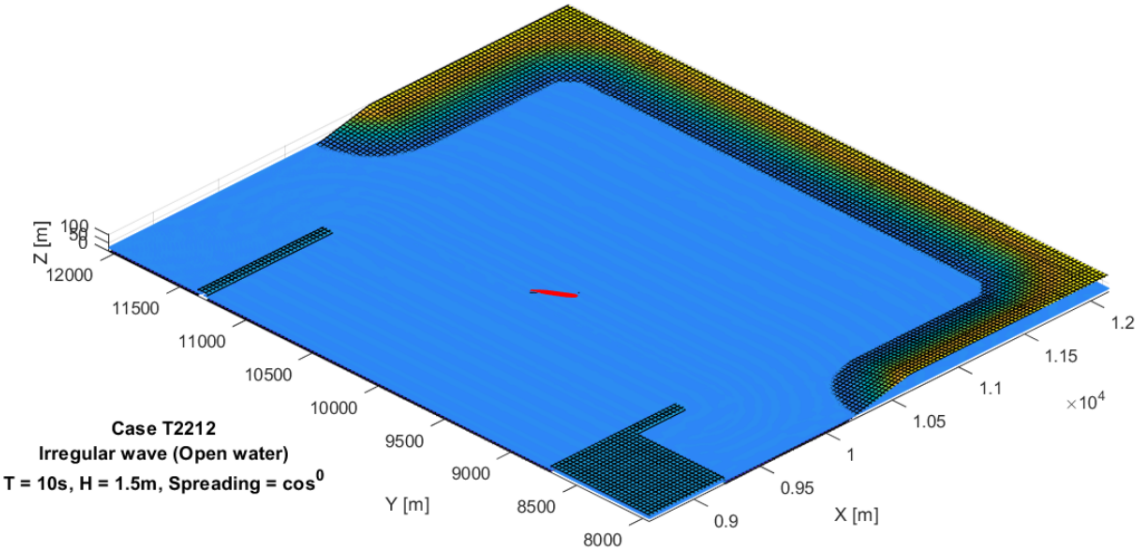

Figure 5.16: Test B1, long-crested wave propagation in open water

In tests B1, the wave conditions are represented by JONSWAP spectra with significant wave height $H_s = 1.5m$ and peak period $T_p = 10s$, propagation direction normal to the wave maker (0° Cartesian). The duration of these simulation should be sufficiently long to minimize the influence of the still initial conditions and ensure a consistent estimation of the wave spectra and wave parameters at different locations. The required duration of the simulation is determined based on the measured wave dataset for test B1, which have a duration of 5 hours in prototype scale. Wave parameters were determined varying gradually with the length of the time series, starting the calculation at 9 minutes after the beginning of the test. Spectral parameters Hm0 (significant wave height) are derived from the wave spectra of the water elevation time series at GHM01, GHM02 and GHM03 with time step of half hour. The results considering different realization times are normalized by the wave parameters associated to the complete time series (excluding the initial 15 minutes and the last 15 minutes of simulation, and normalized with Hm0 at the end of measurement). For test B1, from Fig.5.18, after 2 hours of the experiment, the total wave heights are only slightly affected by increasing the length of the time of simulation, the deviation of Hm0 are within 1% with after 2 hours measurement, which means the wave condition are almost fully developed respect to the end of measurement. It is reasonable to consider a simulation time in SWASH of 3 hours.

Instantaneous maps (at the end of simulation) on simulated water surface elevation of test B1 is given on Fig.5.17. The difference in wave frequency is clearly visible in the plot.

The calculate wave height at the different measure locations are given on Table.5.5. Only three measuring gauges are available for the comparisons in the test of open water cases as in test A1.1 and A1.2.

An underestimation of energy in SWASH simulation of test B1 at the high frequency tail

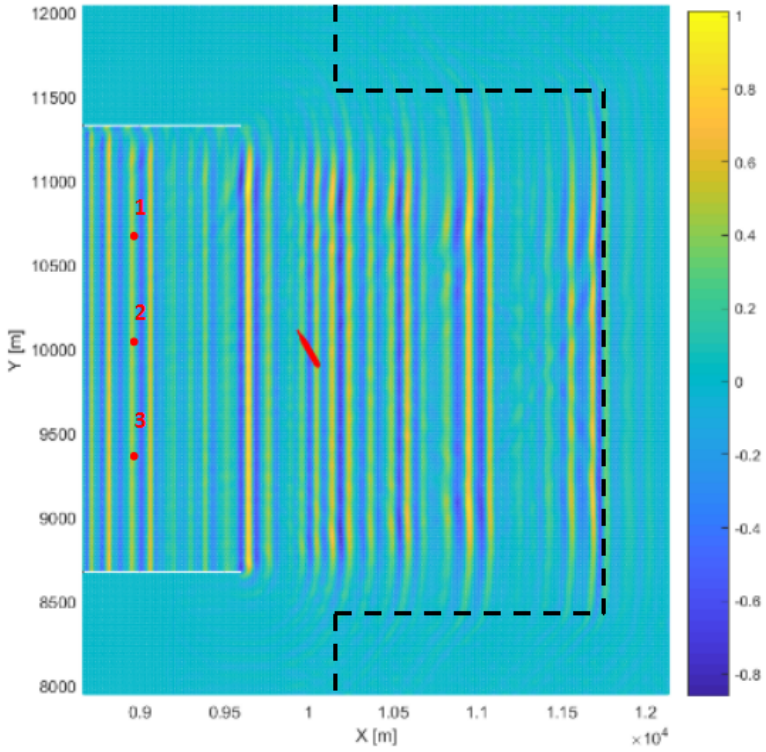

Figure 5.17: Wave map at the end of simulation (Test B1)

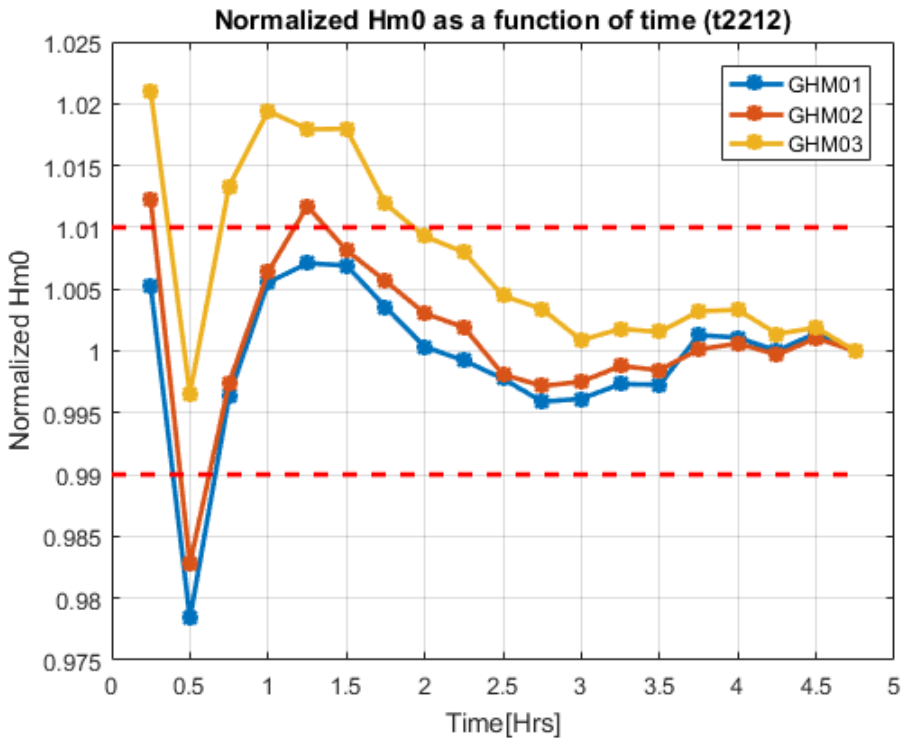

Figure 5.18: Normalized Hm0 variation over time (Test B1).

Table 5.5: Measured and simulated significant wave height (Test B1)

Wave gauge	Hm0 Measured	Hm0 Simulated	Difference
GHM01	1.32	1.21	8.3%
GHM02	1.32	1.21	8.3%
GHM03	1.43	1.21	15.4%

of the spectrum was expected due to the relatively scarce grid resolution for those (short) waves, however, the reported differences are very small.

Similar as in test A1.1 and A1.2, bigger deviations of Hm0 among three wave gauges in measurements than in SWASH simulation in both cases test B1. The averaged measured and simulated waves spectra for simulation B1 at three gauges are given in Fig.5.19, the energy of high frequency wave components in simulation are underestimated than in model test in test B1, better fits at both low and high frequency zone are shown in simulation C1.

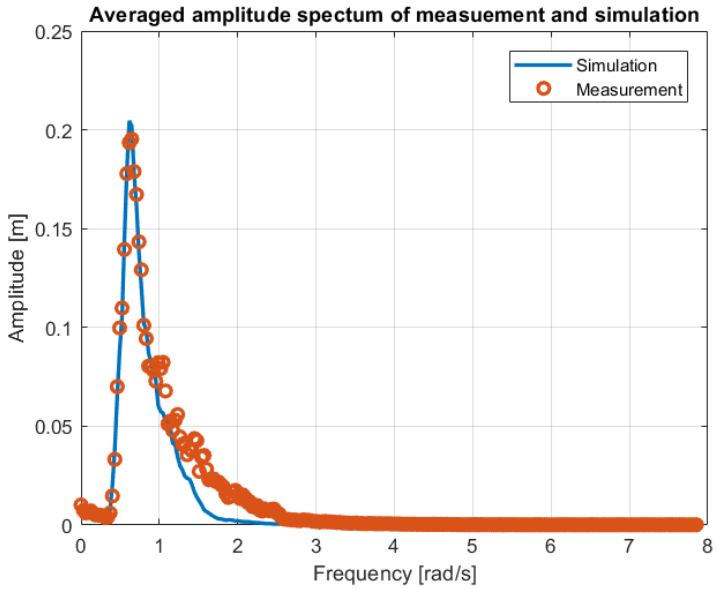

Figure 5.19: Averaged amplitude density spectrum over gauges (Test B1)

The measured and computed forces and moments density spectra with both 'Full FFT' Method and 'Partial overlapping FFT' method acting on the ship during test B1 are compared in Fig.5.20 and Table.5.6.

The overall magnitude of simulated results (significant forces and moments derived from spectrua) with both 'Full FFT' method and 'Partial Overlapping FFT' method are in good agreement as shown in Fig.5.20, the peak of density spectra from 'Full FFT' method have a little bit shift towards to high frequency zone (it is more obvious in spectra of F_y, M_x and M_z), this is because the precision of DIFFRAC calculation is 0.0001 rad/s, therefore the precision of step increment in DIFFRAC calculation should not over 0.0001 rad/s, otherwise the accumulated error will influence the overall result (peak of responses may shift to high frequency zone).

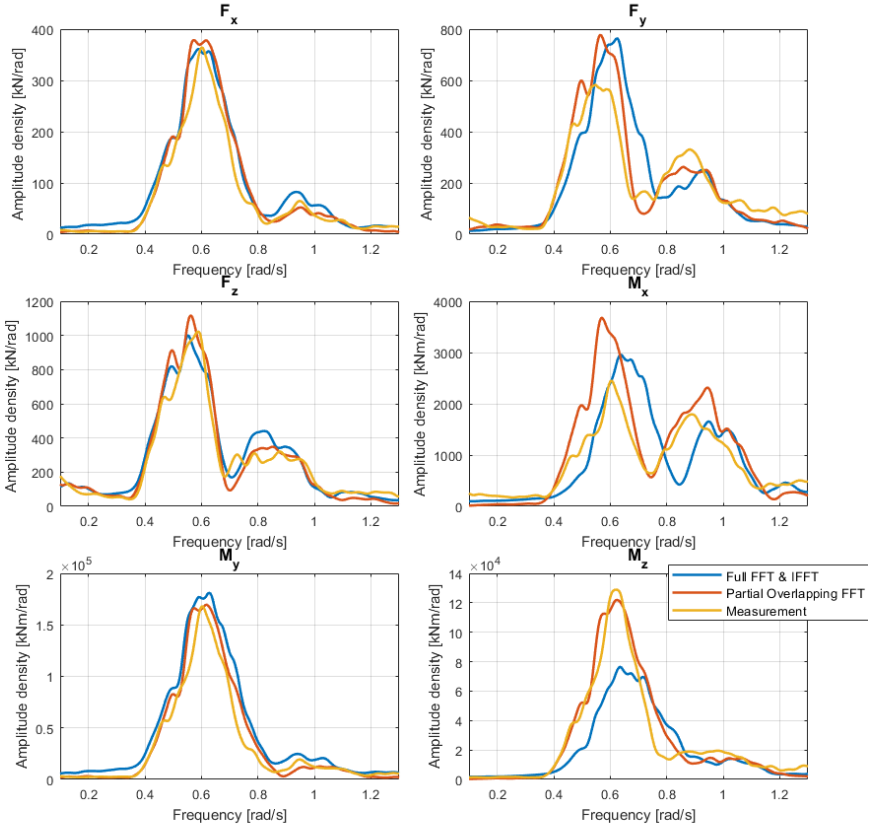

Figure 5.20: Amplitude density spectra of forces and moments from measurement and simulation (Test B1).

Table 5.6: Measured and simulated significant wave force and moment, and deviation with respect to Measurement, 'P O FFT' is 'Partial Overlapping FFT' (Test B1)

Mode	'Full FFT' [MN/ MNm]	Difference	'P O FFT' [MN/ MNm]	Difference	Measurement [MN/ MNm]
Fx	3.07	16.38%	3.08	16.75%	2.64
Fy	6.28	14.03%	6.32	14.83%	5.51
Fz	8.68	5.95%	8.94	9.24%	8.19
Mx	27.29	16.58%	27.29	39.29%	23.41
My	1545.27	27.73%	1381.65	14.21%	1209,79
Mz	679.13	-27.53%	1002.91	7.02%	937.08

All the response spectra from measurement and simulation fit quite well, only excluding the response spectra of roll moment M_x. This mismatch may be related to the underestimation of viscous effect in simulation, because the scaling used in the physical model tests is based on the Froude number and the fluid viscosity is not properly handled, the Reynolds number is incorrectly represented, the viscous effect of water is much more important in roll and yaw motion than in other degree of freedoms, therefore the relatively significant overestimation of ship response in roll motion in simulation can be expected, the simulated yaw moment are lower than result from measurement, which is on the contrary of simulated roll moment, the same underestimation also shows up in test A1.1 and A1.2 with regular waves, the difference is probably related to an external factor, i.e. the error during measurement.

A better overview of time domain simulated wave force is given in Fig.5.21. With 'Full FFT' method, the wave force and moment time series without initial period can also be reproduced and be compared with measurement data. For spectral wave simulation, the simulated force and moment time trace are not in phase with the measurements, however, some response envelopes can be seen in both measurement and simulation at the same time in all 6 components, which means the wave data and ship response are in phase in both simulation and measurement respectively. The same as shown in Fig.5.20, the simulated yaw moment is obviously smaller than the measurement.

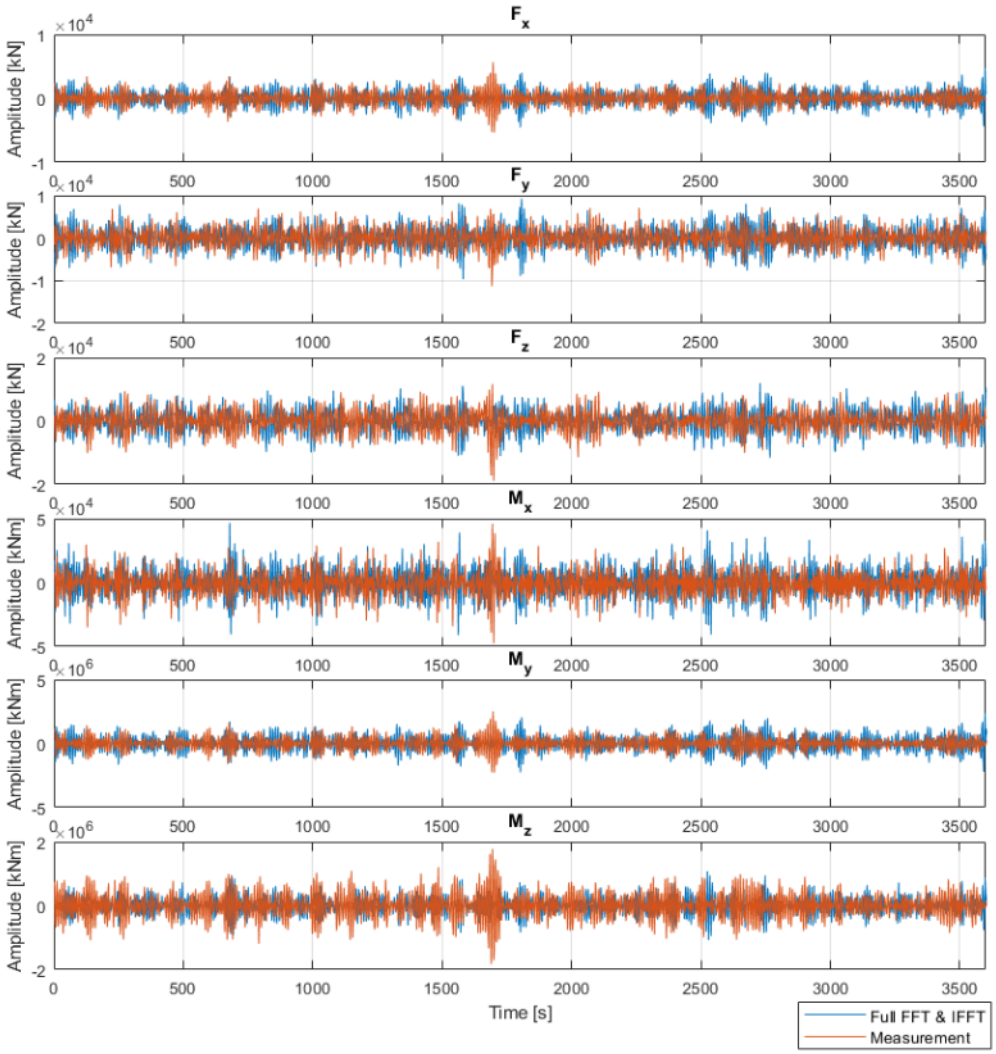

Figure 5.21: The last 1 hour response time series from measurement and simulation (Test B1).

5.6 Test C1: Short-crested waves with ship in open water

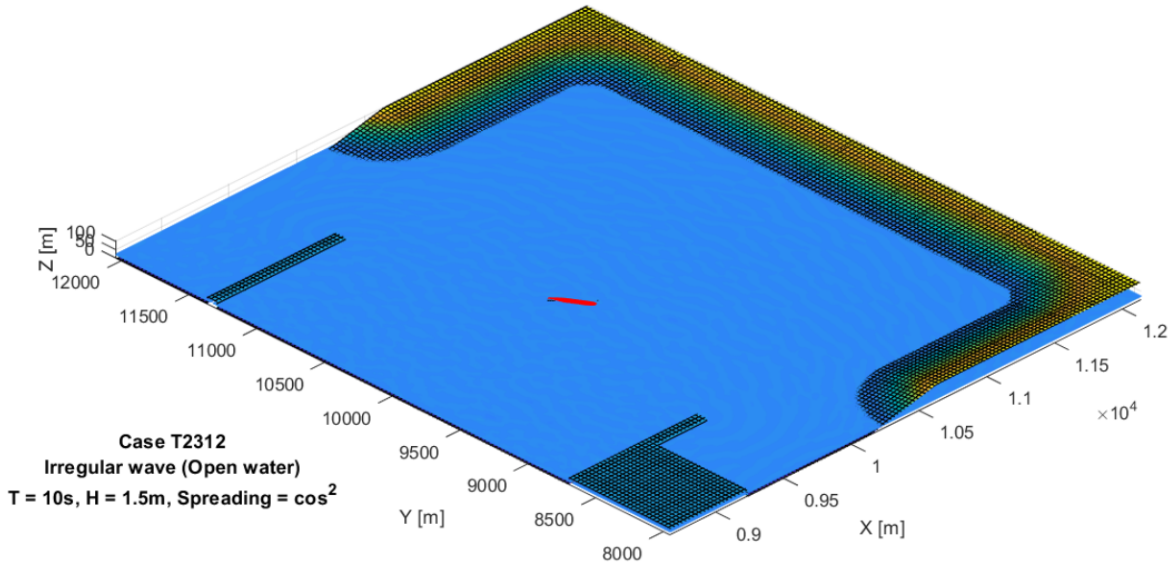

Figure 5.22: Test C1, short-crested wave propagation in open water

In test C1, short-crested wave simulation are represented by JONSWAP spectra with significant wave height $H_s = 1.5m$ and peak period $T_p = 10s$, propagation direction normal to the wave maker (0° Cartesian), with directional spreading factor cos^2.

The same as SWASH simulation in test B1, the required duration of the simulation is determined based on the measured wave dataset for test C1, from Fig.5.24, the wave is almost fully developed after the first 2 hours, so it is justifiable to consider a simulation time in SWASH of 3 hours.

Instantaneous maps on simulated water surface elevation of test C1 is given on Fig. 5.23. The difference in wave frequency and directional spreading are clearly visible in the plot.

The calculated wave height at the different measured locations available for these tests are given on Table.5.7.

Table 5.7: Measured and simulated significant wave height (Test C1).

Wave gauge	Hm0 Measured	Hm0 Simulated	Difference
GHM01	1.23	1.18	4.1%
GHM02	1.27	1.18	7.1%
GHM03	1.32	1.20	9.1%

With including the directional spreading character, the measured wave height at all three gauges in test C1 is indeed smaller than in test B1. This is well simulated in SWASH model, similar as in tests A1, bigger deviations of significant wave height among three wave gauges in measurements than in SWASH simulation in both test C1. The averaged measured and simulated waves spectra for simulation C1 at three gauges is given in

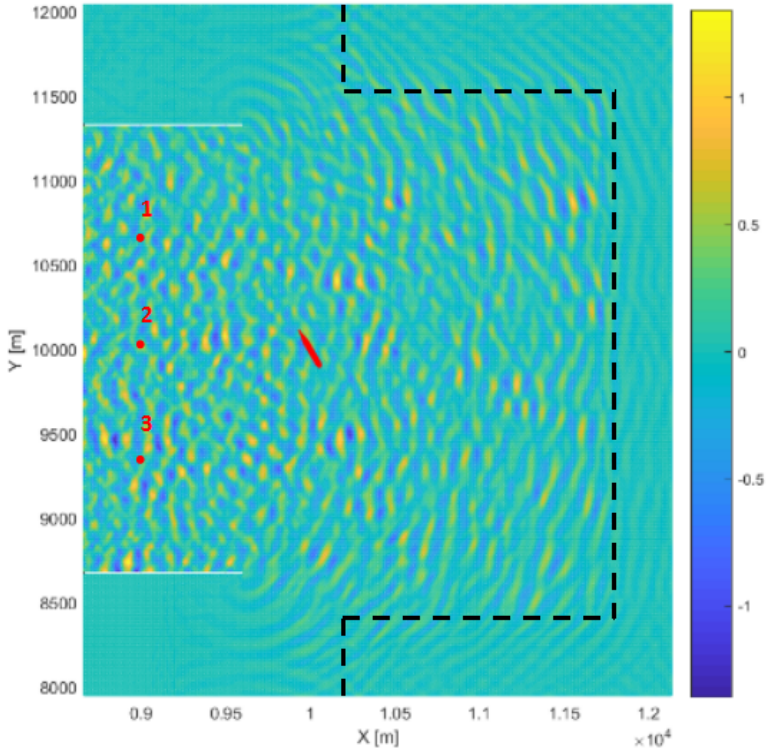

Figure 5.23: Fully developed wave map (Test C1)

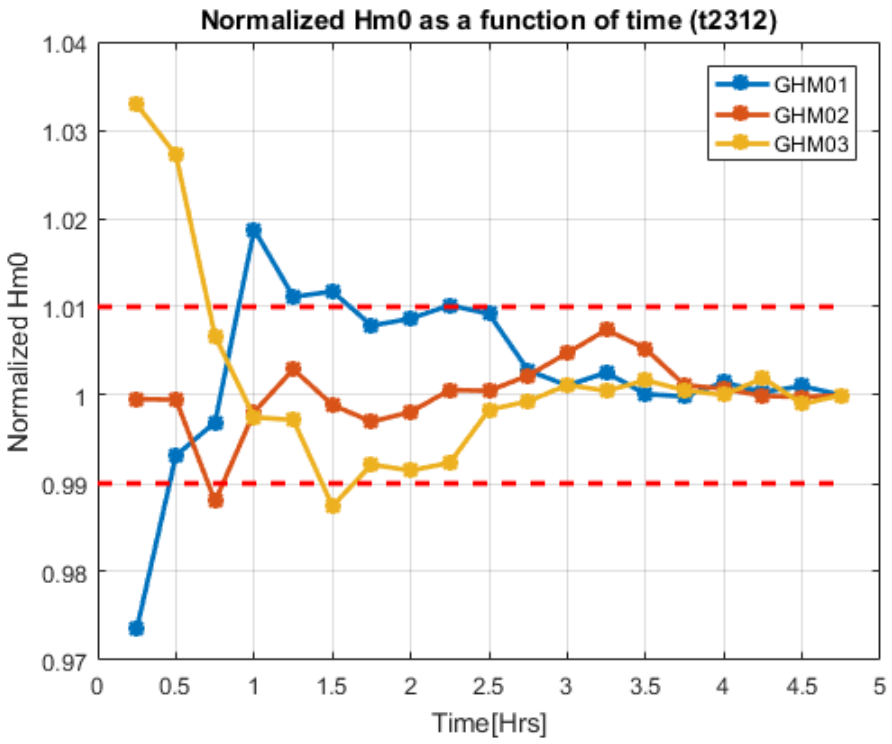

Figure 5.24: Normalized Hm0 variation over time (Test C1).

Fig.5.25. Better performance at both low and high frequency zone are shown in test C1 than in B1.

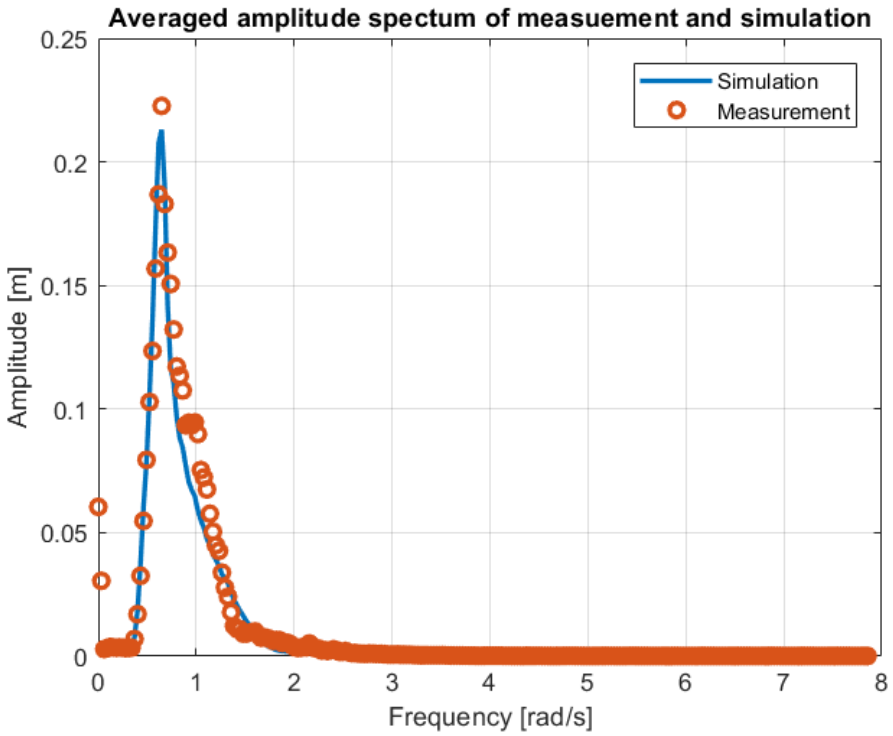

Figure 5.25: Averaged amplitude density spectrum over gauges (Test C1)

For test C1, with including the wave directional spreading, the energy in both wave spectrum and response spectra are spreading out from the peak frequency. As shown in Table.5.7, Hm0 of test C1 is lower than the value in case B1 for both measurement and simulation. in the validation of case C1 the results of simulation with both 'Full FFT' method and 'Partial Overlapping FFT' method are given, since this test case is also did by Dobrochinski in year 2014, therefore the performance of Harberth can also be involved.

The measured and simulated response are shown in Fig.5.26 and Table.5.8

Table 5.8: Measured and simulated significant response amplitudes (Test C1)

Mode	'Full FFT' [MN/ MNm]	Difference	'P O FFT' [MN/ MNm]	Difference	Harberth Difference	Measurement [MN/ MNm]
Fx	2.95	10.25%	1.76	-7.36%	-9.20%	1.90
Fy	7.16	-43,99%	5.25	-58.9%	2.00%	12.78
Fz	16.81	10.26%	7.49	-50.85%	17.90%	15.25
Mx	23.10	-11.28%	25.89	-0.57%	-0.80%	26.04
My	986.55	15.21%	898.07	4.88%	-5.00%	856.32
Mz	420.54	-44.50%	668.38	-11.79%	-27.50%	757.67

Deviations in the measured and computed spectra of forces and moments can be attributed to different sources of inaccuracies, i.e. the wave modeling, the coupling tool, the computations of DIFFRAC, and the limitation on the measurement. In view of that, the results of test C1 among measurements and simulations with 'Full FFT' method and

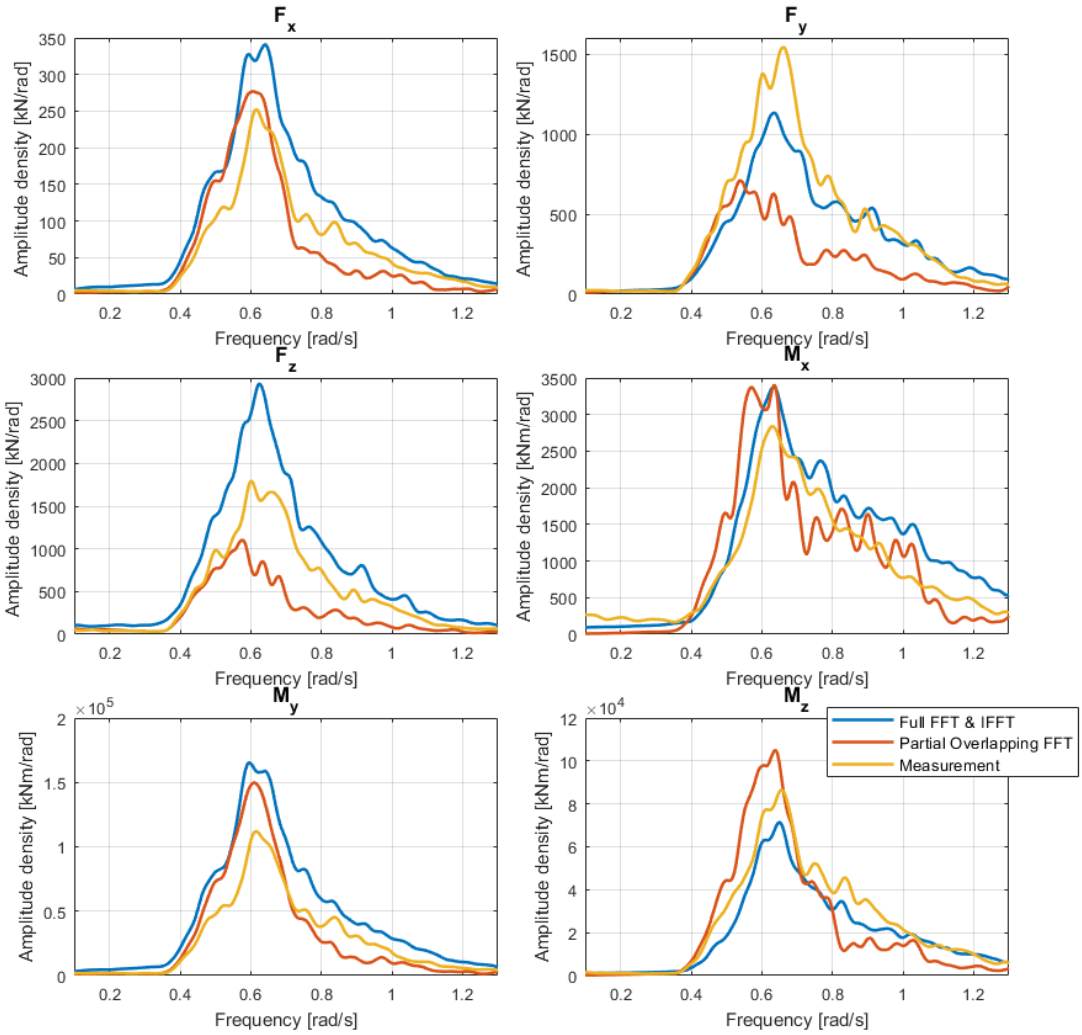

Figure 5.26: Amplitude density spectra of forces and moments from measurement and simulation (Test C1).

'Partial Overlapping FFT' methods considered satisfactory, but less comparable the results from Herbarth calculation, the reported underestimation of yaw moment is the same as the conclusion from test A1.1 and A1.2.

Bigger deviations show up in the comparison of results from 'Partial Overlapping FFT' method and measurement, the comparisons of measured and simulated wave height and 1D-spectra are in good agreement, so the difference between measured and computed forces and moments are not likely significantly related to the modelled wave energy and periods. The same applies for the coupling tool, which has shown to be accurate for unidirectional wave case. Therefore, differences in forces/moments can be attributed to the directional character of the simulated and measured waves, also the potential uncertainties in defined wave directions for short-crested wave in 'Partial Overlapping FFT' method (this is also why the amplitude density spectra of 'Partial Overlapping FFT' Method is more coarse than the result from measurements and 'Full FFT' method).

The last 1 hour time series of measurement and simulation are given in Fig.5.27.

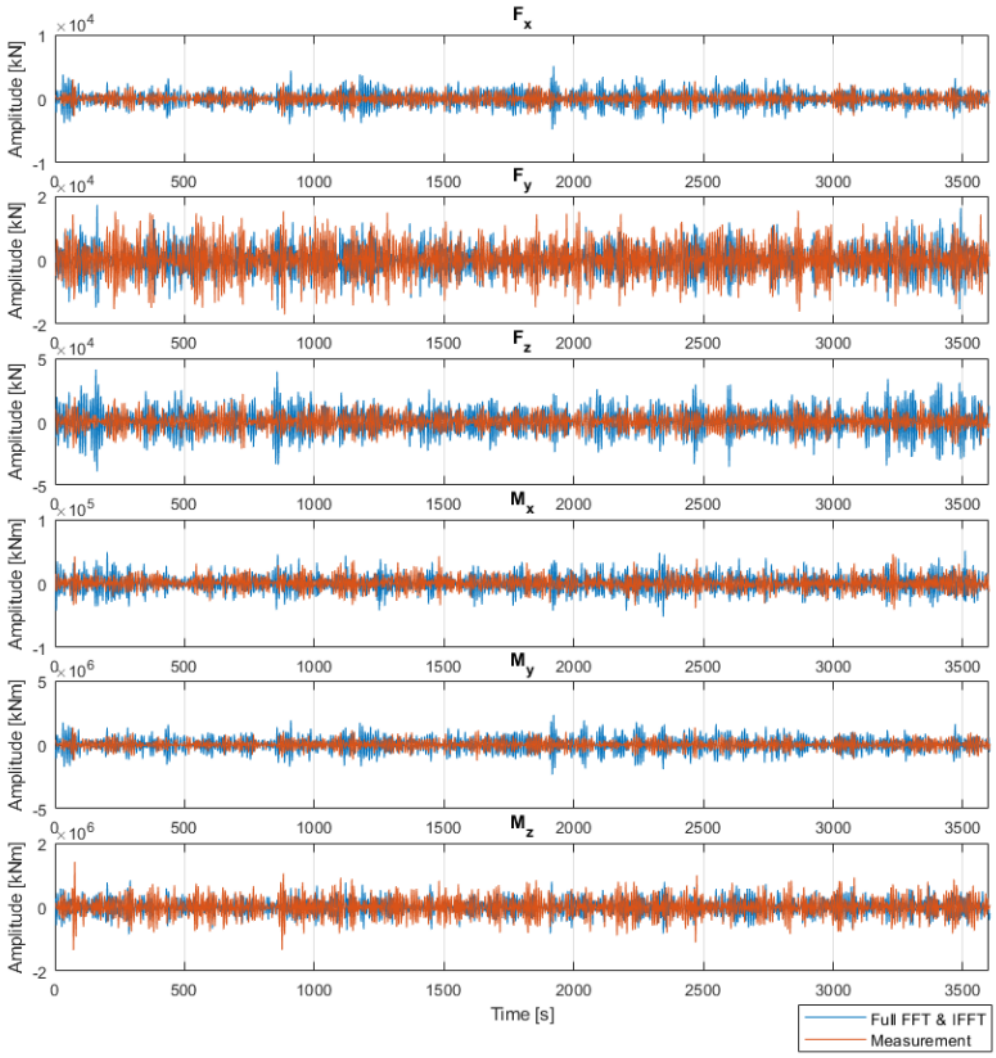

Figure 5.27: The last 1 hour response time series from measurement and simulation (Test C1).

5.7 Test A2, B2 and C2: waves with ship in harbour basin

5.7.1 Model preparation

Test series 2 considers a harbour situated in the middle of the testing basin. The harbour layout is composed by vertical (i.e. quay walls) and a porous slope in the outer side of the wall, between the harbour and the wave maker as shown in Fig.5.28 These structures were included in SWASH simulations by imposing their horizontal/vertical dimensions, porosity and D_{n50} (stone diameter, the mesh size of structures).

The vertical walls surrounding the harbour are 15m wide, 50m high (from the bottom level), and have a porosity set as 0 (minimum value of 0.1 is used by SWASH in the computations). The porous slope is placed in the outer side of the vertical wall in order to reduce wave reflection back towards the wave maker. In the numerical model it was implemented as a porous structure (p=0.45) with slope of 1:3 (the porosity is the same as the gravel slope), starting at 85m from the wall. The top of the sloping structure is approximately 28m high measuring from the bottom of the basin (8m above the mean water level), all the mentioned mesh are shown in Fig.5.5 and 5.6, basin geometry and structure is given in Fig.5.28, color coding means the height of the structures with respect to the bottom (z = 0m).

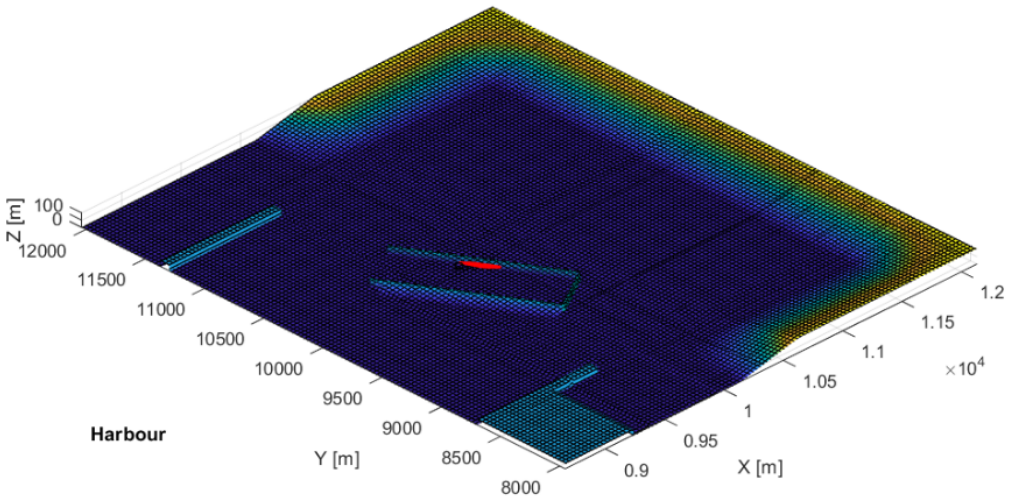

Figure 5.28: Basin bottom with harbour geometry and gravel slop

5.7.2 SWASH Simulations of tests A2, B2 and C2

Together with the same wave mesh mentioned in simulation series 1, the holistic basin layout of three wave model are given in

The measured wave dataset are complete for three different wave conditions (Test A2, B2 and C2), with data measured at all wave gauges (GHM01 to GHM08) indicated on Fig.5.2. The influence of the length of the analyzed time series on the calculated wave

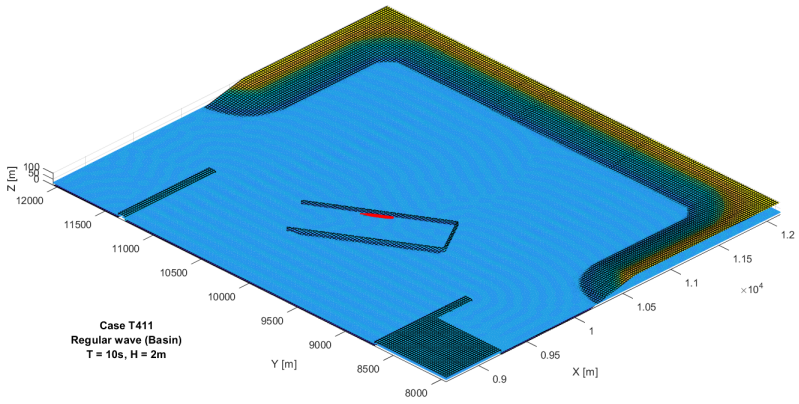

Figure 5.29: Test case A2, regular wave in basin with structure

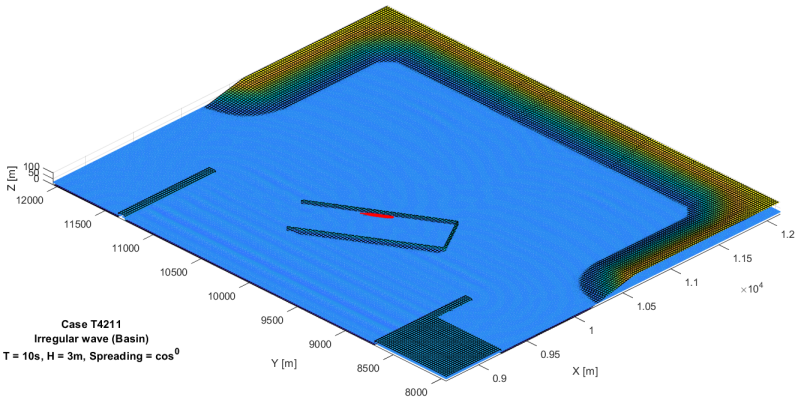

Figure 5.30: Test case B2, long-creted wave in basin with structure

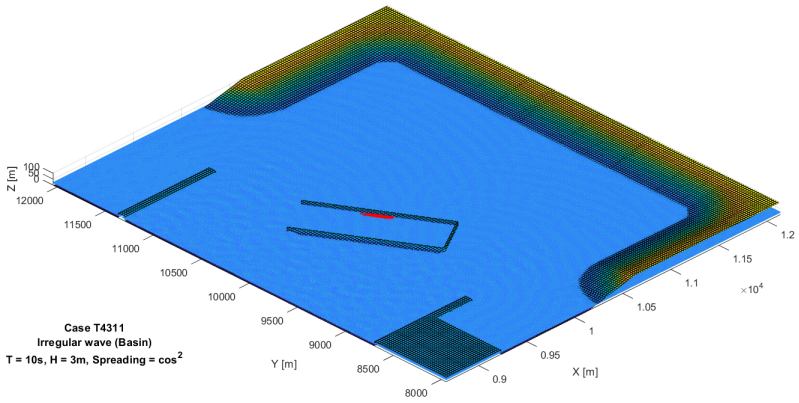

Figure 5.31: Test case C2, short-crested wave in basin with structure

spectra parameters for test A2, B2 and C2 are shown in Fig.5.32,5.33 and 5.34 respectively. With 3 hours time series the convergence is considered sufficient. Therefore the duration of the numerical simulations is set as 3 hours. The first 9 minutes are excluded from both the measured and numerically simulated time series to prevent the influence of the initial conditions on the analysis.

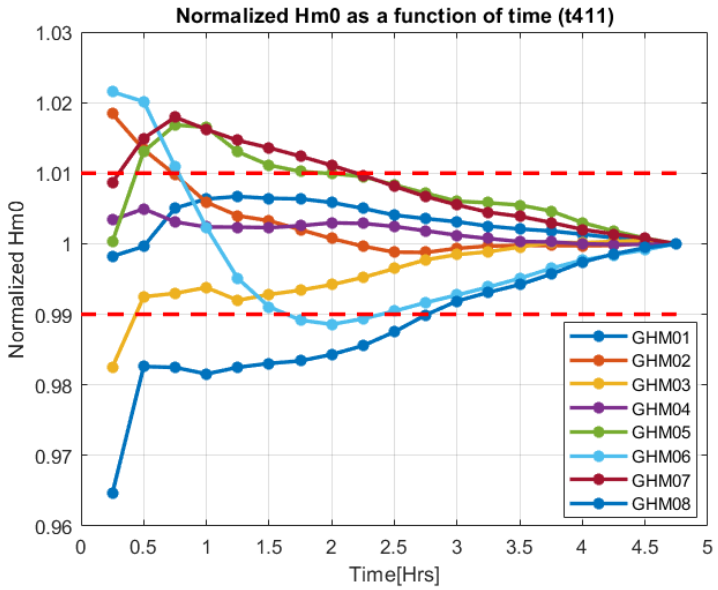

Figure 5.32: Hm0 variation of time (test case t411 (A2))

The significant wave height from measurements and simulations at all gauges are shown in Table.5.9 and 5.10. The significant wave height at wave gauges outside the harbour (GHM01 to 04) from simulation fit well with the results from measurement, however, in SWASH simulation significant wave height at all wave gauges locate within the harbour (GHM05 to 08) greatly reduced with respect to the wave outside the basin. In model test,

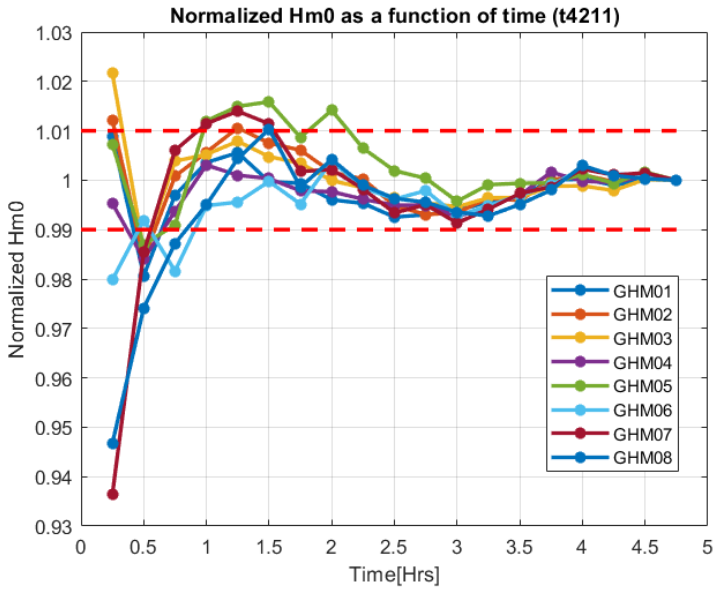

Figure 5.33: Hm0 variation of time (test case t4211 (B2))

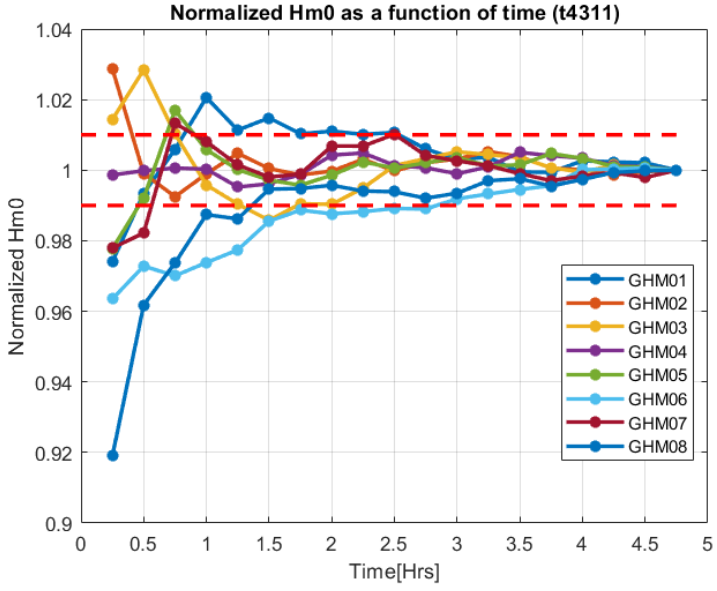

Figure 5.34: Hm0 variation of time (test case t4311 (C2))

the significant wave height along all wave gauges are much uniform than in simulation, this phenomenon because of the harbour is open to the wave maker, and the wall are vertical and very smooth and reflective, therefore the energy dissipation from wave-wall interaction is very small in model test, to investigated potential reasons of this difference, the map of significant wave height of the whole domain are given in Fig.5.35, 5.36 and 5.37

Table 5.9: Measured and simulated significant wave height for test A2

Wave gauge	Test A2 Hm0 [m]		
	Measured	Simulated	Difference(%)
GHM01	0.89	1.01	13.48
GHM02	1.00	1.00	0.00
GHM03	1.00	1.03	3.16
GHM04	1.07	1.10	2.80
GHM05	1.00	0.66	-34.23
GHM06	0.92	0.32	-65.22
GHM07	0.99	0.22	-77.78
GHM08	0.78	0.30	-61.54

Table 5.10: Measured and simulated significant wave height for test B2 and C2

Wave gauge	Test B2 Hm0 [m]			Test C2 Hm0 [m]		
	Measured	Simulated	Difference(%)	Measured	Simulated	Difference(%)
GHM01	3.35	2.99	-10.53	3.46	2.99	-13.47
GHM02	3.22	3.01	-6.21	3.37	3.03	-10.19
GHM03	3.44	3.00	-12.88	3.40	2.98	-12.41
GHM04	3.92	3.19	-18.83	3.36	2.65	-21.22
GHM05	2.99	1.26	-57.88	3.35	1.07	-58.09
GHM06	2.30	1.06	-54.22	2.95	1.20	-59.21
GHM07	2.53	1.05	-58.55	2.34	1.09	-53.46
GHM08	2.05	1.12	-45.36	2.68	1.14	-57.54

The map of significant wave height for all three cases are shown in Fig.5.35, 5.36 and 5.37. From the maps of significant wave height of the whole domain, the harbour is indeed affecting the wave propagation, as there is a sheltered area in lee side. To some extents, this means the structure is well presented, however, as shown in all figures, the gravel slope beside the wall expected to dissipate the wave energy and lead a reduction of significant wave height, in simulation the influence of this dissipation layer is marginal, since for all three case, the wave field in between wave makers and port is uniform, this may because of the porosity of this small sponge layer is not well defined in simulation (higher than real value), however this still can not explain the reduction of wave height inside the port (low energy dissipation outside the port should induce higher wave height within the port), so it seems very likely that position of the sponge layer is not well defined in simulation (partially inside the port, therefore the wave energy inside the port is partially dissipated), however, from Fig.5.5, this possibility is very small, the other potential reason may because of considerable numerical dissipation, for wave propagation in open water, the simulated significant wave height at GHM01 to 03 with 4x4m grid has been proved sufficient with comparing the significant wave height from model test, however, when including harbour, a finer grid precision may have to be applied to well simulate the wave behaviour around the structure, or at least a locally finer grid (curvilinear grid) around

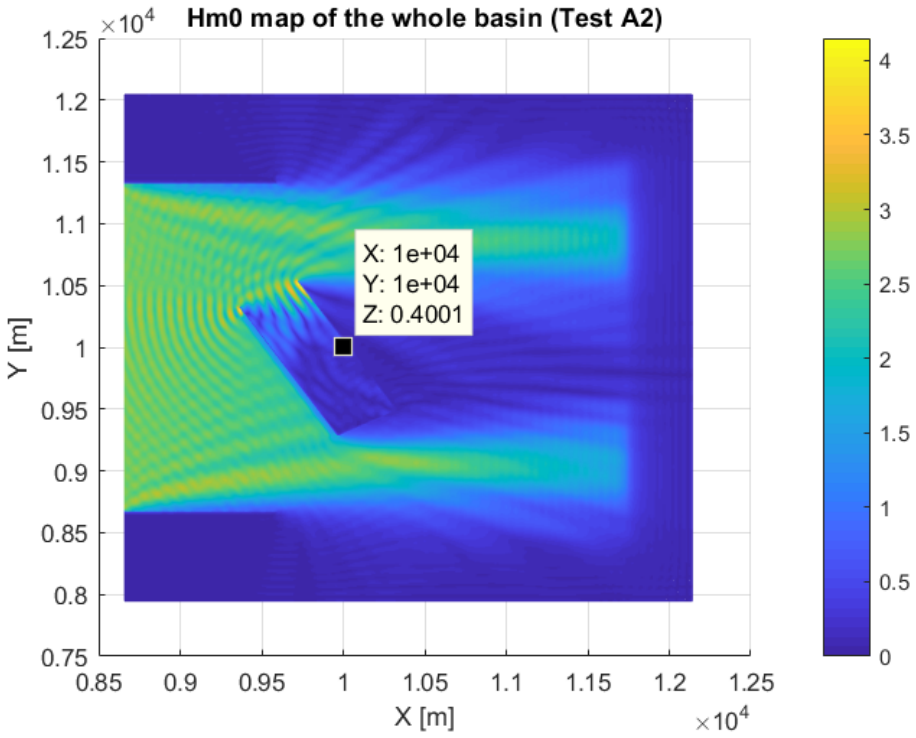

Figure 5.35: Hm0 of the whole domain (Test A2)

the structure should be applied (100 grids/per wave length is recommended from The SWASH Team (2017)).

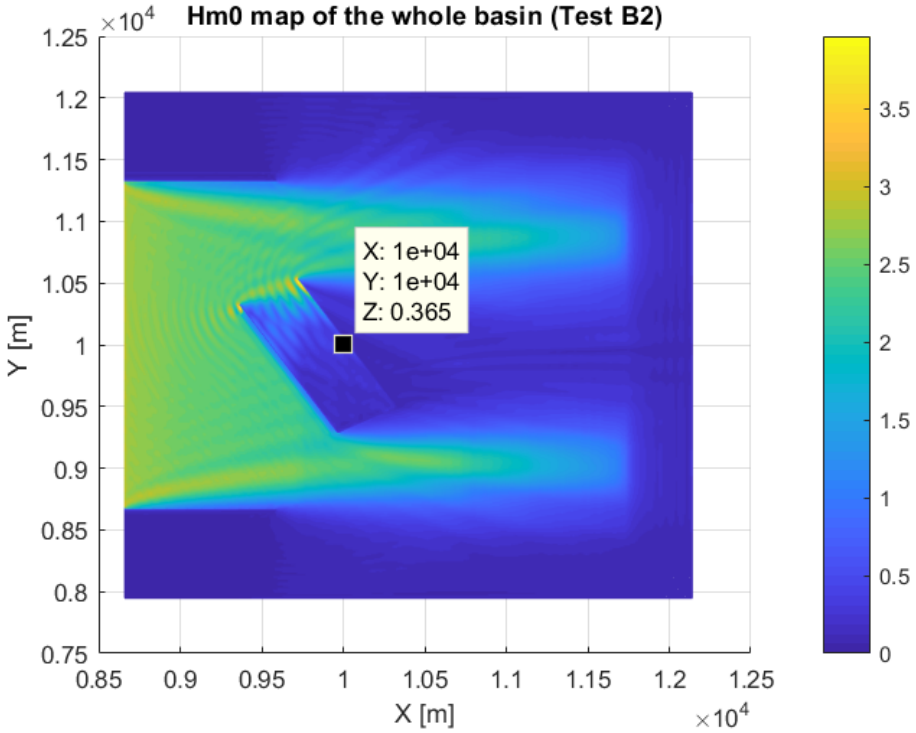

Figure 5.36: Hm0 of the whole domain (Test B2)

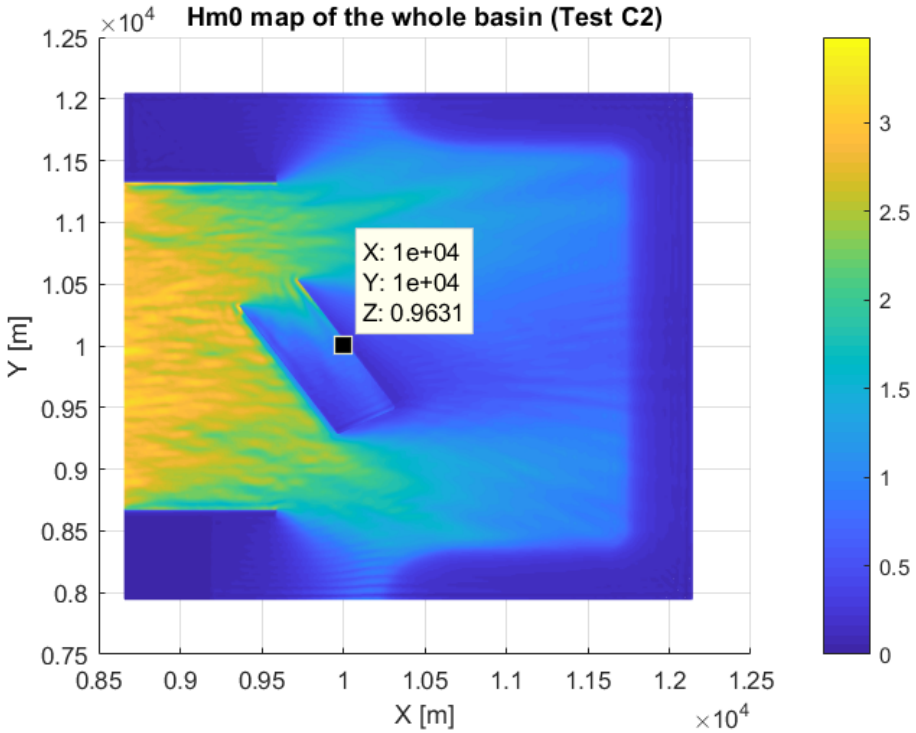

Figure 5.37: Hm0 of the whole domain (Test C2)

5.8 Conclusion

- During validation, the SWASH model has been proven to be capable of reproducing the complex wave propagation in open water case, in this case involving considerable wave reflection, wave diffraction and non-linearities. SWASH model setting with 30 grid points/wave length ($30/\lambda$) has been proven sufficiently for wave simulation, to couple SWASH with DIFFRAC, 4 vertical layers with smooth layer ditribution are required.
- In model test of wave propagating in the basin with port, the superposition of incident wave and reflected wave near the wall produces higher waves, however this phenomenon is not shown in executed SWASH simulation, the reason has to be investigated. The difference between wave modelling and wave simulation is the main potential source of inaccuracies to the overall approach. This may not be due to the limitations in SWASH model, but the wrong model setting, for irregular waves such impertinent model setting is hard to be investigated only by comparing the wave spectrum against the wave data at gauges. If the computed wave information provided to the coupling tool and DIFFRAC model is wrong, it will likely result in the incorrect forces, making the overall approach inaccurate.
- Detailed information about the setup of model test is of prime importance when setting up numerical models aiming to reproduce the experiments. The lack of information limits the capacity of drawing conclusions and understanding possible disagreements between measured and modelled results.
- For unidirectional wave, including both regular and long-crested spectral wave, the approach with 'Partial overlapping FFT' has been proven with good performance.
- For more complicated wave condition including wave directional spreading and more non-linearities during wave development, the simulated wave forces and moments spectra from 'Partial overlapping' method is less stable than in unidirectional wave case. This instability mainly comes from the potential uncertainties within wave direction calculation, which can come from SWASH simulation and the coupling tool. Regarding the results from 'Full FFT' method, the computed forces and moments are in agreement with in both time domain and frequency domain for open water case, the influence of the linear potential model for the radiated waves and the assumption of relatively small ship motions could not be addressed based on the validation results because in the model tests the ship is restrained to the fixed position.
- The developed coupling tool to combine SWASH and DIFFRAC models in order to predict wave forces acting on a moored ship is consistent and can be considered for future applications.

Chapter 6

Final considerations

6.1 Conclusions

The main objectives of this study, as proposed in Chapter 1, are:

- Analyse the overall approach identifying the contribution of the different steps and associated assumptions/simplifications to the accuracy of the calculations;
- Develop a coupling tool to combine the wave model SWASH and the 3D diffraction model DIFFRAC in order to compute wave forces acting on floating bodies;
- Investigate the influence of SWASH model definitions in the predictions of forces acting on moored ship;
- Validate the combination SWASH/DIFFRAC for the computation of the wave fields and resulting forces acting on a moored ship.

The SWASH model is able to handle in a robust way the relevant physical processes involved in non-linear wave propagation through intermediate and shallow waters, possibly taking into consideration complex port geometries. The overall results indicate that the SWASH model results are consistent provided that: i) the number of vertical layers is sufficient (especially in relatively deep waters); ii) the horizontal resolution of the computational grid is sufficient; iii) important terms of the momentum equation are modelled with higher-order numerical schemes (especially for non-linear waves in relatively deep waters). Possible inaccuracies in this sense refer to amplitude errors, while dispersion errors have shown to be a minor issue for the tested conditions. The SWASH model computations times are very sensitive to the horizontal grid resolution, so usually a trade-off has to be made between the required accuracy of the results and the acceptable computation time.

The wave simulations of the validation tests show that generally the SWASH model results compare well with the measured dataset when do not involve the structure, albeit that the numerical model setup may differ from the scale tests in a number of characteristics, e.g. representation of the porous slopes and bottom friction, properties of the wave makers to

absorb reflected waves. The absence of a clear restriction in this sense makes SWASH a potential candidate for practical applications.

A computational tool was developed to make the coupling between the SWASH model outputs and DIFFRAC model inputs, enabling the combination of the two models to calculate wave forces on moored ships. The tool proved to be accurate for the simplified tested conditions in Chapter 4 and the validation tests in Chapter 5, for even complicated wave case (including structure), the SWASH simulation has big deviations with model test data, therefore the performance of developed coupling tool can not be investigated. The performance of the tool is optimal in shallower waters (say $kd < 3$). For relatively short waves the vertical distribution of wave quantities is more curved and additional vertical layers should be considered in the SWASH modelling in order to accurately prescribe the wave velocities and pressures along the hull of the ship. Nonetheless, waves with these characteristics are generally less relevant in coastal regions.

Linear potential theory is applied in the DIFFRAC model for the computations of the wave-body interactions, so the non-linearities in the scattered and radiated waves are assumed to be sufficiently small. The wave height and the body motions are also assumed sufficiently small compared to the body dimensions so that the first-order forces acting on the restrained body dominate the second-order corrective loads. Further, the DIFFRAC model considers only mean second-order forces and moments.

The result of the studied approach (SWASH + coupling tool + DIFFRAC) for the testing cases considered in the validation indicate that measured and computed forces and moments acting on a restrained ship are generally in good agreement. More pronounced differences occurred for 'roll' and 'yaw' moments, but these can be associated to inaccuracies on the measurements and other external factors effect in simulation. Overall disagreements might also be related to deviations in the simulated wave fields and in the DIFFRAC computations of forces.

The practical considerations given in the previous paragraphs the answer to the research question of the study:

To which extent can the SWASH wave model and the DIFFRAC model be combined in order to accurately compute wave forces acting on moored ships?

Each computational tool considered in the proposed approach (the wave model SWASH, the developed coupling tool, and the diffraction model DIFFRAC) can contribute to the inaccuracy of the computed wave forces acting on a moored ship.

Although the SWASH model has shown to be physically consistent and a robust numerical tool, the wave modelling is the main potential source of inaccuracies to the overall approach. Errors in the wave model can be related to insufficient computational grid resolution and the use of first-order schemes for relatively important terms, but also due to a misrepresentation of the simulated area, e.g. on the bathymetry definition, bottom friction coefficients, implementation of structures and boundary conditions, this is clearly shown for SWASH simulation case with harbour geometry.

The coupling tool is generally sufficiently accurate without introducing additional requirements to the wave simulations. In such cases the coupling procedure requires additional

vertical layers to be considered in the SWASH simulations.

The computations of first-order forces with the DIFFRAC model will be reliable provided that the general model setting are consistent and the hull of the ship and wave information are properly defined. Relatively larger deviations can occur for the second-order forces computed with DIFFRAC. In practical applications this simplifications will impact the computed drift forces, although the relative errors are expected to be reduced when the incident short waves are small and the low-frequency loads are dominated by the low-frequency waves.

Under those conditions the potentiality of the proposed approach is remarkable relative to current methods. In deeper and more complicated areas, widely available tools may be applied to compute the wave loads acting on a floating body.

6.2 Recommendations

The items listed below include possible improvements to the numerical tools used in this study and potential subjects for future research.

1. Investigate the effect of different combination of four discretization methods of advection terms in momentum equations, the influence of different combination may not significantly affect the water elevation in SWASH simulation, but the velocity components in each layer, therefore, the influence is hard to be investigated within limit number of simulations but may greatly influence the results of diffraction analysis (not only about DIFFRAC).
2. In 'Partial overlapping FFT' method, the biggest potential uncertainty is from the calculation of wave directions of short-crested wave. The 'Max entropy method' has been verified against unidirectional wave with including both regular and irregular long-crested wave, but the effect of duration of simulation and the complexity of the wave still needs to be investigated.
3. In the phase of validation, some of the phenomenon only exist in model test (i.e. standing wave in open water case), which have a big possibility from the limitation of the size of the model basin, therefore simulation in model scale is recommended to eliminate the influence.
4. Investigate *scale effects* on viscous bottom friction in physical scale model tests. Understand its occurrence and consequences to short wave propagation over relatively large distances and damping of seiching modes in semi-enclosed basins. Perform sensitivity tests with a numerical wave model, varying the bottom friction formulation and coefficient in order to comprehend the wave damping in scale model tests and its relation to wave damping in prototype scales.
5. In this project, the validation for the case including harbour geometry is not managed to fit with the results from model tests, but the SWASH simulation in (Rijnsdorp et al.,) fits very well with the reference cases for complicated basin geometry with even extreme wave case. therefore, performing additional systematic tests with the

proposed modelling chain (SWASH model + coupling tool + DIFFRAC model) considering non-linear waves and variable bottom topography is important to investigate the limitation of this coupling chain. Compare results with measurements and/or other numerical tools, identifying disagreements and possible limits of application. A verification against typical frequency-domain diffraction models based on linear potential theory could give insight on the applicability of those tools in shallow waters, where non-linearities in the incident waves are not negligible.

6. SWASH simulation is quick and accurate for independently usage, to couple SWASH with other software in order to calculate the force acting on the offshore structure, a guideline for representing coastal and port structures in SWASH model simulations (e.g., breakwaters, quay walls, access channel) in recommended, this because the friction coefficient of structure can not be included in SWASH simulation, the possible method to reduce the wave reflection can be increasing the porosity of the structures.

7. Verify the applicability of proposed modelling approach with the SWASH and DIFFRAC models in an existing practical case.

References

Bakkedal, E. (2014). Alternative methods of realizing the sea spectrum for time-domain simulations of marine structures in irregular seas. (June).

Bijleveld, H. J. M. (2004). Projectbeschrijving R&D Haves EZ-LIP: H3896.40 Validatie golfkrachten op schepen.

Bingham, H. B. (n.d., apr). A hybrid Boussinesq-panel method for predicting the motion of a moored ship. *Coastal Engineering*(1), 21–38. doi: 10.1016/S0378-3839(00)00002-8

Butt, T. (2010). Infragravity Waves: Part 1. (June). Retrieved from `http://www.surfscience.org/articles/infragravity-waves-part-1`

Dobrochinski, J. P. H. (n.d.). A combination of SWASH and Harberth to compute wave forces on moored ships. *Tu Delft*(October).

Hasselmann, K. (1962). On the non-linear energy transfer in a gravity-wave spectrum: Part 1. General theory. *Journal of Fluid Mechanics*. doi: 10.1017/S0022112062000373

Journée, J., Massie, W. (2002). Offshore Hydromechanics. *Electrochimica Acta*. doi: 10.1097/DCC.0b013e318276822f

Krogstad, H. E. (2000a). LINEAR WAVE THEORY Random waves and wave statistics. *Science And Technology*, *45*(February), 197–208.

Krogstad, H. E. (2000b). LINEAR WAVE THEORY Regular waves. *Science And Technology*(February). doi: http://folk.ntnu.no/oivarn/hercules_ntnu/LWTcourse/lwt_new_2000_Part_A.pdf

Lygre, A., Krogstad, H. E. (n.d.). *Maximum Entropy Estimation of the Directional Distribution in Ocean Wave Spectra* (No. December). doi: 10.1175/1520-0485(1986)016<2052:MEEOTD>2.0.CO;2

MARIN. (2017). *DIFFRAC: User Guide* (Tech. Rep.). Retrieved from `www.marin.nl`

Mathuranathan. (2011). FFT and spectral leakage. (January). Retrieved from `https://www.gaussianwaves.com/2011/01/fft-and-spectral-leakage-2/`

MELLINK, B. (2012). Numerical and experimental research of wave interaction with a porous breakwater. (1230166).

Monteban, D. (2016). Numerical modelling of wave agitation in ports and access channels. (June).

Munk, W. H. (2010). ORIGIN AND GENERATION OF WAVES. *Coastal Engineering Proceedings*. doi: 10.9753/icce.v1.1

Rahman, M., Riordan, D., Susilo, A., Mousavizadegan, S. H. (n.d.). The fast Fourier transform applied to estimate wave energy spectral density in random sea state. , *115*, 133–144.

Rijnsdorp, D. P., Smit, P. B., Zijlema, M. (2014). Non-hydrostatic modelling of infragravity waves under laboratory conditions. *Coastal Engineering*, *85*, 30–42. doi: 10.1016/j.coastaleng.2013.11.011

The SWASH Team. (n.d.). SWASH User Manual version 4.01A.

van der Molen, W. (2006). *Behaviour of Moored Ships in Harbours.*

van der Molen, W., Wenneker, I. (2008). Time-domain calculation of moored ship motions in nonlinear waves. *Coastal Engineering*. doi: 10.1016/j.coastaleng.2008.01.001

van Dongeren, A., Klopman, G., Reniers, A., Petit, H. (n.d.). High-Quality Laboratory Wave Generation for Flumes and Basins. *Ocean Wave Measurement and Analysis (2001)*(October 2015), 1190–1199. doi: 10.1061/40604(273)120

Zijlema, M., Stelling, G. S. (2005). Further experiences with computing non-hydrostatic free-surface flows involving water waves. *International Journal for Numerical Methods in Fluids*. doi: 10.1002/fld.821

Zijlema, M., Stelling, G. S., Smit, P. B. (2011). Simulating nearshore wave transformation with non-hydrostatic wave-flow modelling. *Conference Proceedings, 12th Int. Workshop on Wave Hindcasting*

and Forecasting, Hawaii, USA, 1–11.

Appendix A

SWASH model

SWASH models water waves by solving the non-hydrostatic Reynolds-averaged Navier-Stokes equations for an incompressible fluid and a free surface. The free surface motion is tracked by applying the non-linear shallow water equations with the addition of a vertical momentum equation and non-hydrostatic pressure in horizontal momentum equations. The numerical approach adopted in SWASH requires much fewer grid cells in the vertical direction than other alternative methods. Additionally, with appropriate conservation properties, the non-linear shallow water equation is able to deal accurately with gradients or discountinuities in the flow and the combined effects of wave-wave and wave-current interaction in shallow water without need of any additional modeling.

In a two dimensional (2D) framework that is bounded by the free surface $z = \zeta(x,t)$ and the bottom $z = -d(x)$, where t is time and x and z are Cartesian co-ordinates (z = 0 is located at the still water level), the governing equations read (Rijnsdorp et al., 2014):

$$\frac{\partial u}{\partial x} + \frac{\partial w}{\partial z} = 0 \tag{7.0.1}$$

$$\frac{\partial u}{\partial t} + \frac{\partial uu}{\partial x} + \frac{\partial wu}{\partial z} = -\frac{1}{\rho}\frac{\partial (p_h + p_{nh})}{\partial x} + \frac{\partial}{\partial x}(v^h \frac{\partial u}{\partial x}) + \frac{\partial}{\partial z}(v^v \frac{\partial u}{\partial z}) \tag{7.0.2}$$

Equation (7.0.1) holds the conservation of mass and equations A.2 and A.3 the conservation of x- and z- momentum. Equations are solved in time t and along directions x and z. u(x,z,t) is the horizontal velocity, w(x,z,t) is the vertical velocity, v^h and v^v are the horizontal and vertical kinematic eddy viscosities, g is the gravitational acceleration, and p_h and p_{nh} are the hydrostatic and non-hydrostatic pressures, respectively. The hydrostatic pressure is expressed in terms of the free surface elevation $\zeta(x,y,t)$ measured from the still water level:

$$p_h = \rho g(\zeta - z) \tag{7.0.3}$$

An expression for the free surface is obtained by considering the (global) mass balance for the entire water column($d(x, y)$ is the still water depth):

$$\frac{\partial \zeta}{\partial t} + \frac{\partial}{\partial x} \int_{-d}^{\zeta} u dz = 0 \tag{7.0.4}$$

The bottom friction term can be included in the horizontal momentum balance equations. The coefficient that can be specified in different ways, including a constant value, the well-known Manning and Chezy roughness coefficients, and the logaritmic wall-law for either smooth or rough beds.

Incident regular or irregular waves are introduced at open boundaries of the computational domain by specifying normal horizontal velocities based on second-order wave theory. Though, in the current version (4.01A) of SWASH only the difference interactions are incorporated. The sum interactions (i.e. bound super harmonics) are not included for efficiency reasons.

The vertically varying velocity amplitude of the primary wave components is related to the shortwave amplitude and determined by linear wave theory. In coastal waters the bound infra-gravity wave component are essentially shallow-water waves, for which the vertical variation is negligible. The velocity amplitude associated to the bound infra-gravity waves is assumed to be vertically constant and is computed based on the free wave components following (Hasselmann, 1962).

To simulate waves entering the domain without reflections at this boundary, a weakly reflective condition allowing outgoing waves is adopted. The total velocity signal is determined as the superposition of the incident velocity signal and a velocity signal of the reflected waves. To estimate the velocity of the reflected wave signal, the reflected waves are assumed to be shallow water waves, progressive, of constant form and propagating perpendicular to the boundary. The depth averaged horizontal velocity can be calculated from mass conservation using surface elevation of the outgoing waves (i.e. the difference between the target surface elevation and the instantaneous surface elevation computed by SWASH). This type of radiation conditions has been shown to lead to good results with nearshore wave conditions, especially for waves approaching the boundary on small angles ($< 30°$).

Two options are available to approximate the onshore boundary condition: the moving shoreline used in inundation or run up computations; and an absorbing condition (e.g. Sommerfeld's radiation condition) which allows the (long) waves to cross the outflow boundary without reflections. The radiation condition may be combined with a sponge layer technique.

Space discretization of the governing equations is carried out in a staggered grid arrangement, in which the velocity components are located at the center of the cell faces and the water level is located at cell center. With this choice non-physical oscillations related to decoupling of the unknowns are prevented. The non-hydrostatic pressure along the vertical terrain-following grid can be given either at the cell center (standard layout) or at the layer interface (box layout).

For the time integration of the continuity and momentum equations an explicit leapfrog scheme in conjunction with a second order explicit time step for advection, a first order explicit time step for the viscosity term and a first order implicit time step for the non-hydrostatic part is used. This variant of the leapfrog is second order accurate in time and does not introduce wave damping. To achieve second order accuracy in space for the approximation of the water depth a higher order interpolation is added, augmented with a flux limiter to avoid unwanted oscillations near sharp gradients. A special treatment of the advection term is required for momentum conservation. This is covered with detail in Zijlema et al. (2011).

The non-hydrostatic pressure is governed indirectly by the local continuity equation. This equation is linked to the momentum equations by means of a second order correction pressure technique. The discretized forms of the equations are combined to give a Poisson equation linking the non-hydrostatic pressure correction at a grid point to its neighbors. As a result, local mass conservation is enforced (Zijlema and Stelling, 2005).

Because mass and momentum are strictly conserved at discrete level, the adopted scheme is able to deal with flows with a wide range of Froude numbers. Once the wave height over depth ratio becomes relatively large, a discontinuity develops as a wave steepens up and develops a vertical face. In such a situation, the model conserves momentum over the discontinuity and energy is dissipated at a rate analogous with that of a bore. Therefore, energy dissipation of a breaking wave is intrinsically considered by SWASH.

However, a high vertical resolution is required to reproduce the observed locations of incipient wave breaking (10 layers), whereas at low vertical resolutions wave breaking is delayed.

To capture wave breaking with only a few vertical layers (say 2 layers) and make the simulations more efficient, the non-hydrostatic pressure can be neglected in the vicinity of a breaking wave, ensuring that a wave develops a vertical face. This approach is initiated once the rate of change of the free surface exceeds a predefined threshold.

Because the time stepping is of explicit type, the stability criteria should be met for a stable solution (i.e. conditional stability). The well-known CFL condition for 2D problem is given by:

$$C_r = \Delta t(\sqrt{gd} + \sqrt{u^2 + v^2})\sqrt{\frac{1}{\Delta x^2} + \frac{1}{\Delta y^2}} \tag{7.0.5}$$

with Δx and Δy the mesh width, Δt the time step, u and v the flow velocity components and C_r the Courant number.

The time step is dynamically adjusted by SWASH in order to keep the Courant number within a user prescribed range. Usually, the minimum Courant number (C_r) is set to 0.2, while the maximum C_r is specified in the range of 0.5 to 0.8. For high, nonlinear waves, or wave interaction with structures with steep slopes (e.g. jetties, quays), a maximum Courant number of 0.5 is advised by the The SWASH Team (2017).

When a large number of vertical layers are taken into account, the standard layout us-

ing explicit central differences for the approximation of vertical non-hydrostatic pressure gradients is sufficiently accurate and preferable due to its robustness. The box layout applying the implicit Keller-box scheme or compact scheme to determine the gradients is recommended at low vertical resolution, say 5 layers or less, because it gives relative low numerical dispersion and dissipation.

Regarding the computational domain in the horizontal plane, it is recommended to keep the area of interest at least two wave lengths away from the boundaries. Additionally, it is wise to choose the grid axes being aligned as much as possible with the dominant wave direction. One should ensure that the spatial resolution is sufficiently high so that the most energetic wave components are resolved accurately on the grid. According to the User Manual, for low waves it is sufficient to take 50 grid cells (or 51 grid points) per peak wave length. For relatively high waves, however, it is recommended to take at least 100 grid cells per peak wave length The SWASH Team (2017).

Numerical settings related to the discretization of advection terms in the momentum equation must be taken into account according to the simulated conditions. The default and recommended settings under non-linear and non-hydrostatic conditions are given in Table 7.1. It is highlighted that some of the recommended schemes are automatically considered by SWASH depending on other model settings. Additional explanation is given on Section 5.4.5 of the The SWASH Team (2017).

Table 7.1: Discretization of advection terms in the momentum equations. BDF: 2^{nd} order Backward Difference Scheme; CDS: 2^{nd} order Central Differences Scheme; UPW: 1^{st} order Upwind Scheme. The highlighted schemes are recommended by the model developer (Marcel Zijlema, personal communication 2014).

Term	**Default**	**Adapted**
$u\frac{\delta u}{\delta x}$ (H. Adv. of H-momentum)	BDF	**BDF** or CDS
$w\frac{\delta u}{\delta z}$ (V. Adv. of H-momentum)	UPW	BDF or **CDS**
$u\frac{\delta w}{\delta x}$ (H. Adv. of V-momentum)	Usually ignored	**BDF** or CDS
$w\frac{\delta w}{\delta z}$ (V. Adv. of V-momentum)	Usually ignored	UPW

When the model is forced with wave spectra, the maximum frequency that should be accurately represented by the model is ideally about 1.5 to 2 times the peak frequency. One must be aware that some so-called evanescent modes might be also included in the input spectra. These modes are a general property of the underlying model equations and show exponential decay with distance from the boundary at which the spectrum is imposed. The frequencies at which the evanescent modes are generated is above the cut-off frequency, which is determined by the dispersive properties of the model equations. Accordingly, the cut-off frequency (f_{cf}) is given by:

$$f_{cf} = \frac{\omega_{cf}}{2\pi} = \frac{2K}{2\pi}\sqrt{\frac{g}{d}} \tag{7.0.6}$$

with K the number of layers used in the model. Hence, the lowest wave period to considered in the model simulation equals $1/f_{cf}$ (waves shorter than that will be removed by SWASH).

SWASH has been extended to cover porous flow and predict partial reflection and transmission through breakwater, for instance. The Forchheimer relation is included in the porous momentum equations by means of two extra friction terms f_l(laminar) and f_t (turbulent), in which the grid cells have a porosity ranging from n=0 (wall) to n=1 (pure water). The friction terms in the momentum equation are MELLINK (2012):

$$f_l = \alpha_0 \frac{(1-n)^2}{n^3} \frac{v}{D_n^2 50} \cdot u \tag{7.0.7}$$

$$f_t = \beta_0 \frac{(1-n)}{n^3} \cdot \frac{1}{D_{n50}} \cdot u \cdot abs(u)..... \tag{7.0.8}$$

where:
n = pore volume/total volume = porosity
u = horizontal flow velocity
v = kinematic viscosity
D_{n50} = normal stone diameter
α_0 = particle-form constant for laminar friction loss (default: 1000)
β_0 = particle-form constant for turbulent friction loss (default: 2.8)

In order to implement a porous structure in a SWASH simulation, the structure height above the bottom level, the characteristic grain size, and porosity should be specified along the domain. SWASH computes an average porosity for a given grid cell based on the porosity and height of the structure relative to the water depth (or vertical dimension of the layer). Therefore, the effect of a porous slope, for example, is approximated as a gradual variation on the average porosity, instead of a physical boundary (the bottom level remains below the structure). Further, the porosity is only taken into account in the horizontal component of the momentum conservation equations, so vertical velocities are not damped by the porous structure.

Space-varying input quantities are imposed to SWASH by means of input grids. The spatial resolution of the input grid is not necessarily the same as that of the computational grid. Structures can be represented in the model in different ways: 1) included in the bathymetry definition (impermeable); 2) by means of porous structures; 3) specifying permanently dry points in the computational grid by means of exception values (impermeable); or 4) combinations of the previous options.

From a stability point of view, the second option is preferred. The other choice may be better when detailed results are required in the vicinity of the (impermeable) structure. In this case the modeller is advised to use a larger threshold of water depth to prevent instabilities. The use of exception values on the computational grid may be problematic when the computations involve parallel processing (The SWASH Team, 2017).

Appendix B

DIFFRAC Model

The program package DIFFRAC calculates the hydrodynamic property of floating or moored bodies in regular waves or wave group in restricted water. The program is applicable to both shallow and deep water.

The hydrodynamics involved follow from 3D potential theory including wave radiation and diffraction. The program DIFFRAC is capable of handling the hydrodynamics of any number of independently moving bodies.

Mathematical formulation of the linearised theory

The fluid is assumed to be ideal and irrotational. For long-crested waves of frequency ω, the free surface displacement ζ and the potential Φ can be related in first order to their spatial factors:

$$\zeta(x,t) = Re(\eta(x,y)e^{-i\omega t}) \tag{8.0.1}$$

$$\Phi(x,t) = Re(\phi(x)e^{-i\omega t}) \tag{8.0.2}$$

The fluid velocities are related to the potential by its gradient:

$$u(x,t) = e^{-\omega t}\nabla\phi \tag{8.0.3}$$

Cartesian coordinates are used.

The sign convention is according to a right-handed space fixed coordinate system with origin in the free surface in the free surface. Also another ship-fixed coordinate system, with axis in the center of gravity will be used Fig.8.1

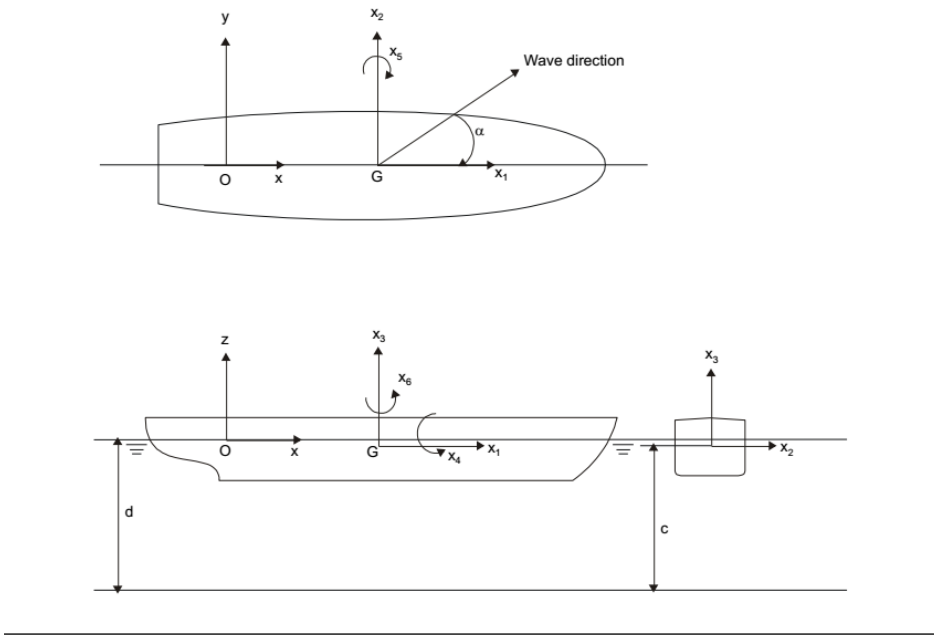

Figure 8.1: The coordinate system in DIFFRAC

The oscillatory motions in the center if gravity are given by:

$$X_j = |X_j|e^{i\omega t}, j = 1..6 \tag{8.0.4}$$

The motions are defined with respect to the center of gravity. The motion variables x_1, x_2 and x_3 stand for the translations surge, sway and heave, while x_4, x_5 and x_6 stand for rotational motions, the so-called Eulerian angles. Since only small oscillatory motions are considered, these Eulaerian angles coincide with the angular displacements in a space-fixed coordinate system. The motions in the center of gravity can be used to compute the motion X in any other point on the body.

The fluid domain will be limited by the following boundaries:

1. The free surface.
2. Bottom surface.
3. The body surface.

The governing set of linearised equations of the first-order potential can be stated as follows:

$$\Delta\phi(x) = 0 \tag{8.0.5}$$

x within th fluid domain V

$$-\omega^2\phi + g\frac{\partial\phi}{\partial z} = 0 \tag{8.0.6}$$

in the plane z = 0, the free surface, g is the gravitational constant

$$\frac{\partial \phi}{\partial n}(x) = -i\omega X \cdot n \tag{8.0.7}$$

x on the rigid body boundary B, where v is velocity of the body and n is normal vector of B pointing into the fluid.

$$\frac{\partial \phi}{\partial n}(x) = 0 \tag{8.0.8}$$

x on the bottom boundary z = -d

In case of open water and a constant water depth, the following analytical expression satisfies these equations:

$$\phi_0 = \frac{g\zeta_a}{\omega}\frac{coshk(z+d)}{coshkd}exp[ik(xcos\alpha + ysin\alpha) - i\omega t] \tag{8.0.9}$$

This so-called incoming wave potential which is used in DIFFRAC.

The relation between the wave length λ and the wave frequency ω is given by the dispersion relation.

In the following it is assumed that there exist M independently moving bodies. Because of the linearization adopted, the velocity potential ϕ can be separated into various quantities:

$$\phi = \phi_0 + \phi_7 + \sum_{m=1}^{M}\sum_{j=1}^{6}\phi_{mj} \tag{8.0.10}$$

where: ϕ_0: incidental wave potential, ϕ_{mj}: potential due to the motion m of body B_j, ϕ_7 = diffracted wave potential.

Substituting (8.0.10) in the free-surface condition on the damping zone, reveals the following boundary conditions for the radiated and diffracted potentials in the damping zone:

$$\frac{\partial}{\partial z}\phi_7(x) - (1 - i\epsilon)\frac{\omega^2}{g}\phi_7(x) = 0 \tag{8.0.11}$$

$$\frac{\partial}{\partial Z}\phi_{mj}(x) - (1 - i\epsilon)\frac{\omega^2}{g}\phi_{mj}(x) = 0 \tag{8.0.12}$$

The solution of equation (8.0.5) through (8.0.6) will be given by an integral equation method using a distribution of sources (Green functions with varying strength) over the domain boundaries.

For the first-order potential a frequency dependent Green function is used that satisfies the free-surface condition and the bottom boundary condition:

$$G = -\frac{1}{r} + \frac{1}{r'} + F(h, \omega) \tag{8.0.13}$$

The Green's function in (8.0.13) gives the amplitude of the potential of an oscillating source of unit strength.

These sources are distributed over the hull surface. By applying the hull boundary condition for the first-order potential, the source strength is found.

According to the decomposition of the velocity potential in equation (8.0.10) the source strength can also be decomposed into several components, e.g.

$$\sigma(x) = \sigma_7(x) + \sum_{m=1}^{M} \sum_{j=1}^{6} \sigma_{mj}(x) \tag{8.0.14}$$

in which M is the total number of bodies and j is the mode of motion(j = 1..6).

The boundary condition for the forced oscillation problem can be described as:

$$\begin{aligned} \frac{\partial}{\partial n}\phi_{mj}(a) &= -i\omega n_j(a) \quad a \in S_m \quad m = 1, ..m \\ &= 0 \quad a \in S_B | S_m \quad = 1, ..6 \end{aligned} \tag{8.0.15}$$

where $n_j(a)$ is the direction cosine vector.

The boundary condition for the diffraction problem is:

$$\frac{\partial}{\partial n}\phi_7 = -\frac{\partial}{\partial n}\phi_0 \tag{8.0.16}$$

in case of a forced oscillation, the integral equation (2,24) results into:

$$-\frac{1}{2}\sigma_{mj}(x) + \int_{S_b} \sigma_{mj}(\vec{\rightarrow} \xi)\frac{\partial}{\partial n}G(\overrightarrow{x}, \overrightarrow{\xi}\epsilon)dS_{\rightarrow\xi} = -i\omega i_j(\rightarrow x)x \in S_M \\ = 0 \quad x \in S_B \; S_M \tag{8.0.17}$$

This integral equation is of Fredholm type of the second kind.

This equation is solved thorough discretization of the body surface and the assumption that the source strength is constant over a discretized part of the body surface. This leads to the following set of linear equations:

$$\left[-\frac{1}{2}l_n + k_n\right]_{-mj} = [\phi\vdots n_j\vdots\phi]^T m = 1...M \\ S_m j = 1...6 \tag{8.0.18}$$

where l_n is the unity matrix and Kn the influence matrix obtained from the Green's function.

Equation (8.0.18) can be solved with standard numerical inversion techniques. Once the source strength is known, the velocity potential $\phi_{mj}(x)$ can easily be calculated with Green function.

From the velocity potential ϕ_7, ϕ_{mj} and Bernouilli's law we can derive the hydrodynamic first-order pressure on all bodies due to the motion j of the body m and due to diffraction.

$$p_{mj} = -\rho(-\omega\phi_{mj}), \quad p_7 = -\rho(-i\omega\phi_7) \tag{8.0.19}$$

The force follows from pressure integration over the mean wetted hull surface:

$$F_k = -\int_{SB}\int p \cdot nkdS \tag{8.0.20}$$

The reaction force in the k^{th} mode on body m due to the motion in the j^{th} mode of the body i we write;

$$F_{kj}^{mi} = \int\int_{SB} p_{ij}n_k dS \quad k, j = 1...6, m, i = 1...M \tag{8.0.21}$$

This reaction force F_{kj}^{mi} can be split into an added mass and a damping term.

$$F_{kj}^{mi} = -\omega^2 a_{kj}^{mi} - i\omega b_{kj}^{mi} \tag{8.0.22}$$

The wave forces acting on body m are as follows:

$$F_k^m = -\rho i\omega \int_{SB} \int (\phi_0 + \phi_7) n_x dSm = 1...M \tag{8.0.23}$$

The equations of motion can then be written as:

$$\begin{aligned}
(m_1 + A_{11})\ddot{x}_1 + A_{12}\ddot{x_2} + ...A_{1m}\ddot{A_{1m}} + B_{11}\dot{x_1} + ..B_{1m}\dot{x_m} + C_{11}x_1 = F^1 \\
A_{m1}\ddot{X}_1 + ...(A_{mm} + m_m)\ddot{x_m} + ...C_{mm}x_m = F^m \\
A_{M1}\ddot{X}_1 + ...(A_{MM} + m_M)\ddot{x_M} + ...C_{MM}x_M = F^M
\end{aligned} \tag{8.0.24}$$

where $x_m = [x_m,\ y_m,\ z_m,\ \phi_m,\ \theta_m,\ \psi_m]^T$ is the motion vector of body m and F^m is the wave exciting force vector $[F_1^m,\ F_2^m],\ F_3^m,\ F_4^m,\ F_5^m,\ F_6^m]^T$ acting on body m.

Appendix C

Dobrochinski (2014)

Figure 9.1: Qualitative summary of SWASH performance with 3 or 2 layers and linear wave conditions. ↓kd = (kd ≤ 1); ↑kd = (kd ≥ 3). "++" = very good; "+" = good; "-" = bad; "- -" = very bad.

Schemes	Horiz. resolution	Dispersion		Amplitude (boundary)		Amplitude /λ		Score
		↓ kd	↑ kd	↓ kd	↑ kd	↓ kd	↑ kd	
Default set	100	++	++	++	-	++	- -	+5
	40	++	++	++	-	++	- -	+5
	20	++	++	++	-	+	- -	+4
	10	+	+	++	-	-	- -	0
Adapted set	100	++	++	++	-	++	++	+9
	40	++	++	++	-	++	++	+9
	20	++	++	++	-	+	+	+7
	10	+	+	++	-	-	- -	0

Figure 9.2: Qualitative summary of SWASH performance with 3 or 2 layers and non-linear wave conditions. ↓kd = (kd $\leq$ 1); ↑kd = (kd $\geq$ 3). "++" = very good; "+" = good; "-" = bad; "- -" = very bad.

Schemes	**Horiz. resolution**	**Dispersion**		**Amplitude (boundary)**		**Amplitude /λ**		**Score**
		↓ kd	↑ kd	↓ kd	↑ kd	↓ kd	↑ kd	
Default set	100	++	++	++	-	++	++	**+9**
	40	++	++	++	-	++	++	**+9**
	20	++	++	++	-	++	++	**+9**
	10	+	+	++	-	++	++	**+7**
Adapted set	100	++	++	++	-	++	++	**+9**
	40	++	++	++	-	++	++	**+9**
	20	++	++	++	-	++	++	**+9**
	10	+	+	++	-	++	++	**+7**

Appendix D

Sketch map of ship model in model test (Bijleveld, 2004)

Figure 10.1: Transducer locations and ship response calculation sketch map.